NASA Contractor Report 191427 Volume I

GASL TR 342

Mach 10 to 20 Electrothermal Wind Tunnel Feasibility Study and Demonstration

Final Report

Volume I
Executive Summary and Analytical Study

by

O.F. Rizkalla and W. Chinitz,
General Applied Science Laboratories, Inc.
77 Raynor Avenue
Ronkonkoma, New York 11779

and

R. Burton
University of Illinois
Urbana, IL 61801

Prepared for
NASA Langley Research Center
Hampton, Virginia 23665

under

Contract NAS1-18450
Task Order 20

November 1991

Executive Summary

The objective of the electrothermal wind tunnel (EWT) concept study is to demonstrate, both analytically and experimentally, the feasibility of a high total pressure and enthalpy airbreathing propulsion test facility. The key element of this wind tunnel is a high-pressure heater developed by GT-Devices which uses a continuous high power (100 to 650 MW) arc discharge to heat cryogenic liquid air (or possibly a surrogate fluid) to high temperature and pressure. The vaporized fluid is mixed with cooler fluid to obtain the desired reservoir conditions, then expanded through a nozzle to produce the test conditions (or expanded directly from the arc). The full scale facility was initially sized to produce Mach 10 to 20 total enthalpies at mass flows up to 17 kg/sec (35 lbm/sec) for total test times of 0.5 seconds.

The experimental work was conducted by GT-Devices and the analytical study was performed by GASL. A summary of each effort follows:

Experimental Study

The objective of the experimental effort was to demonstrate operation of the key component of the Electrothermal Wind Tunnel (EWT), the liquid capillary arc in a subscale, pulsed-type test bed. Operation of the liquid capillary arc requires pumping a cryogenic liquid into a tube of large length to diameter ratio, maintaining a continuous arc discharge in the tube, and producing a stable effluence of high pressure, high temperature vaporized gas suitable for expansion through a supersonic nozzle. The primary goal of this effort was production of up to 0.5 kg/sec of air at a pressure of 10,000 psi (ultimately 60,000 psi) and temperature of 20,000°K for a period of 2 milliseconds. These conditions were chosen to match the capacity of the available capacitor bank at GT-Devices.

Operation of the arc was successfully achieved, although with liquid nitrogen rather than liquid air, and at substantially reduced pressure, e.g. 4500 psi. A number of experimental problems were encountered, the most significant of which were:

1) Lack of movement of the intensifier pump piston due to the presence of water ice;
2) Leakage of pump high pressure seals at cryogenic temperature;
3) The occurrence of capillary arc quenching during liquid injection.

Lack of motion of the piston due to water ice formation was successfully overcome by adding additional external plumbing hardware to allow control of the internal atmosphere.

Attempts to identify and eliminate leakage of the pump high pressure seals were unsuccessful. However, procedures were established to allow pump operation at reduced pressures of about 4600 psi for about 1000 psi gas pressure on the piston base.

The intensifier pump is a relatively small component of the system and we believe that the problems encountered should not be difficult to correct. Investigation into an alternative approach is also warranted, i.e., downrating the pressure goal to 30,000 psi (for demonstration of the concept) so that a commercially available unit can be used.

The phenomenon of arc quenching was observed early in the program. It became clear that quenching is caused by trying to initiate an arc in a capillary that contains too much initial fluid mass for the available power. By shortening the capillary, while maintaining essentially the same power input, the initial liquid mass is reduced and the available input power can establish to maintain a stable arc. Two experimental tests were performed in which the capillary length was reduced from the original 13 cm to 5 cm. A stable arc was successfully established in both tests. Test parameters and results for these two shots are summarized in the following table.

Experimental Results for 5 cm Long Capillary

Parameter	Shot 22	Shot 23
Capacitor bank charging voltage, kV	4.24	3.79
Pump piston base He pressure, psi	6.00	1200
Peak pump LN_2 pressure, psi	2571	4458
Pump LN_2 pressure at discharge initiation, psi	873	2241
Peak current, kA	40	36
Average power input, MW	44	37
Plasma pressure at capillary exit, psi	5147	4559
Plasma pressure at nozzle throat, psi	2575	2175
Test time, steady current, msec	1.1	1.1
Test time, steady capillary pressure, ms	1.8	1.9
Test time, steady nozzle throat pressure, ms	1.5	1.6

None of the problems described detract from the anticipated capabilities of the liquid capillary arc or the EWT concept. They do, however, indicate the need for a development effort on the cryogenic components of the system and on the arc. It should be emphasized

that the principal difficulties have been associated with the development of a suitable cryogenic pump; not with the operation of the capillary arc. Establishment of a stable arc discharge appears to be relatively straightforward, as suggested by the last two test shots in this program.

Analytical Study

The primary objective of the analytical studies was to optimize the performance of the EWT facility with respect to test flow quality, including the use of surrogate gases where necessary to improve oxygen recombination in the facility nozzle, and to determine the impact on simulation capability and scramjet flow processes. In addition, a conceptual design for the full scale facility, and a preliminary design for the pilot facility were to be provided. However, as work progressed, a number of critical issues surfaced which were addressed to assess their severity and to indicate possible solutions. The pilot facility concept was subsequently determined to be inappropriate due to scale and facility nozzle throat heat transfer considerations and was therefore postponed in favor of resolving the critical issues, among which are throat heat transfer, the facility power supply, and test gas composition for air simulation. Attention was focussed away from the use of surrogate gases since the fidelity of the simulation is compromised and because the calculations presented herein indicate that additional oxygen recombination does not occur with the surrogate mixture investigated.

The subjects investigated and the conclusions reached are summarized below. Given these conclusions, the simulation potential of the EWT is then assessed in the context of two test times, 25 milliseconds and 0.2 seconds.

1) Gas Conditions in the Mixing Chamber

The conditions in the mixing chamber (reservoir) were calculated assuming chemical equilibrium in the chamber and were corrected for non-ideal (thermally imperfect) gas effects due to interparticle repulsion. The assumption of chemical equilibrium was verified by finite rate calculations at several conditions. One of the key results of these calculations is that significant oxygen dissociation occurs in the arc and mixing chamber even at the design pressures for the facility, and that the very high pressures favor formation of nitric oxide as a primary dissociation product. The results also indicate that imperfect gas effects significantly increase the required reservoir pressure at the design point conditions, namely Mach 10, 12, 16, and 20 inlet and combustor entrance conditions for a 1000 psf flight path. Ionization is minimal, however, due to the high pressures. The total pressure varies from 120 atmospheres for Mach 10 direct-connect simulation to 38,000 atm for Mach 20 free jet. The total temperatures produced do not present a problem since the arc generates 10,000 to 20,000 degrees Kelvin in the capillary. If thermally imperfect gas effects are added and a maximum containable pressure of 13,000 atm (~200,000 psia) is assumed, then full total pressure simulation is achievable up to Mach 16 free jet and up to Mach 20 direct connect. However, direct-connect simulation is limited by facility nozzle performance (to Mach 16), not containment pressure.

2) Facility Nozzle Chemical Kinetic Performance

One-dimensional chemical nonequilibrium calculations were made to assess the extent to which the dissociation products recombine in the facility nozzle for various area distributions and expansion rates. Nitric oxide and atomic oxygen are the products of greatest concern due to their effects on autoignition and apparent heat of combustion of the fuel. Although neither is desirable since they will not occur in significant quantities in flight, atomic oxygen is considered more deleterious to a ground test simulation than nitric oxide.

Two types of facility nozzles were considered: direct connect (d.c.) and free jet (f.j.) The former would simulate scramjet combustor entrance conditions, while the latter would simulate conditions in the flowfield behind the shock wave of a vehicle forebody inclined at 8 degrees to the flight direction.

For all the conditions except Mach 16 direct connect and Mach 20 (d.c. and f.j.), the high local densities allow equilibrium to prevail in the nozzle up to the chemical freezing point. The small fraction of energy tied up in ionization is also in equilibrium with the flow conditions, but has no noticeable effect on the flow or the chemistry during the expansion.

The nozzle exit compositions for simulated Mach 10 and 12 conditions contain zero atomic oxygen. For Mach 16 free-jet simulation, the atomic oxygen which freezes is between one and three mole percent for expansion angles between two and ten degrees, respectively, whereas four to seven percent freezes for direct-connect simulation. Nitric oxide is present at concentrations between four and six mole percent for all the conditions and nozzle geometries investigated. Varying the expansion half-angles between two and ten degrees results in only minor changes in the test gas composition for Mach 10 to 12 simulation, but at higher flight conditions the composition becomes increasingly sensitive to the expansion angle. Hence, expansion angles may have to be lower than those typically used for facility nozzles, in addition to utilizing the following means to improve the simulation quality of the test gas:

Oxygen replenishment and three body recombination enhancement demonstrate significant potential for conditions up to and including Mach 16 simulation. Specifically, although the nitric oxide cannot be reduced (see η_n below), the oxygen lost to NO can be replaced with almost no additional formation of dissociation products. At Mach 16 conditions, the atomic oxygen that remains in the test gas can be reduced to trace amounts by adding efficient third bodies to the flow to catalyze the oxygen three body recombination reaction. Water is an extremely efficient catalyst, but leaves behind trace amounts of hydroxyl radicals and hydrogen in both atomic and molecular form. This situation is slightly worse for Mach 16 direct connect simulation. However, these latter contaminants can probably also be reduced to trace amounts by optimizing the water concentration and/or increasing the simulated flight dynamic pressure. Since the required total pressure for Mach 16 direct-connect

simulation is only about 2200 atmospheres, higher pressures can be produced, albeit at the expense of higher throat heat flux.

At Mach 20, the oxygen in the test gas mixture consists mostly of atomic oxygen and hence does not seem to be suitable for scramjet combustion simulation. Therefore, Mach 16 seems to represent an upper simulation limit with respect to test gas quality.

A nozzle chemical kinetic performance parameter was identified which correlates the amount of recombined oxygen in the nozzle to the reservoir entropy, s_t, pressure, P_t, enthalpy, H_t, and the slope of the (conical) nozzle wall ($\tan\theta$) for the conditions and geometries examined. The parameter is

$$\eta_n = \frac{s_t \ell n\left(\frac{P_t(atm)}{\tan\theta}\right)}{H_t}, \quad (K^{-1}),$$

The implication of the observed trend with regard to the fraction of recombined oxygen is that nitric oxide is always formed somewhere in the reservoir or nozzle at the conditions considered and, once formed, the oxygen lost to nitric oxide can not be recovered. This parameter also correctly predicts the conditions at which a reflected shock tunnel produces 100% atomic oxygen after expansion, but has not been tested further.

3) Facility Nozzle Throat Heat Flux

The transient heat flux calculations for the facility nozzle throat indicate that cooling the throat region at conditions above those for Mach 12 simulation will probably require innovative engineering solutions. However, it is postulated that the problem does not limit the capabilities of the facility to any greater extent than those mentioned above. At these conditions, the surface temperature for a (semi-infinite) copper heat sink throat approaches the free stream temperature over a test time of 0.2 seconds which, for Mach 16 simulation, is 7000 K. The table below summarizes the results for the design point calculations, listing the heat transfer coefficient, the surface temperature after a 0.2 second test, and the average heat flux over the test duration.

Calculated Average Heat Transfer at the Facility Nozzle Throat
Copper Heat Sink; Initially Cooled to 70 K

Flight M	Configuration	h(Btu/in^2-s-° F)	T_w (K) at t=0.2 sec	q(Btu/in^2-s) (average)
10	Direct Connect	0.0061	560.	37.
10	Free Jet	0.017	1380.	98.
12	Direct Connect	0.018	1900.	160.
12	Free Jet	0.051	3450.	415.
16	Direct connect	0.0850	6300.	1030.
16	Free jet	0.260	7100.	3150.
20	Direct connect	0.627	9600.	10,100.
20	Free jet	2.310	10700.	46,500.

The heat flux at Mach 16 is about one order of magnitude greater than at the stagnation point of a ballistic missile during reentry at low altitude. The implication is that cooling a Mach 16 throat does not seem to represent a quantum leap in current technology. However, the severity of the problem may dictate that the test time be scaled back to facilitate a feasible solution.

For a 25 msec test duration, the wall temperature rises to about one-half that of a 0.2 second test, and the average heat flux is about 75% of the values listed above. Hence, the heat sink approach will probably suffice through Mach 16 if rapid surface oxidation (i.e., combustion) can be avoided.

The cooling techniques envisioned for a 0.2 second test are heat sinks through Mach 12 and ablation or transpiration cooling at Mach 16. At Mach 16, the most attractive approach from both cost-conscious and technical viewpoints seems to be the use of ablative inserts. Tungsten coated with an oxidation resistant material or graphite ablation/oxidation might result in acceptable ablation rates and hence throat area changes. Transpiration cooling the throat at this condition requires coolant mass flow rates of about ten times that of typical high heat transfer rate applications. Of course, both of these techniques must be evaluated with respect to their effect on the uniformity of the exit flow.

4) Power Supply Options

The power requirement for the EWT, based on a 50% arc efficiency, is estimated at 650 MW for Mach 20 simulation, and 225 MW for Mach 16 simulation. Selection of the most cost-effective type of power supply was based on test time, operating cost, safety, and maintenance. For test times on the order of one second, the flywheel approach (rotating machinery) seems to be the most appropriate power supply, whereas capacitor banks seem more attractive for test times of around 25 milliseconds. The installed costs are estimated at $60M for the flywheel, and $7M for the capacitor banks. The cost of a power supply for Mach 16 energy levels is about the same for a one second test duration with the flywheel, whereas for a 25 msec test, the cost is reduced to $1.5M for capacitor banks.

Based on throat heat flux and power supply considerations, the cost and risk associated with an EWT facility designed for 25 msec of test time is significantly reduced from that of a 0.2 second test facility. Since the simulation capability remains essentially unchanged, however, a preliminary performance map for the EWT was constructed which represents both test durations. The results of these calculations are shown in the Figure below, which maps the portions of the flight envelope where acceptable nozzle performance, containable total pressures, throat heat flux considerations, and power supply limits are met. The solid lines represent flight paths for flight dynamic pressures of 500 to 2000 psf. The dashed and dotted lines bound the simulation regime for the direct-connect and free-jet conditions, respectively. Simulation is limited to Mach 16 by the total pressure and heat flux generated at the throat, assuming that the throat can be cooled. The remainder of the flight envelope is bounded by power (mass flow) limitations and nozzle performance, as shown. Note that the simulation envelope does not take into account off-design performance of the cryogenic arc or cryogenic pump and capillary mass flow limitations. A preliminary design of the full scale facility is necessary before such factors can be properly accounted for.

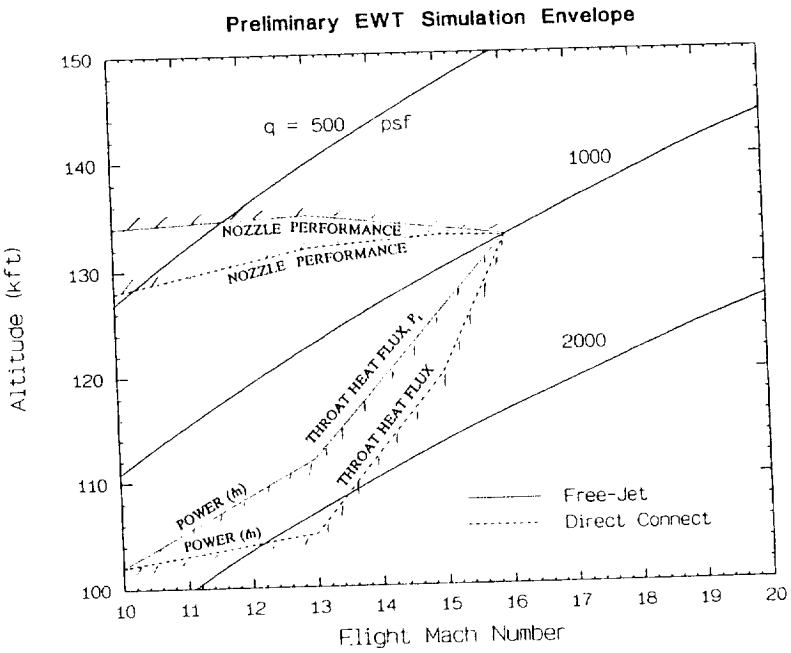

Foreword

This report was prepared by General Applied Science Laboratories, 77 Raynor Avenue, Ronkonkoma, NY 11779, under NASA Contract NAS1-18450, Task 20, and is identified by the contractor as GASL TR 342. The NASA program monitors were Earnest Mackley and Dennis Bushnell. The authors are pleased to acknowledge their guidance, cooperation, and assistance in carrying out this effort. The research was performed during the period January 1, 1990 to August 31, 1991.

Table of Contents

Table of Contents (continued)

List of Illustrations

List of Illustrations (continued)

List of Illustrations (continued)

List of Tables

1.0 Introduction

A renewed national interest in hypersonic flight has generated a need for ground testing airbreathing propulsion systems at simulated flight conditions above Mach 10.[1-5] In order to properly interpret the test data and relate model performance to the full scale engine, true simulation of the relevant flow characteristics of the test gas is required. Herein lies the crux of the problem which has continually frustrated the hypersonic airbreathing propulsion community. Proper simulation of the flow physics and chemistry at hypervelocity conditions requires duplication of the local temperature, density, velocity, and gas composition, and scale. The latter implies that the model must be appropriately sized (preferably to full scale) to closely simulate the residence time of the gas in the engine, and particularly in the combustor, where the time required to mix and react the fuel and oxidizer is of the order of the residence time. In addition, the facility test time must be sufficient to allow establishment of viscous-dominated phenomena such as separated flow regions, and to simulate nonadiabatic and catalytic wall effects, although the latter is less critical at these flight conditions[6]. All facilities currently in operation are limited in one or more of these requirements because they cannot produce the requisite energy levels for sufficient duration, and/or cannot obtain the proper distribution of energy among the various energy states of the test gas, i.e., translation and dissociation.

The two methods available for adding energy to a fluid to obtain the required test conditions are thermally, through pressure and temperature, and kinetically, through velocity. The more effective means of energy addition is the latter approach which has been shown[7,8,9] to be capable of duplicating both the total enthalpy and total pressure, as well as the mixture composition. However, in keeping with the stated limitations, the power requirements are such as to confine the facility to submillisecond test times and small core flow areas, thereby precluding its use as an engine test facility (although it has been shown[7,8,9] to be useful as a hypervelocity propulsion research facility). In point of fact, the most effective means of energy addition is probably a combination of the two. However, such a facility is barely conceptualized at this point.

The first-named method is by far the most common, and is the only one that has been applied to an engine test facility. Simply stated, the energy is added by various means to a fluid at rest, then the hot, high pressure fluid is expanded through a nozzle to obtain the test conditions. Although the total temperature requirement for hypervelocity simulation can be met, the principal disadvantage is an inability to tolerate or contain the total pressure required and to obtain the proper test gas mixture composition. Hence, either the test static pressure is sacrificed or the pressure is simulated at the expense of high static temperature, but the test mixture composition is incorrect in either case due to contamination with combustion products or to early freezeout of the gas in the nozzle, or both.

The relative total pressure capabilities of the various test facility concepts are summarized in Figure 1. The total pressure required to simulate conditions for a typical NASP-type trajectory (1000 psf) is plotted as a function of flight Mach number for the freestream and for inlet and combustor entrance conditions. The total pressure is seen to vary exponentially with flight Mach number, and combustor inlet (c.i.) total pressure quickly exceeds 1000 atmospheres above about Mach 14. However, combustion and arc heaters are typically limited in total pressure to between only 100 and 200 atmospheres (Mach 8 to 10, c.i.) due to high plenum heat transfer rates and to arc stability and electrode burnout, respectively. Reflected shock tunnels (RST) can generate at most about 2,000 to 3,000 atmospheres (Mach 12, c.i.) due to structural limitations of the driver tube. In addition, test times are of the order of milliseconds. A free-piston-driven expansion tube can theoretically duplicate conditions which correspond to total pressures of 70,000 to 100,000 atmospheres (> Mach 25, c.i.) by increasing the velocity via an unsteady expansion wave, but does so again at the expense of test time and model size.

If both the total enthalpy and pressure can be generated by providing sufficient power efficiently, without the aid of combustion, then the test static flow properties after expansion will closely approximate the desired conditions and nozzle chemical freezeout will be delayed (owing to the high pressure), resulting in a distribution of thermal energy states in the test gas which more closely approximates that of natural air. This report describes a study which takes an important first step in the development of such a facility.

The objective of the present research has been to demonstrate, both analytically and experimentally, the feasibility of building a high total pressure and enthalpy, airbreathing propulsion test facility. The key element of this wind tunnel is a heater developed by GT-Devices which uses a continuous high power (100 to 650 MW) arc discharge to heat cryogenic liquid air (or a surrogate fluid) to high temperature and pressure. This concept is an extension of existing electrothermal plasma jet technology developed for electrothermal guns[10] and space thrusters.[11] The vaporized fluid, which is initially confined to a small diameter tube, referred to herein as the capillary, is mixed with more fluid to obtain the desired reservoir conditions, then expanded through a nozzle to produce the test conditions. A schematic illustrating the facility concept is shown in Figure 2.

The concept differs from conventional arc heaters in that, first and foremost, the small diameter capillary allows arbitrarily high pressures to be generated, limited only by the material strength of the chamber walls. In the limit of a large outer to inner diameter ratio, this pressure is essentially the tensile strength of the material. However, higher pressures can be tolerated by pre-stressing and multilayering the vessel. Second, the use of a liquid prevents electrode and insulator burnout because the liquid's high density and optically thick qualities absorb radiation which otherwise reach the electrodes and the capillary walls. An added benefit is an increase in the energy conversion efficiency to between 50 and 60 percent, in contrast to the 30 to 40 percent efficiency of conventional arcs.

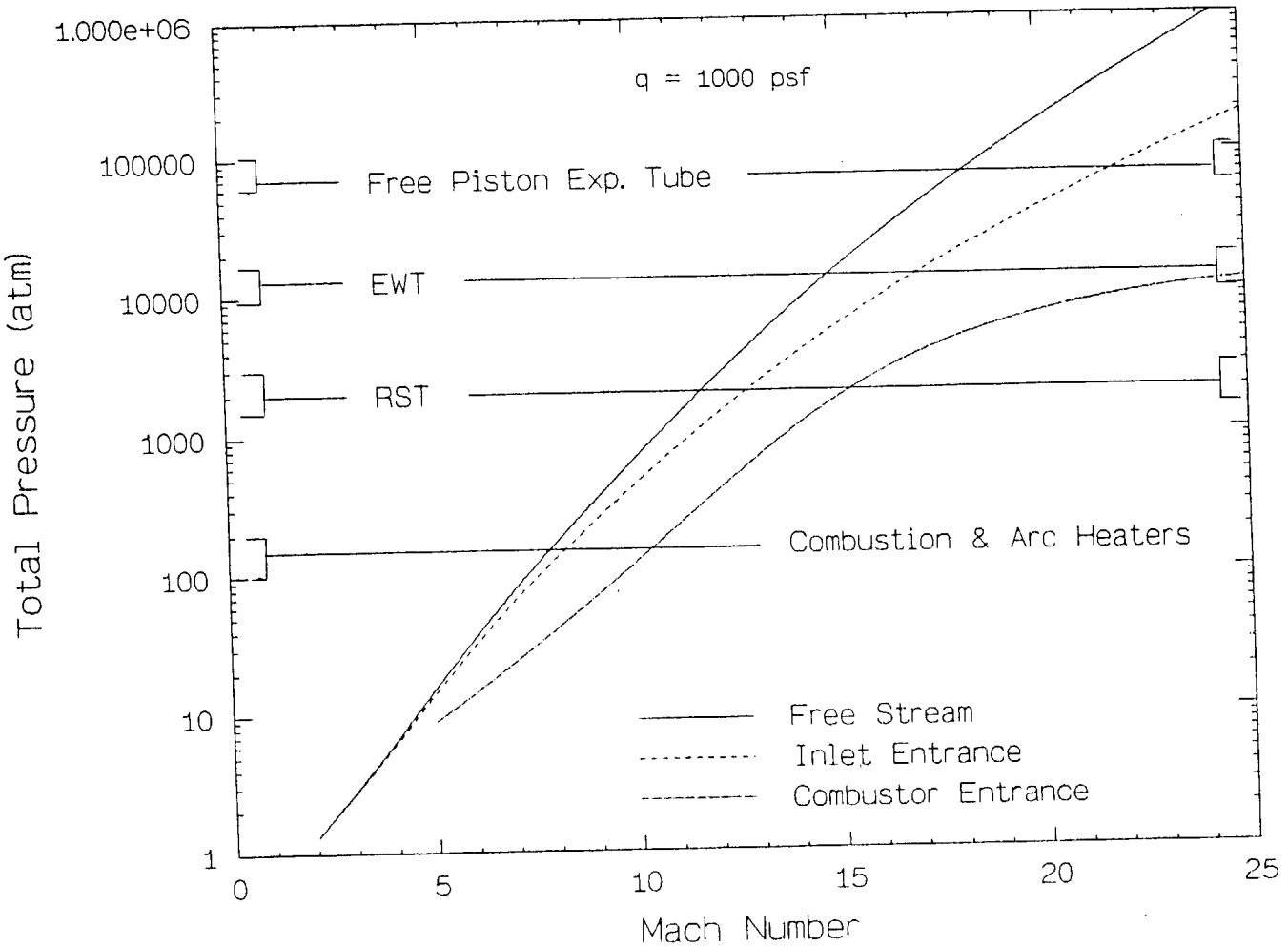

FIGURE 1. TOTAL PRESSURE SIMULATION CAPABILITY

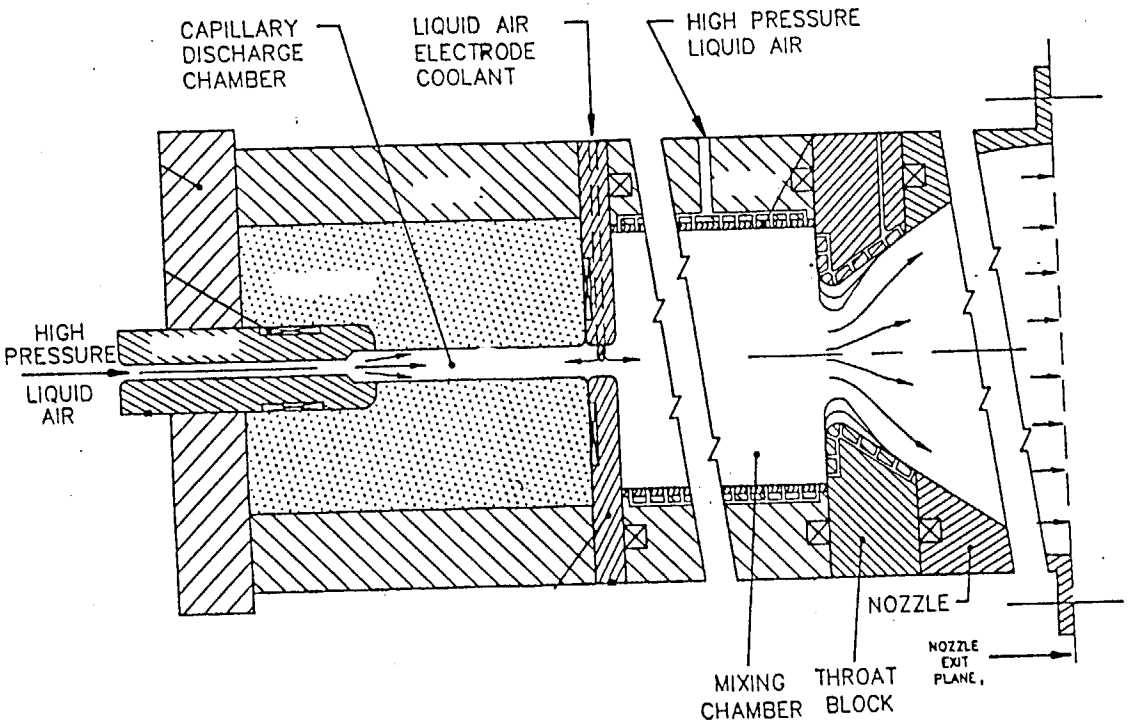

FIGURE 2. SCHEMATIC OF THE ELECTROTHERMAL WIND TUNNEL CONCEPT

In addition to obtaining true simulation of the flow variables, the high pressure was expected to improve the simulation qualities of the gas because dissociation of the reservoir gas would be reduced, and the chemistry during the expansion would remain in equilibrium longer. Therefore, the portion of the thermal energy that is in dissociation after chemical freezing should be minimized.

The facility, and thus the power supply, was conceptualized to produce mass flows up to 17 kg/sec (36 lbm/sec) for test times up to 0.5 seconds at simulated Mach 20 test conditions. The nozzle exit area for a free-jet test (i.e., simulated inlet entrance conditions) is 2 ft^2. Table 1 shows the free-stream and free-jet test conditions for the selected facility design points.

The objective of the experimental work was to demonstrate stable operation of the capillary arc with a cryogenic liquid as the working fluid. To this end, a subscale electrothermal wind tunnel (EWT) was designed, built, and tested at GT-Devices. The wind tunnel consisted of basically three components; a capillary arc designed for 60,000 psi maximum pressure, a cryogenic pump (also designed for 60,000 psi) to feed cryogenic liquid to the capillary at mass flows up to 0.5 kg/sec, and a supersonic nozzle to receive and expand the vapor effluent. The capacitor bank and pulse-forming network supplied enough power to produce a 40 MW arc for a period of 2 milliseconds. Figure 3 shows a schematic of the subscale wind tunnel which was tested (see Volume II of this report).

Operation of the arc was successfully achieved, although with liquid nitrogen rather than with liquid air, and at substantially reduced pressures (e.g, 4550 psi) due to pump difficulties. A number of other problems were encountered, although none negated any of the anticipated capabilities of the EWT concept. However, they do indicate the need for further development of the cryogenic components of the system and of the prediction of the characteristics of cryogenic capillary arc operation.

The objective of the analytical study was to determine and optimize the performance of the full-scale facility with respect to flow quality. In addition, technically challenging areas which might be encountered in the full-scale and $1/30^{th}$-scale pilot facilities were to be investigated and possible solutions identified. Specifically, the real gas conditions in the mixing chamber (reservoir) required to produce the test flow were determined for the design point conditions. The chemical kinetic performance of the facility nozzle is a major concern and was investigated in detail to indicate the extent to which the dissociated reservoir mixture recombined in the nozzle. For conditions at which an unacceptable test gas mixture is produced, methods to maximize the performance were investigated, e.g., nozzle geometry optimization, oxygen replenishment, three-body recombination enhancement, etc.

TABLE 1. FLIGHT AND TUNNEL CONDITIONS

For M_∞ = 10 to 20 flight at a dynamic pressure of 1000 psf, the following table describes the flight free-stream flow parameters.

Flight Parameters

M	V	Alt	q_∞	H_t		ρ V/A	$Re/10^6$	$P_{t\ approx}$
	ft/sec	ft/1000	lbs/ft^2	Btu/lb	ft^2/sec^2	lb/ft^{2}sec	1/ft	atm.
10	10,036	110.5	1000	2019	53.02 x 10^6	6.513	6.422	266
12	12,228	119	1000	3097	77.51 x 10^6	5.316	5.113	587
16	16,700	133	1000	5687	142.32 x 10^6	3.852	3.564	2554
20	21,255	144	1000	9145	228.89 x 10^6	3.043	2.735	7996

For the scramjet test facility in a free-jet test mode simulating the Mach number under a vehicle forebody at eight (8) degrees to the flight direction, the table below describes the facility requirements. A two (2) square-foot nozzle exit area is assumed.

Free-Jet Tunnel Flow Parameters (2 Ft^2 Exit)

M_∞	q_∞	M_L	q_L/q_∞	$\rho V_L/\rho V_\infty$	Re_L/Re_∞	H_{t_L}	p_{t_L}	Wa
	lbs/ft^2					Btu/lb	atm	lbs/sec
10	1000	7.28	2.75	2.81	1.79	2012	174	36.6
12	1000	8.2	3.119	3.178	1.85	2987	312	33.8
16	1000	9.594	3.736	3.80	1.87	5572	832	29.3
20	1000	10.55	4.207	4.275	1.81	9025	1534	26.0

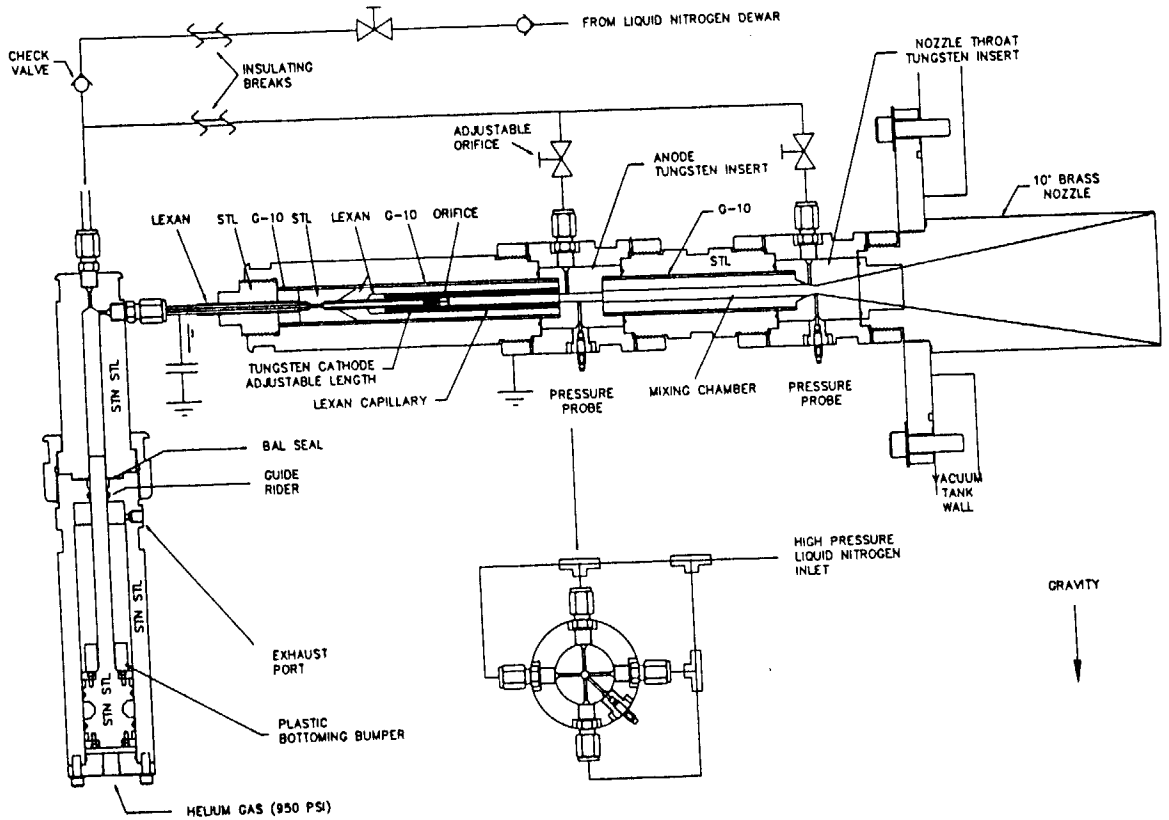

FIGURE 3. SCHEMATIC OF SUBSCALE DEMONSTRATION EWT FACILITY

Another major concern is the heat flux generated at the throat of the facility nozzle. The combination of high temperatures and pressures produce throat heat flux rates which, above about Mach 14, will require innovative solutions to prevent significant interaction between the test gas and the nozzle wall. Several possible techniques were investigated in this regard, among which are ablative inserts and transpiration cooling. The most attractive approach at this time from both cost-conscious and technical viewpoints seems to be the use of ablative inserts. However, the severity of the problem at Mach 16 may dictate that the test time be scaled back to facilitate a more feasible solution, such as a heat sink.

The results of the performance study indicate that the full-scale facility can produce a satisfactory test flow up to about Mach 16, where the throat heat flux rates, pressure containment, and chemical freezing in the nozzle all become limiting factors.

Finally, the power levels required to produce such high energies and mass flows indicate that the power supply will be the major cost driver in the full-scale facility. To a large extent this cost is a function of the type of power supply chosen. A study to determine the most cost-effective type of power supply for this application concluded that it is heavily dependent on the desired test time. Rotating machinery is most appropriate for test times on the order of one second, whereas capacitor banks seem more attractive for test times of around 25 milliseconds.

The next section describes the calculations made to predict the mixing chamber (reservoir) conditions.

2.0. Gas Conditions in the Mixing Chamber (Reservoir)

The function of the mixing chamber (reservoir) of the EWT is to receive the arc-heated gases discharged from the capillary and dilute them with additional fluid to achieve the desired gas composition, pressure, and enthalpy. Simulating Mach 10 to 20 scramjet test conditions in the EWT facility requires that the test gas be generated in the mixing chamber at true total enthalpy and pressure. At these flight conditions (especially above Mach 15), the test gas will be highly dissociated and partially ionized in the mixing chamber. The state of the gas will therefore differ significantly from perfect gas predictions, and must be calculated appropriately.

An effect of particular concern in this regard is the high total pressure generated by a gas (air) which is calorically imperfect and dissociates at total enthalpy levels typical of the hypervelocity regime. These characteristics were fully accounted for in the calculations made here. Additionally, the high reservoir densities tend to increase the macroscopic effects of intermolecular forces, driving the gas away from its typically assumed thermally perfect state. Calculations were made to assess the magnitude of this phenomenon, however they were not coupled with the chemistry as this would have required an extensive effort.

The selected flight conditions for which the mixing chamber properties were determined correspond to those given in Table 1. The calculations were made with an in-house equilibrium chemistry code, "EqState", which is described below. Use of both natural air and surrogate gases (mixtures of O_2, N_2, and Ar) was considered. The surrogate gas and air calculations are subsequently detailed for both the free jet and direct connect simulation conditions. Graphical representations of the mixing chamber properties also allow for other conditions to be interpolated. Compressibility effects at the reservoir conditions are then examined. Finally, some observations are made which reflect upon the impact of these calculations towards the performance of the facility nozzle.

2.1. Description of the EqState Code

The stagnation state calculations were made using an in-house code, "EqState", which calculates static and stagnation conditions both upstream and downstream of normal or oblique shock waves. Either frozen (variable gamma) or equilibrium chemistry may be assumed at each state, as well as across the shock. Given the initial conditions (pressure, temperature, and velocity), and the initial species concentrations, mass, momentum, and energy are conserved to obtain the conditions across the shock. The total enthalpy and entropy are conserved to arrive at the stagnation state. An equilibrium solution is obtained by utilizing the CREK chemistry package developed by D. Pratt[12], which minimizes the Gibbs free energy. This version of CREK is formulated to permit a set of species which exist in an ideal, homogeneous gas-phase mixture.

The thermodynamic properties of each component of the gas take the form of polynomial temperature coefficients for the specific heat at constant pressure, the enthalpy, and the entropy. The temperature range for the components of air is 298 to 24,000 degrees Kelvin, and includes ionized species. The coefficients for the range from 298 to 5,000 K were obtained from Gordon and McBride[13], while the temperature coefficients from 5,000 to 24,000 K were compiled in-house from various sources, e.g., Hilsenrath[14]. The species included in the calculations and their temperature coefficients are listed in Table 2.

EqState was modified for this study to calculate the frozen or equilibrium properties across oblique shocks of arbitrary wave angles. Given the flow deflection angle, δ, in addition to the initial conditions, the shock angle, θ, is obtained from considerations of the geometry of the oblique wave and the continuity equation. The relation is

$$\tan \delta = \frac{[(1-\beta) \tan \theta]}{[1+\beta \tan^2\theta]}$$

where ß is the ratio of upstream to downstream densities ρ_1/ρ_2. Since the deflection angle δ is known, the error in the assumed shock angle can be obtained by comparing the left and right hand sides of the equation. A Newton-Raphson type iteration is used to converge on the shock angle. The validity (existence) of a solution is verified by checking that the total enthalpy is conserved across the wave. It will not be conserved if the input deflection angle is above the maximum for an attached shock at a particular set of initial conditions.

A series of calculations were made to compare EqState with the available literature. Figures 4 and 5 show the free stream stagnation pressure and temperature as a function of Mach number for a 1000 psf flight path as calculated by EqState and from Hansen[15,16]. Agreement is seen to be excellent up to about Mach 18. At these conditions, Hansen's curve fit for the compressibility function becomes increasingly inaccurate[16]. Agreement between EqState and the Mollier diagrams of Moeckel and Weston[17] is good. Also shown for comparison are the curves for a perfect gas, $\gamma = 1.4$.

Calculations were also made to verify that the properties across oblique shocks were being correctly predicted. These calculations are not discussed here, but this version of the code has been subsequently used in many computations involving oblique shocks across which significant heat was released from hydrogen-air (and H_2-O_2) reaction (i.e., equilibrium oblique detonation waves). In all the cases examined, the calculated shock angle and downstream conditions agreed with the available literature.

Table 2. Temperature coefficients for Cp, h, s, for components of high temperature air (Reference 2).

```
ELEMENTS  HI TEMP CHEMISTRY w/IONS
E          .548597D-3 0.0000000
N+        14.0061500 4.0000000
O+        15.9988500-1.0000000
A+        39.9474500 1.0000000

                                                                                    8.
THERMO
N2                  JX9/65N+ 2.E  2.00 0.00 0.G    300.000 24000.000
 0.28963194D 01 0.15154866D-02-0.57235277D-06 0.99807393D-10-0.65223555D-14
-0.90586184D 03 0.61615148D 01 0.36748261D 01-0.12081500D-02 0.23240102D-05
-0.63217559D-09-0.225772530-12-0.10611588D 04 0.23580424D 01
-0.63217559D-09-0.225772530-12-0.10611588D 04 0.23580424D 01
 0.35629875D+01 0.55076464D-03-0.11275757D-06 0.97308112D-11-0.23949919D-15
-0.11816970D+04 0.23347563D+01

O2                  JX9/65O+ 2.E  2.00 0.00 0.G    300.000 24000.000
 0.36219535D 01 0.73618264D-03-0.19652228D-06 0.36201558D-10-0.28945627D-14
-0.12019825D 04 0.36150960D 01 0.36255985D 01-0.18782184D-02 0.70554544D-05
-0.67635137D-08 0.215559930-11-0.10475226D 04 0.43052778D 01
-0.67635137D-08 0.215559930-11-0.10475226D 04 0.43052778D 01
 0.42234946D+01 0.27618072D-03-0.34479165D-07 0.33461225D-11-0.87166645D-16
-0.18315161D+04-0.30217827D+00

A                   XX0000A+ 1.E  1.00 0.00 0.G    300.000 24000.000
 0.25000000D+01-0.00000000D+00-0.00000000D+00-0.00000000D+00-0.00000000D+00
-0.74537500D+03 0.43661076D+01 0.25000000D+01-0.00000000D+00-0.00000000D+00
-0.00000000D+00-0.000000000+00-0.74537500D+03 0.43661076D+01
-0.00000000D+00-0.000000000+00-0.74537500D+03 0.43661076D+01
 0.24425760D+01 0.20039480D-04 0.11062574D-08-0.85805080D-12 0.59103430D-16
-0.65754781D+03 0.47684504D+01

NO                  JX6/63N+ 1.0+ 1.E  2.00 0.G    300.000 24000.000
 0.31890000D 01 0.13382281D-02-0.52899318D-06 0.95919332D-10-0.64847932D-14
 0.98283290D 04 0.67458126D 01 0.40459521D 01-0.34181783D-02 0.79819190D-05
-0.61139316D-08 0.15919076D-11 0.97453934D 04 0.29974988D 01
-0.61139316D-08 0.15919076D-11 0.97453934D 04 0.29974988D 01
 0.40265559D+01 0.21895516D-03-0.33697776D-07 0.28557753D-11-0.69511790D-16
 0.95266701D+04 0.18941598D+01

N                   JX3/61N+ 1.E  1.00 0.00 0.G    300.000 24000.000
 0.24502682D 01 0.10661458D-03-0.74653373D-07 0.18796524D-10-0.10259839D-14
 0.56116040D 05 0.44487581D 01 0.25030714D 01-0.21800181D-04 0.54205287D-07
-0.56475602D-10 0.20999044D-13 0.56098904D 05 0.41675764D 01
-0.56475602D-10 0.20999044D-13 0.56098904D 05 0.41675764D 01
 0.21512169D+01 0.11381697D-04 0.41759829D-07-0.39307636D-11 0.10347405D-15
 0.56798887D+05 0.67884744D+01

O                   JX6/62O+ 1.E  1.00 0.00 0.G    300.000 24000.000
 0.25420596D 01-0.27550619D-04-0.31028033D-08 0.45510674D-11-0.43680515D-15
 0.29230803D 05 0.49203080D 01 0.29464287D 01-0.16381665D-02 0.24210316D-05
-0.16028432D-08 0.38906964D-12 0.29147644D 05 0.29639949D 01
-0.16028432D-08 0.38906964D-12 0.29147644D 05 0.29639949D 01
 0.23707167D+01 0.61978856D-04-0.14923527D-08-0.24070972D-12 0.15175868D-16
 0.29368901D+05 0.60421714D+01

E                   XX0000E  1.00 0.00 0.00 0.G    300.000 24000.000
 0.25000000D+01 0.00000000D+00 0.00000000D+00 0.00000000D+00 0.00000000D+00
-0.74510992D+03-0.11735000D+02 0.25000000D+01 0.00000000D+00 0.00000000D+00
 0.00000000D+00 0.000000000+00-0.74510992D+03-0.11735000D+02
 0.00000000D+00 0.000000000+00-0.74510992D+03-0.11735000D+02
 0.25000000D+01 0.00000000D+00 0.00000000D+00 0.00000000D+00 0.00000000D+00
-0.74510992D+03-0.11735000D+02
```

TABLE 2. (Continued)

```
N2+                  XX0000N+ 2.E  1.00 0.00 0.G   300.000 24000.000
 0.29073906D+01 0.11956061D-02-0.17123167D-06 0.95032496D-11-0.17969049D-15
 0.17906339D+06 0.68555503D+01 0.29073906D+01 0.11956061D-02-0.17123167D-06
 0.95032496D-11-0.17969049D-15 0.17906339D+06 0.68555503D+01
 0.29073906D+01 0.11956061D-02-0.17123167D-06 0.95032496D-11-0.17969049D-15
 0.17906339D+06 0.68555503D+01

O2+                  XX00000+ 2.E  1.00 0.00 0.G   300.000 24000.000
 0.53113509D+01-0.88229012D-03 0.18913235D-06-0.10860789D-10 0.19438677D-15
 0.13709662D+06-0.63310571D+01 0.53113509D+01-0.88229012D-03 0.18913235D-06
-0.10860789D-10 0.19438677D-15 0.13709662D+06-0.63310571D+01
 0.53113509D+01-0.88229012D-03 0.18913235D-06-0.10860789D-10 0.19438677D-15
 0.13709662D+06-0.63310571D+01

NO+                  XX0000N+ 1.0+ 1.E  1.00 0.G   300.000 24000.000
 0.42572272D+01 0.70026398D-05-0.10239430D-07 0.37576346D-11-0.13193645D-15
 0.11586592D+06-0.98682264D+00 0.42572272D+01 0.70026398D-05-0.10239430D-07
 0.37576346D-11-0.13193645D-15 0.11586592D+06-0.98682264D+00
 0.42572272D+01 0.70026398D-05-0.10239430D-07 0.37576346D-11-0.13193645D-15
 0.11586592D+06-0.98682264D+00

N+                   XX0000N+ 1.00 0.00 0.00 0.G   300.000 24000.000
 0.24359303D+01 0.46631664D-04 0.69411300D-09-0.23205306D-12 0.71659160D-17
 0.22568537D+06 0.53375241D+01 0.24359303D+01 0.46631664D-04 0.69411300D-09
-0.23205306D-12 0.71659160D-17 0.22568537D+06 0.53375241D+01
 0.24359303D+01 0.46631664D-04 0.69411300D-09-0.23205306D-12 0.71659160D-17
 0.22568537D+06 0.53375241D+01

O+                   XX00000+ 1.00 0.00 0.00 0.G   300.000 24000.000
 0.29287151D+01-0.39171128D-03 0.86145060D-07-0.53210888D-11 0.10281547D-15
 0.18792426D+06 0.18307374D+01 0.29287151D+01-0.39171128D-03 0.86145060D-07
-0.53210888D-11 0.10281547D-15 0.18792426D+06 0.18307374D+01
 0.29287151D+01-0.39171128D-03 0.86145060D-07-0.53210888D-11 0.10281547D-15
 0.18792426D+06 0.18307374D+01

O-                   XX00000+ 1.E  2.00 0.00 0.G   300.000 24000.000
 0.18754903D+01 0.32387412D-03-0.11846887D-07-0.74902520D-12 0.32286199D-16
 0.10454200D+05 0.87469047D+01 0.18754903D+01 0.32387412D-03-0.11846887D-07
-0.74902520D-12 0.32286199D-16 0.10454200D+05 0.87469047D+01
 0.18754903D+01 0.32387412D-03-0.11846887D-07-0.74902520D-12 0.32286199D-16
 0.10454200D+05 0.87469047D+01

A+                   XX0000A+ 1.00 0.00 0.00 0.G   300.000 24000.000
 0.27162466D+01-0.70048198D-04 0.92083731D-08-0.55677708D-12 0.12891905D-16
 0.18294332D+06 0.45550237D+01 0.27162466D+01-0.70048198D-04 0.92083731D-08
-0.55677708D-12 0.12891905D-16 0.18294332D+06 0.45550237D+01
 0.27162466D+01-0.70048198D-04 0.92083731D-08-0.55677708D-12 0.12891905D-16
 0.18294332D+06 0.45550237D+01
```

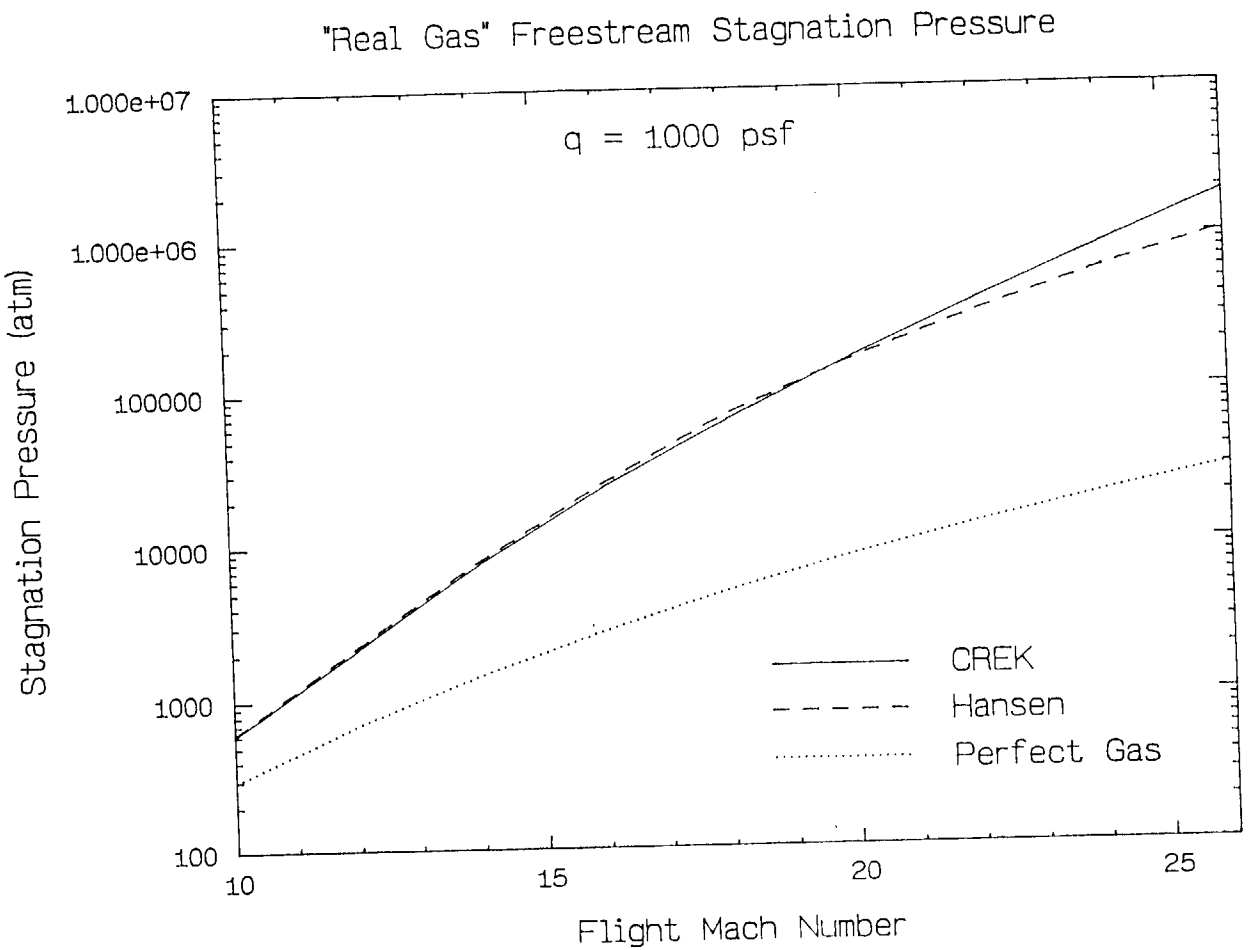

FIGURE 4. COMPARISON OF EQSTATE-CALCULATED FREESTREAM STAGNATION PRESSURE WITH REFERENCE 13 AND A PERFECT GAS

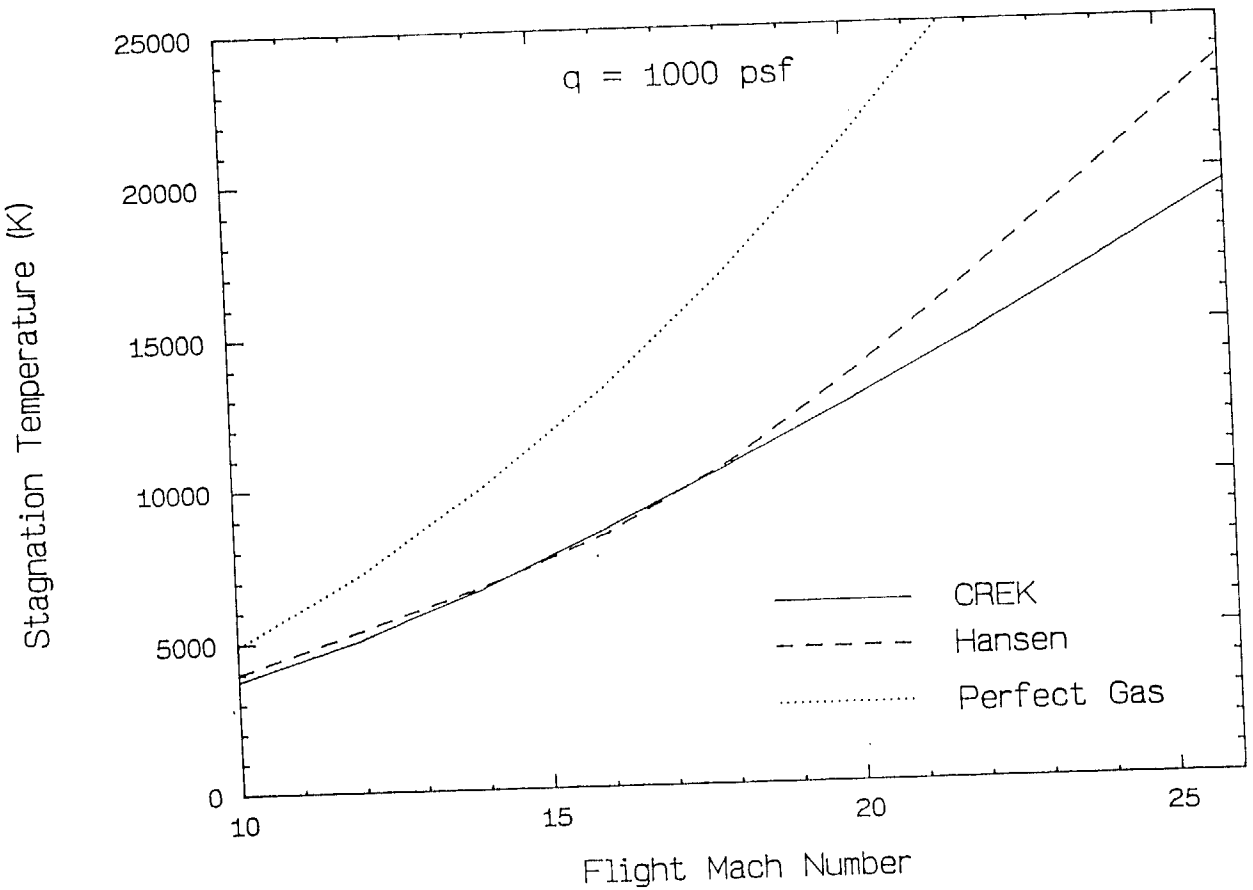

FIGURE 5. COMPARISON OF EQSTATE-CALCULATED FREESTREAM STAGNATION TEMPERATURE WITH REFERENCE 13 AND PERFECT GAS

2.2. Surrogate Test Gas

Initially, the objective of this part of the study was to determine the stagnation conditions in the mixing chamber for a surrogate test gas mixture which maximized the recombination of molecular oxygen in the facility nozzle. The surrogate gas was to be composed of the nominal concentration of oxygen in air, with the balance being some mixture of argon and nitrogen. Replacement of some of the nitrogen in air with an inert gas was thought to increase both the concentration of oxygen in the reservoir and its recombination rate in the nozzle by reducing the formation of atomic nitrogen and oxides of nitrogen. In particular, the nitric oxide which forms tends to reduce the formation of oxygen in two ways. First, NO tends to freeze during the expansion in the nozzle, tying up oxygen atoms which could otherwise recombine, and second, the reaction mechanisms involving NO also tie up and at some conditions produce additional atomic oxygen, thereby retarding the formation rate of molecular oxygen. These effects will be discussed in section 3 on the chemical kinetic performance of the facility nozzle.

The substitution of some of the nitrogen with an inert (perfect) gas also affects the stagnation state, reducing both the level of dissociation of the mixture and the variation of the mixture specific heat with temperature. The net effect is to reduce the total pressure and to increase the total temperature for a given simulated flight condition (total enthalpy). To illustrate the magnitude of these effects, an equivalent flight path for an argon-oxygen atmosphere (21 mass percent O_2) was first constructed based upon equal flight dynamic pressures of 1000 psf. Stagnation conditions for these flight paths were then calculated as a function of Mach number. The stagnation pressure is shown in Figure 6 for both free stream and free jet conditions. (The free jet condition is defined as the conditions behind the shock wave of an eight-degree forebody.)

For a given Mach number, the required stagnation pressure for the surrogate test gas is in fact seen to be significantly below that for air over the entire flight path (note the log scale of the ordinate). At the Mach 16 free jet condition, for example, the stagnation pressure for air is almost 8500 atmospheres (125,000 psia), while for the surrogate gas it is about 800 atm (11,800 psia). Simulating the Mach 20 free jet condition requires a total pressure for the surrogate gas of only 2000 atm (29,400 psia), whereas for air it is almost 40,000 atm (588,000 psia).

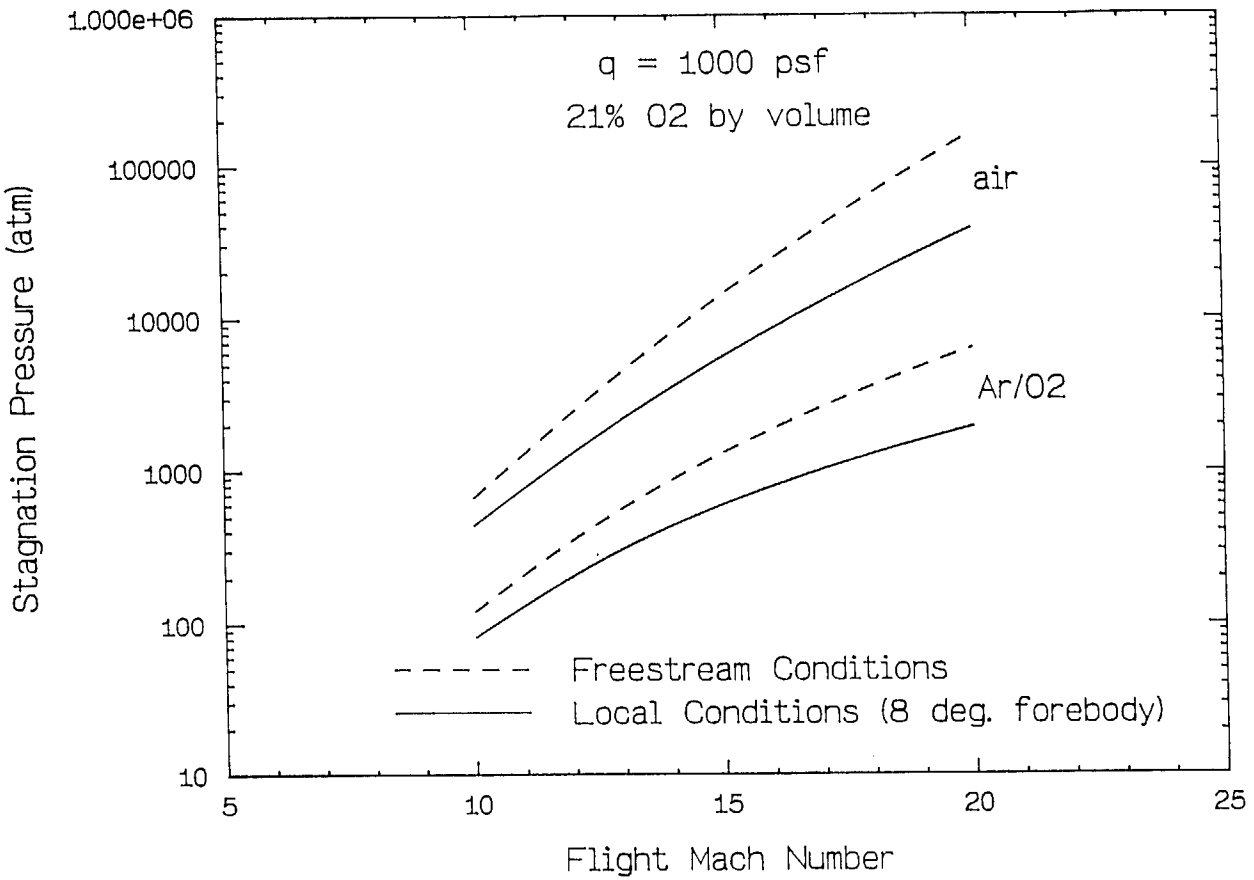

FIGURE 6. TOTAL PRESSURE SIMULATION REQUIREMENTS FOR AIR AND AR/O_2 SURROGATE GAS (21 MOLE PERCENT O_2)

Obviously, differences in total pressure of this magnitude would have a significant impact on the composition of the test gas chosen for these conditions, as 3200 atm is within reach of current materials and throat cooling technologies, while 40,000 atm is not. However, while the lower pressure required by the surrogate gas is more favorable from the containment and cooling points of view, it tends, along with the high temperatures generated, to negate the advantages of a partially inert test gas by reducing the nozzle kinetic performance. That is, for a given simulated total enthalpy, the lower total pressure induces additional dissociation in the mixing chamber, and the lower mixture density in the nozzle reduces the level of recombined molecular oxygen. Nevertheless, an attempt was made to optimize the composition for each flight condition for which a "reasonable" mixing chamber pressure (to be defined subsequently) was generated and for which nozzle kinetic performance was maximized.

2.2.a. Effect of Surrogate Gas Composition on Reservoir Pressure

In order to optimize the surrogate test gas composition, it was necessary to first determine the effect of the composition on the stagnation or mixing chamber pressure. (Subsequently, chemical kinetic calculations would determine whether the surrogate mixture composition chosen is favorable from the point of view of oxygen recombination.) The composition of the surrogate mixture was changed by varying the molar concentration of argon from 0 to 89 percent with the balance being a mixture of nitrogen and 21 mole percent oxygen. Stagnation conditions were then calculated for each mixture at each of the four flight conditions considered (Mach 10, 12, 16, and 20). The results of the calculations for the free jet conditions are presented in Figures 7 and 8. Figure 7 shows the effect of varying the surrogate mixture composition on the calculated stagnation pressure for equilibrium chemistry and for a perfect gas, while Figure 8 shows the same for the stagnation temperature. Based upon GT-Devices' experience with electrothermal capillaries, it was determined that a "reasonable" maximum allowable mixing chamber pressure was about 6,000 atm (88,200 psia). Hence, the composition of the test gas for each flight condition was determined based upon this maximum reservoir pressure. Based on this criterion, simulating Mach 10 and 12 conditions requires reservoir pressures which fall below 6000 atm, allowing the composition to remain that of air. The Mach 16 and 20 free jet conditions, however, require approximately 9,000 and 40,000 atm, respectively, for air. Imposing a 6,000 atm maximum pressure yields a test gas composed of 17.5 mass percent argon for the Mach 16 condition and 64 percent argon for the Mach 20 condition.

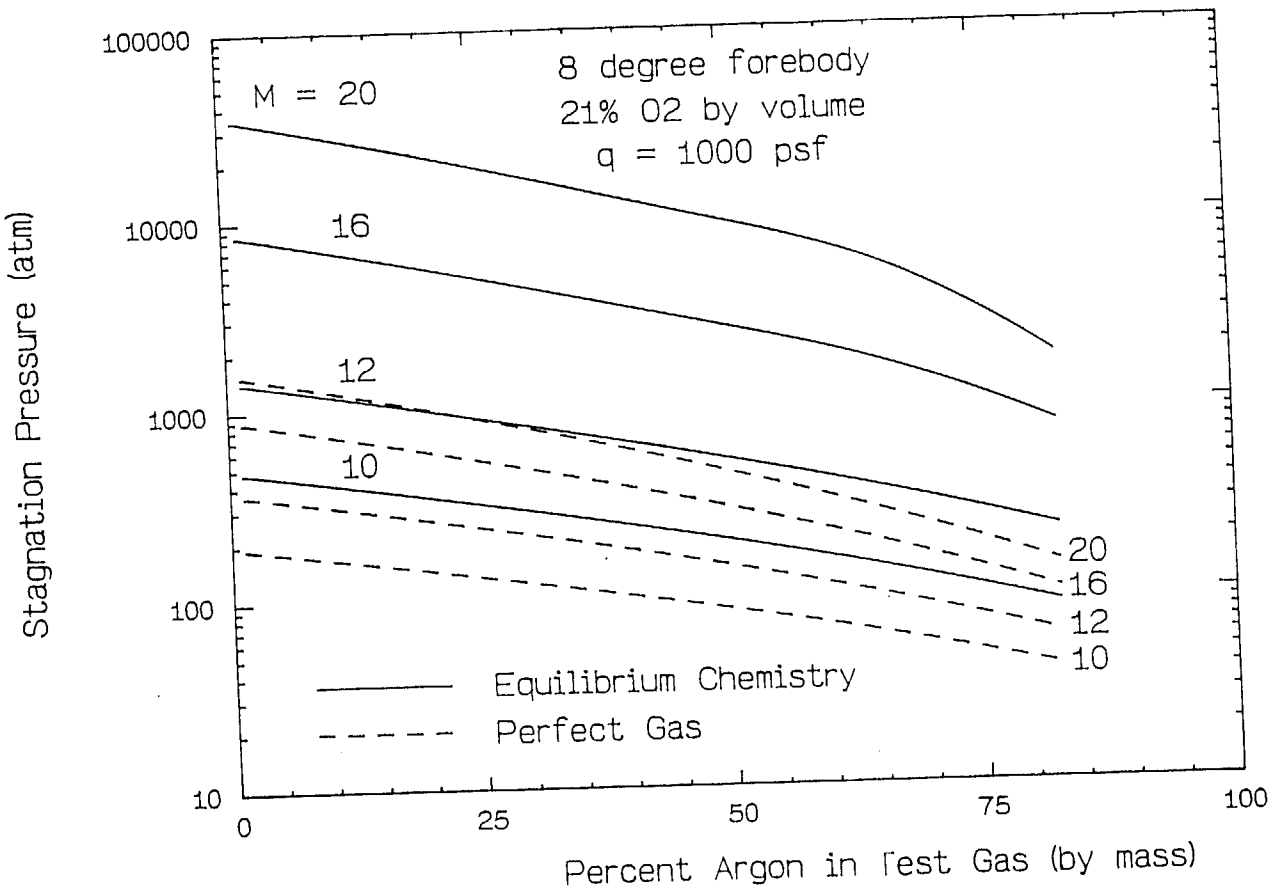

FIGURE 7. THE EFFECT OF SURROGATE TEST GAS COMPOSITION ON REQUIRED FREE-JET STAGNATION PRESSURE

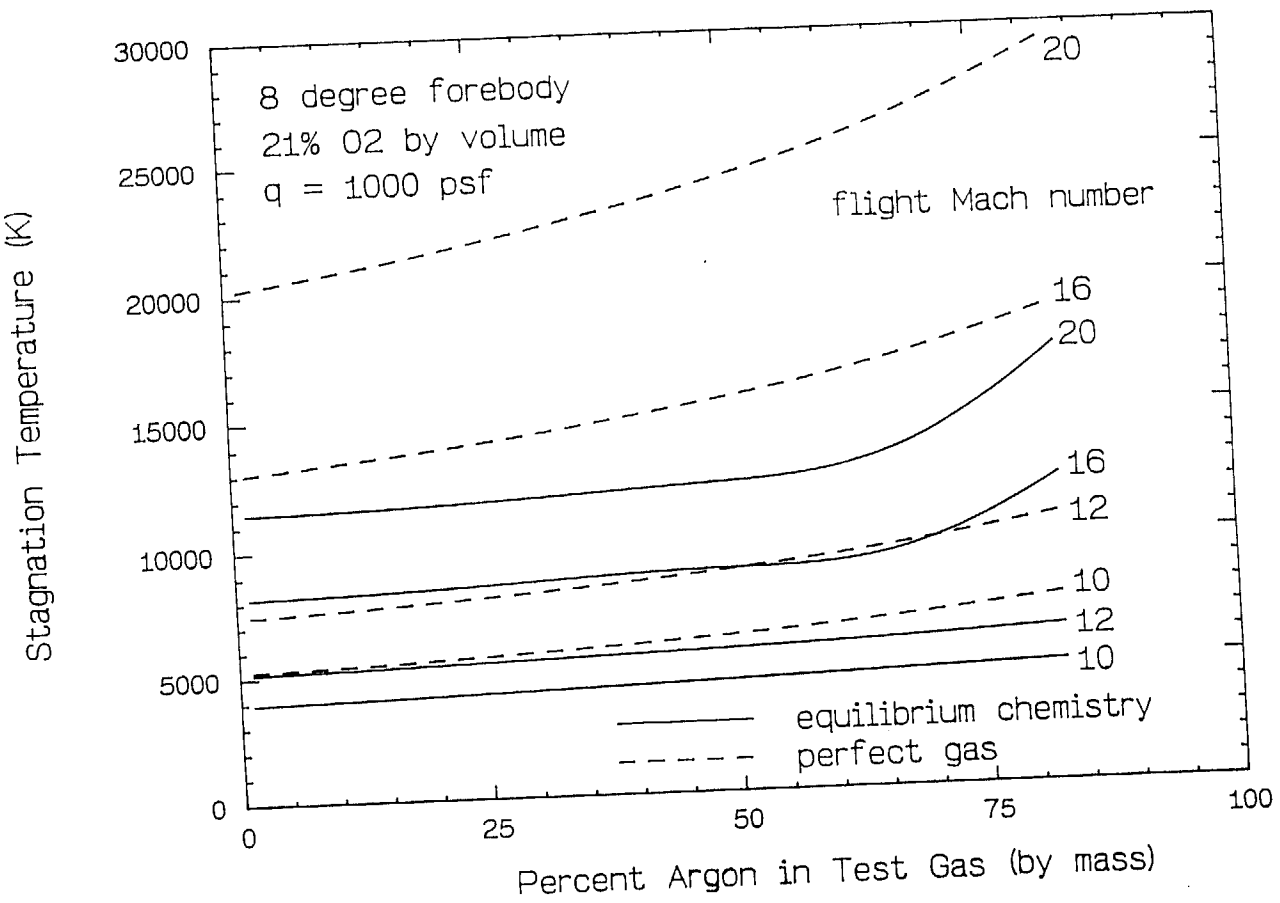

FIGURE 8. THE EFFECT OF SURROGATE TEST GAS COMPOSITION ON REQUIRED FREE-JET STAGNATION TEMPERATURE

Subsequently, it was decided that while 6,000 atm represents the upper limit of GT-Devices' experience base, it is well below current and projected maximum capillary containment pressures which fall between 10,000 and 13,600 atm (150,000 and 200,000 psia). Furthermore, the use of a surrogate gas for hypervelocity combustion testing introduces a variety of complications (e.g., different thermodynamic and transport properties, different ignition delay and reaction times, etc.) which make interpretation of test results more difficult. Consequently, the focus of attention in the calculations shifted from the surrogate gas to pure air. The calculations made for air are described in section 2.3.

2.2.b. Free Jet Mixing Chamber Conditions

The complete set of conditions (free stream, local, and reservoir) for the free jet mode, including species concentrations, are listed in Table 3. The Mach 10 and 12 mixing chamber compositions show increasing levels of nitric oxide formation, but relatively low concentrations of atomic oxygen. Given the tendency of NO to freeze in the nozzle, it seems unlikely that there will be complete recombination to molecular oxygen. The situation is quite different for the surrogate gases at Mach 16 and 20 total enthalpies, however, as significant amounts of atomic oxygen form due to the near complete dissociation of O_2, while the argon substitution prevents additional formation of NO. In addition, small amounts of NO and argon begin to ionize.

2.2.c. Direct Connect Mixing Chamber Conditions

The direct connect mode of operation implies that the facility must duplicate conditions which feed directly into a scramjet combustor. It was therefore necessary to estimate conditions across the inlet. In this connection, a generic two dimensional inlet configuration was chosen from Reference 18. The combustor entrance conditions are representative of those downstream of a low contraction ratio, adiabatic inlet. Mixing chamber conditions were calculated from the combustor entrance static conditions in a manner identical to the free jet calculations. However, the total pressure loss across the inlet was large enough to avoid using a surrogate gas for all the flight conditions considered. Thus, the direct connect mixing chamber conditions are described in the next section on the air calculations.

2.3. Air Test Gas

The previous section described the calculations made to limit mixing chamber pressures in the EWT to those which were commensurate with GT-Devices' experience with electrothermal capillaries. However, maximum containment pressures of 10,000 to 13,000 atm would enable the use of air at the higher flight Mach numbers if containment, nozzle kinetics, and throat cooling problems can be overcome. Direct connect simulation conditions were calculated exclusively for air, and hence they are also described here.

Table 3. Conditions for Free Jet Mode of Operation
(Surrogate gas mixtures for Mach 16 and 20) q_∞=1000 psf

	Mach 10 (air)			Mach 12 (air)		
	Free stream	Free jet $P_t/P_{t\infty} = 0.658$	Mixing Chamber	Free stream	Free jet $P_t/P_{t\infty} = 0.541$	Mixing Chamber
Pressure	696 N/m^2	3610 N/m^2	6480 psia (441 atm)	480 N/m^2	3200 N/m^2	19,700 psia (1340 atm)
Temperature (K)	233	420	3750	240	492	5010
Density (kg/m^3)	0.0104	0.0299	41.2	0.697^{-2}	0.0227	91.3
Compressibility (z)	1	1	1.05	1	1	1.11
Velocity (m/s)	3060	3000	0.0	3730	3660	0.0
Mach number	10	7.31	0.0	12	8.26	0.0
Species mass fractions						
N_2	0.75555	0.75555	0.71430	0.75555	0.75555	0.68733
O_2	0.23155	0.23155	0.17525	0.23155	0.23155	0.11859
Ar	0.01290	0.01290	0.01290	0.01290	0.01290	0.01290
NO	0.0	0.0	0.088325	0.0	0.0	0.14532
N	0.0	0.0	0.13049^{-4}	0.0	0.0	0.38292^{-3}
O	0.0	0.0	0.92008^{-2}	0.0	0.0	0.035469
e^-	0.0	0.0	0.0	0.0	0.0	0.25154^{-5}*
N_2^+	0.0	0.0	0.0	0.0	0.0	0.0
O_2^+	0.0	0.0	0.0	0.0	0.0	0.0
NO^+	0.0	0.0	0.0	0.0	0.0	0.74086^{-5}
N^+	0.0	0.0	0.0	0.0	0.0	0.0
O^+	0.0	0.0	0.0	0.0	0.0	0.0
Ar^+	0.0	0.0	0.0	0.0	0.0	0.0
O^-	0.0	0.0	0.0	0.0	0.0	0.25471^{-5}

* Mole Fraction

Table 3. (Continued)

	Mach 16 (17.5% Argon by mass)			Mach 20 (64% Argon by mass)		
	Free stream	Free jet $P_t/P_{t\infty} = 0.369$	Mixing Chamber	Free stream	Free jet $P_t/P_{t\infty} = 0.306$	Mixing Chamber
	$\gamma_\infty = 1.39$			$\gamma_\infty = 1.46$		
Pressure	263 N/m^2	2780 N/m^2	87,400 psia (5950 atm)	158 N/m^2	2640 N/m^2	84,900 psia (5780 atm)
Temperature (K)	250	686	8410	250	1060	13200
Density (kg/m^3)	0.385^{-2}	0.0148	233	0.270^{-2}	0.0107	144
Compressibility (z)	1	1	1.26	1	1	1.15
Velocity (m/s)	4990	4900	0.0	5950	5860	0.0
Mach number	16	9.62	0.0	20	9.76	0.0
Species mass fractions						
N_2	0.60476	0.60476	0.51595	0.1720	0.17199	0.056003
O_2	0.22024	0.22024	0.032145	0.1880	0.18797	0.52299^{-2}
Ar	0.1750	0.1750	0.17500	0.6400	0.6400	0.63755
NO	0.0	0.0	0.14712	0.0	0.28895^{-4}	0.027849
N	0.0	0.0	0.019903	0.0	0.0	0.10175
O	0.0	0.0	0.10924	0.0	0.0	0.16595
e^-	0.0	0.16242^{-3}*	0.0	0.0	0.0	0.31501^{-2}*
N_2^+	0.0	0.0	0.43882^{-5}	0.0	0.0	0.23158^{-3}
O_2^+	0.0	0.0	0.88806^{-5}	0.0	0.0	0.82055^{-4}
NO^+	0.0	0.0	0.45587^{-3}	0.0	0.0	0.13849^{-2}
N^+	0.0	0.0	0.35262^{-6}	0.0	0.0	0.36993^{-3}
O^+	0.0	0.0	0.14869^{-5}	0.0	0.0	0.34786^{-3}
Ar^+	0.0	0.0	0.15330^{-5}	0.0	0.0	0.24403^{-2}
O^-	0.0	0.0	0.15640^{-3}	0.0	0.0	0.79399^{-3}

* Mole fraction

2.3.a. Free Jet Mixing Chamber Conditions

The mixing chamber conditions required to simulate Mach 16 and 20 free jet conditions with air as the test gas were computed in a manner similar to the surrogate gas calculations described above. These conditions are shown in Table 4. The values of most interest are the mixing chamber pressures and species concentrations. The pressures for the Mach 16 and 20 conditions are seen to be 8640 atm (127,000 psia) and 38,000 atm (559,000 psia), so that based upon the sole constraint of a 200,000 psia maximum containment pressure, free jet simulation is limited to Mach 17.5 (at a flight dynamic pressure of 1000 psf).

2.3.b. Direct Connect Mixing Chamber Conditions

The direct connect conditions for the four flight conditions were calculated as discussed in section 2.2.c., and are shown in Table 5. The total pressures generated here are relatively low compared with the free jet simulation conditions due to the total pressure loss across the inlet. Given that the total enthalpy remains constant, it is expected that additional dissociation would take place compared with the free jet condition. On the other hand, pressures (and hence densities) of this magnitude, particularly at free jet reservoir conditions, introduce compressibility effects which must be quantified to determine the extent to which the gas deviates from ideal behavior. This subject is examined in section 2.4.

2.3.c. Graphical Description of Mixing Chamber Conditions

The mixing chamber calculations made for air were plotted and curve-fit to allow for interpolation of other conditions. Figures 9 through 13 show the total temperature, total pressure, and species mole fractions as a function of flight Mach number for the defined range of free jet and direct connect conditions ($q_\infty = 1000$ psf). The ideal gas total pressure and total temperature are plotted in Figure 9, while the major and minor ($x_i < 0.001$) mole fractions for the free jet and direct connect conditions are shown in Figures 10 through 13, respectively.

Table 4. Conditions for the Free Jet Mode of Operation with air, q=1000 psf
(See Table 3 for Mach 10 and 12 conditions with air)

	Mach 16			Mach 20		
	Free stream	Free jet $P_t/P_{t\infty} = 0.360$	Mixing Chamber	Free stream	Free jet $P_t/P_{t\infty} = 0.238$	Mixing Chamber
Pressure	267 N/m^2	2760 N/m^2	127,000 psia (8640 atm)	171 N/m^2	2560 N/m^2	559,000 psia (38,000 atm)
Temperature (K)	252	665	8240	261	872	11800
Density (kg/m^3)	0.369^{-2}	0.0145	335	0.228^{-2}	0.0102	960
Compressibility	1	1	1.46	1	1	2.8 (?)
Velocity (m/s)	5090	5010	0.0	6480	6380	0.0
Mach number	16	9.80	0.0	20	11.0	0.0
Species mass fractions						
N_2	0.75555	0.75555	0.65487	0.75555	0.75555	0.59326
O_2	0.23155	0.23155	0.039947	0.23155	0.23155	0.023123
Ar	0.01290	0.01290	0.01290	0.01290	0.01290	0.012894
NO	0.0	0.0	0.180520	0.0	0.0	0.17977
N	0.0	0.0	0.016220	0.0	0.0	0.077073
O	0.0	0.0	0.94973	0.0	0.0	0.11038
e^-	0.0	0.0	0.11382^{-3}*	0.0	0.0	0.61315^{-3}*
N_2^+	0.0	0.0	0.32860^{-5}	0.0	0.0	0.29249^{-3}
O_2^+	0.0	0.0	0.73697^{-5}	0.0	0.0	0.65860^{-4}
NO^+	0.0	0.0	0.40235^{-3}	0.0	0.0	0.20761^{-2}
N^+	0.0	0.0	0.0	0.0	0.0	0.40218^{-4}
O^+	0.0	0.0	0.0	0.0	0.0	0.34296^{-4}
Ar^+	0.0	0.0	0.0	0.0	0.0	0.60044^{-5}
O^-	0.0	0.0	0.15144^{-3}	0.0	0.0	0.98907^{-3}

* Mole fraction

Table 5. Conditions for the Direct Connect Mode of Operation (air), q=1000 psf

	Mach 10			Mach 12		
	Free stream	Direct Connect $P_t/P_{t\infty} = 0.183$	Mixing Chamber	Free stream	Direct Connect $P_t/P_{t\infty} = 0.150$	Mixing Chamber
Pressure	696 N/m^2	63,000 N/m^2	1,800 psia (123 atm)	480 N/m^2	60,800 N/m^2	5,470 psia (372 atm)
Temperature (K)	233	1300	3700	240	1500	4870
Density (kg/m^3)	0.0104	0.169	10.2	0.697^{-2}	0.141	25.5
Compressibility (z)	1	1	1.01	1	1	1.03
Velocity (m/s)	3060	2660	0.0	3727	3350	0.0
Mach number	10	3.79	0.0	12	4.46	0.0
Species mass fractions						
N_2	0.75555	0.75534	0.71627	0.75555	0.75492	0.69392
O_2	0.23155	0.23131	0.17124	0.23155	0.23082	0.10799
Ar	0.01290	0.01290	0.01290	0.01290	0.01290	0.01290
NO	0.0	0.44646^{-3}	0.084109	0.0	0.13613^{-2}	0.13091
N	0.0	0.0	0.20122^{-4}	0.0	0.0	0.51751^{-3}
O	0.0	0.0	0.015460	0.0	0.13022^{-5}	0.053750
e^-	0.0	0.0	0.0	0.0	0.0	0.39555^{-5}*
N_2^+	0.0	0.0	0.0	0.0	0.0	0.0
O_2^+	0.0	0.0	0.0	0.0	0.0	0.0
NO^+	0.0	0.0	0.0	0.0	0.0	0.75545^{-5}
N^+	0.0	0.0	0.0	0.0	0.0	0.0
O^+	0.0	0.0	0.0	0.0	0.0	0.0
Ar^+	0.0	0.0	0.0	0.0	0.0	0.0
O^-	0.0	0.0	0.0	0.0	0.0	0.20220^{-5}

* Mole Fraction

Table 5. (Continued)

	Mach 16			Mach 20		
	Free stream	Direct Connect $P_t/P_{t\infty} = 0.0902$	Mixing Chamber	Free stream	Direct Connect $P_t/P_{t\infty} = 0.0390$	Mixing Chamber
Pressure	267 N/m^2	55700 N/m^2	31,800 psia (2160 atm)	171 N/m^2	53,100 N/m^2	91,600 psia (6230 atm)
Temperature (K)	252	2050	7860	261	2720	10,700
Density (kg/m^3)	0.369^{-2}	0.0947	85.1	0.228^{-2}	0.0672	164
Compressibility (z)	1	1	1.10	1	1	1.22
Velocity (m/s)	5090	4700	0.0	6480	5960	0.0
Mach number	16	5.38	0.0	20	5.90	0.0
Species mass fractions						
N_2	0.75555	0.75115	0.66696	0.75555	0.74036	0.58836
O_2	0.23155	0.22620	0.026307	0.23155	0.20146	0.011952
Ar	0.01290	0.01290	0.01290	0.01290	0.01290	0.012896
NO	0.0	0.94184^{-2}	0.13974	0.0	0.032536	0.12005
N	0.0	0.0	0.023177	0.0	0.11074^{-5}	0.11013
O	0.0	0.32500^{-3}	0.13042	0.0	0.012740	0.15412
e^-	0.0	0.0	0.17560^{-3}*	0.0	0.0	0.90695^{-3}*
N_2^+	0.0	0.0	0.25700^{-5}	0.0	0.0	0.17634^{-3}
O_2^+	0.0	0.0	0.50060^{-5}	0.0	0.0	0.32305^{-4}
NO^+	0.0	0.0	0.38391^{-3}	0.0	0.0	0.17076^{-2}
N^+	0.0	0.0	0.0	0.0	0.0	0.42125^{-4}
O^+	0.0	0.0	0.10094^{-5}	0.0	0.0	0.36915^{-4}
Ar^+	0.0	0.0	0.0	0.0	0.0	0.37426^{-5}
O^-	0.0	0.0	0.99443^{-4}	0.0	0.0	0.48566^{-3}

* Mole fraction

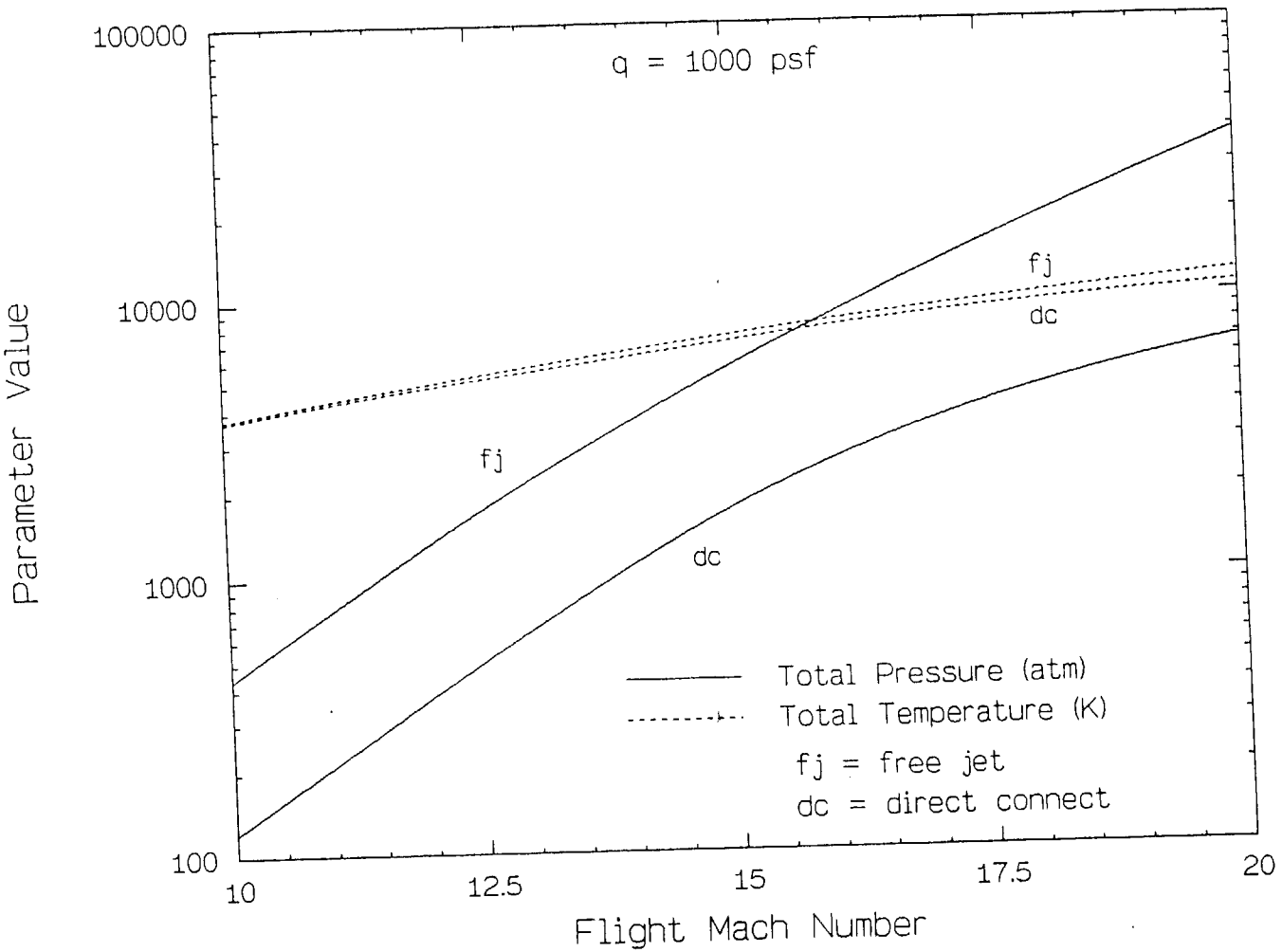

FIGURE 9. REQUIRED FREE-JET AND DIRECT-CONNECT RESERVOIR CONDITIONS VERSUS MACH NUMBER

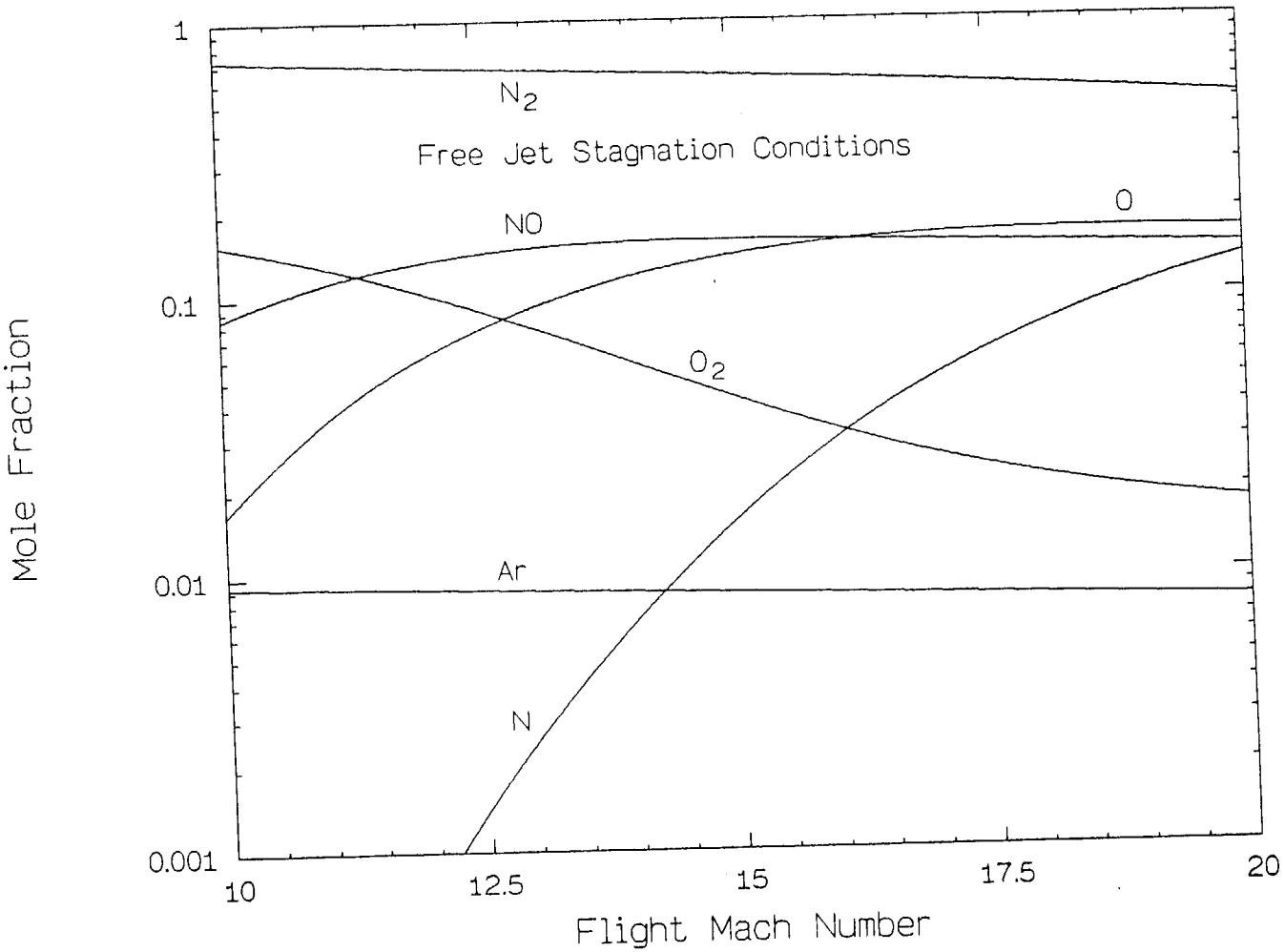

FIGURE 10. THE COMPOSITION OF AIR AT REQUIRED RESERVOIR CONDITIONS FOR FREE-JET SIMULATION (MAJOR SPECIES)

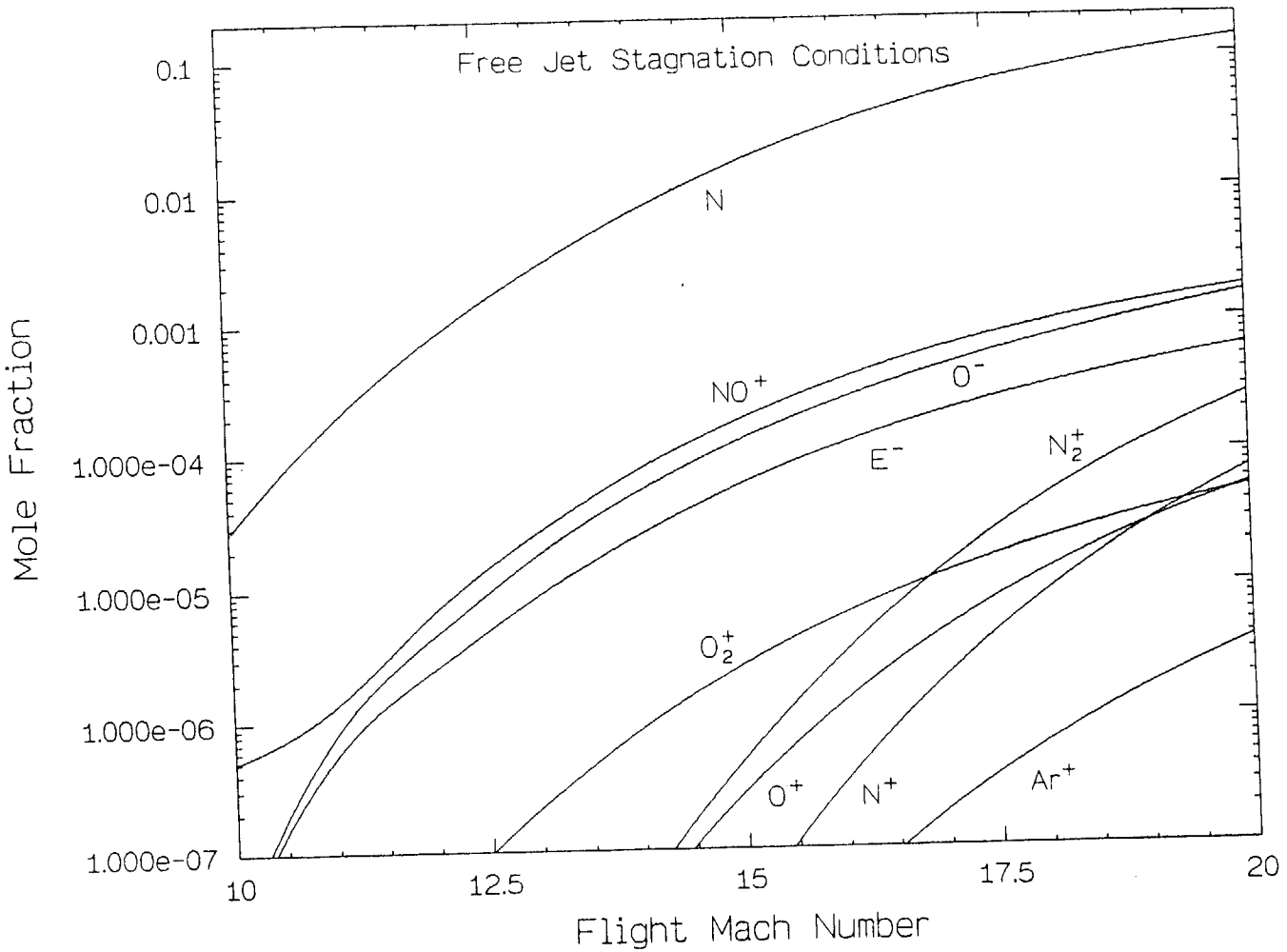

FIGURE 11. THE COMPOSITION OF AIR AT REQUIRED RESERVOIR CONDITIONS FOR FREE-JET SIMULATION (MINOR SPECIES)

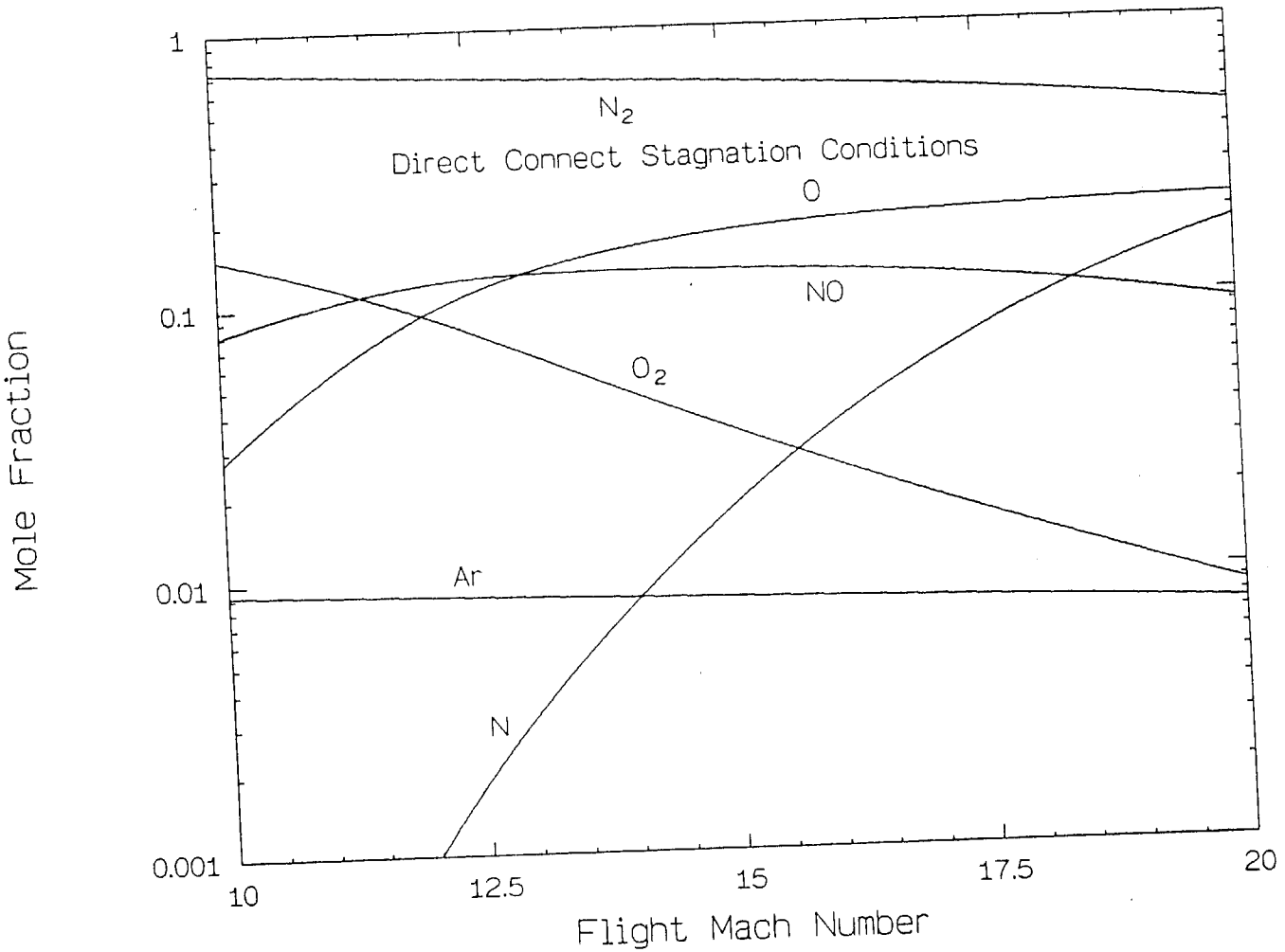

FIGURE 12. THE COMPOSITION OF AIR AT REQUIRED RESERVOIR CONDITIONS FOR DIRECT-CONNECT SIMULATION (MAJOR SPECIES)

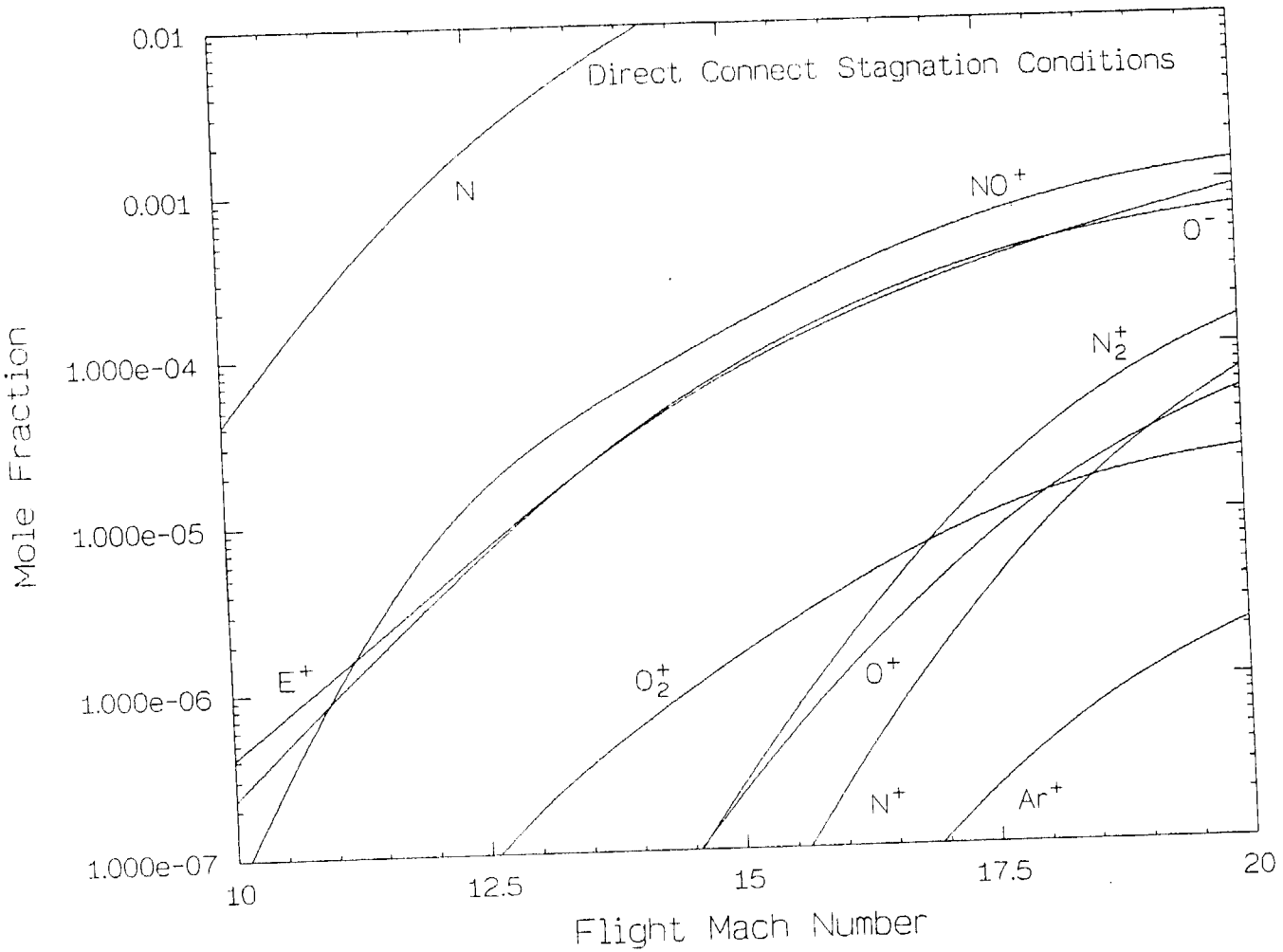

FIGURE 13. THE COMPOSITION OF AIR AT REQUIRED RESERVOIR CONDITIONS FOR DIRECT-CONNECT SIMULATION (MINOR SPECIES)

2.4. Compressibility Effects

The conditions encountered in the mixing chamber are such that the two assumptions which justify use of the ideal gas equation of state to describe each of the constituents of the mixture of species become invalid. The first assumption, Dalton's law of partial pressures, fails to hold since intermolecular repulsion exerts a significant force on the gas at high densities (compared with the density at standard conditions. At moderate densities, molecular attraction dominates.). Second, the assumption that the individual constituents of the gas are point masses also breaks down because at high densities, the molecules occupy a volume which is substantial compared to the total volume of the gas. The net effect in both cases is to raise the pressure above that which the ideal gas equation of state predicts for a given temperature and density.

The ideal gas equation of state can be corrected for real gas effects at high pressures (expressed in terms of the compressibility, Z) by introducing a power series expansion in the mixture molar volume,

$$Z = p\bar{v}/R_o T = 1 + \frac{B(T)}{\bar{v}} + \frac{C(T)}{\bar{v}^2} + \ldots$$

where $\bar{v}$ is the molar volume, R_o is the universal gas constant, and the temperature dependent functions B(T) and C(T) are the second and third "virial coefficients". These coefficients represent the deviation from ideal behavior when collisions involving two and three molecules, respectively, become important in the gas. The range of validity of the virial expansion is limited by the convergence of the series, which begins to diverge at about the density of the liquid state of the gas.[19] The virial coefficients can be obtained experimentally or calculated from a semi-empirical potential function which describes the intermolecular forces as a function of the separation distance between the molecules. Only the second and third virial coefficients B(T) and C(T) have been calculated here, as they represent the most significant contribution to the compressibility factor of a gas.
The potential function chosen for calculating the properties of air at typical conditions in the mixing chamber is the Lennard-Jones (6-12) potential,

$$\varphi(r) = 4\epsilon\left[\left(\frac{\sigma}{r}\right)^{12} - \left(\frac{\sigma}{r}\right)^{6}\right],$$

where ϵ is the maximum energy of attraction between two molecules, r is the separation distance between them, and σ is the collision diameter, or the value of r for which the potential energy φ is zero. This model is one of the most commonly used and gives a realistic representation of the intermolecular forces between simple, non-polar, angle-independent (spherical) molecules. The term $(\sigma/r)^{12}$ represents the repulsive energy between molecules, while $(\sigma/r)^6$ is the attractive energy. The force constants ϵ and σ are determined either from experimental measurements of B(T) or from the principle of corresponding states which predicts that the constants are functions only of the critical properties of the gas.

The analytically integrated second and third virial coefficients for this potential function were obtained from Reference 19 and are tabulated in terms of reduced variables. Figures 14 and 15 from Reference 19 show the reduced virial coefficients B^* ($= B/b_0$) and C^* ($= C/b_0^2$) as a function of the reduced temperature T^* [$=T/(\epsilon/k)$], where k is the Boltzmann gas constant, and b_0 [$=(2/3)\pi N\sigma^3$] is the volume consumed by one mole of molecules each of collision diameter σ. The analytically generated curves are shown with experimental data for several gases.

The agreement is seen to be excellent for the second virial coefficient (except for hydrogen and helium, which must be calculated incorporating quantum effects[19]). Note that for reduced temperatures of greater than 20, B^* begins to decrease from its maximum. This occurs because at very high temperatures, the force of molecular collisions is such that inter-penetration between molecules occurs, resulting in an effective decrease in the collision diameter, and hence a reduction in the compressibility correction. This is seen macroscopically as a slight drop in pressure at the given temperature and density.

On the other hand, agreement for the third virial coefficient is not as good. Poor agreement is expected however with carbon dioxide and ethylene as they are not spherical molecules, and with the light gases (hydrogen, deuterium, and helium) because of quantum effects[19]. Disagreement with the other gases is due partly to an uncertainty in the determination of C(T) from measured compressibility effects and partly to the approximate empirical nature of the potential function.[19]

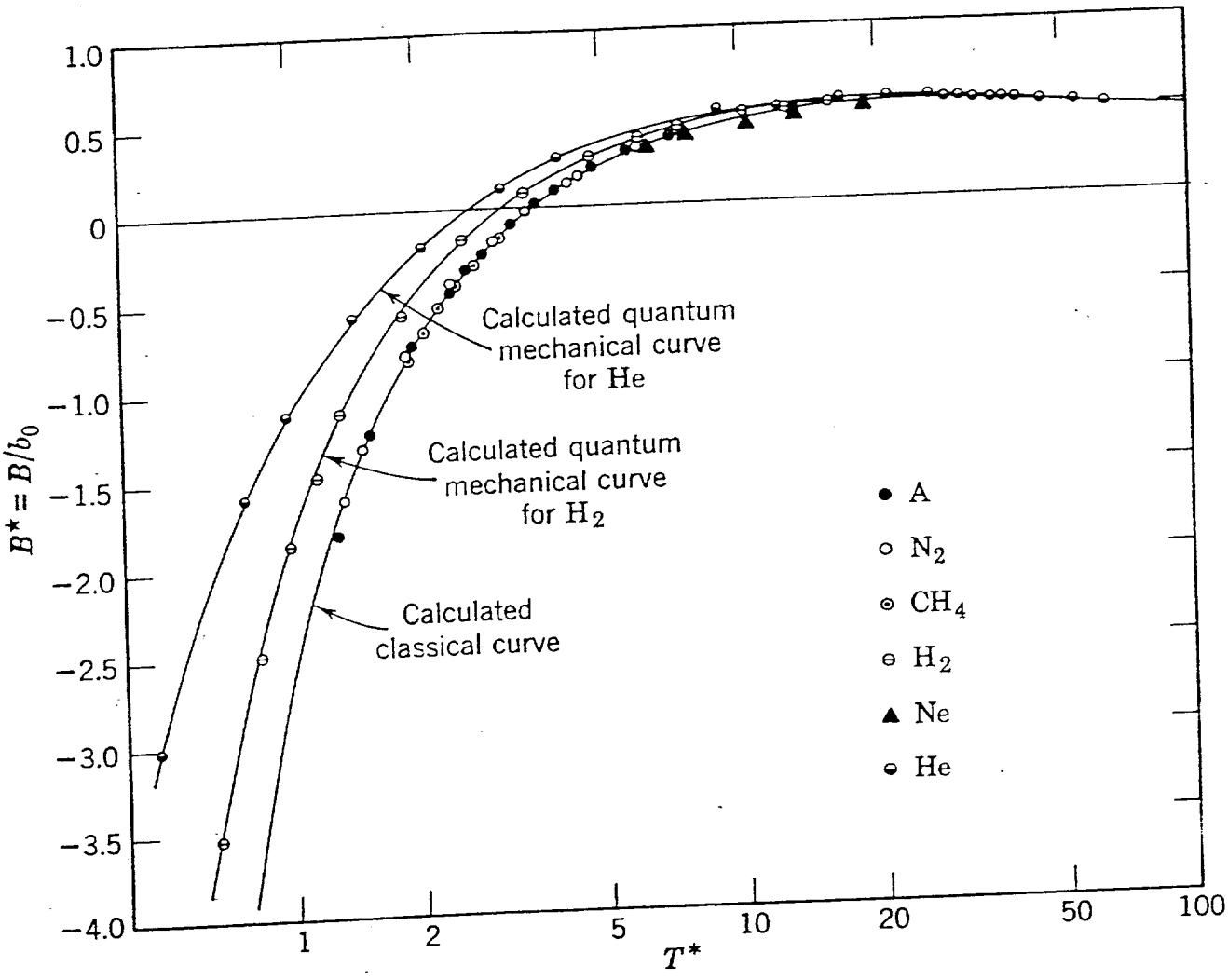

FIGURE 14. THE REDUCED SECOND VIRIAL COEFFICIENT FOR THE LENNARD-JONES POTENTIAL

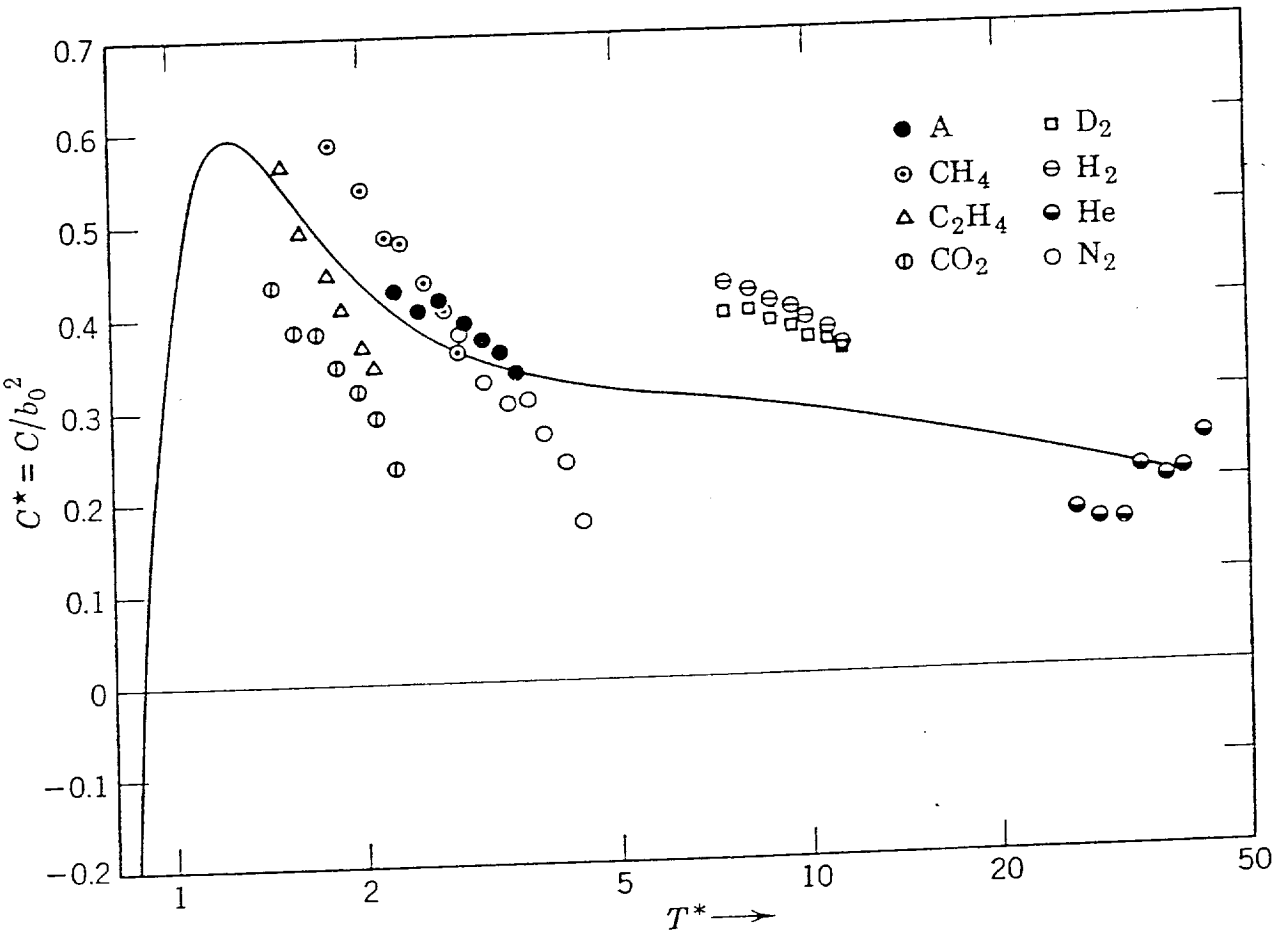

FIGURE 15. THE REDUCED THIRD VIRIAL COEFFICIENT FOR THE LENNARD-JONES POTENTIAL

Although the discussion has thus far been restricted to single component gases, the second and third virial coefficients for mixtures can be approximated provided that the force constants for each component of the gas are known. In the absence of experimental data, the force constants can be calculated for the Lennard-Jones potential, as described above, from the critical point properties of the substance. The relations are:

$$\frac{\epsilon}{k} = 0.77T_c$$

$$b_0 = \frac{1.864T_c}{p_c}, \qquad T(K),\ p\left(\frac{N}{m^2}\right)$$

The force constants used for the Lennard-Jones potential are listed in Table 6. Note that ionized species are not included since this potential function is not valid for charged molecules. In spite of this limitation, it was expected that the calculation should produce meaningful results since the products of the molar concentrations of the ionized species are small for the cases of interest. The mixture virial coefficients are given by

$$B(T)_{mix} = \sum_{i=1}^{ns} \sum_{j=1}^{ns} x_i x_j B_{ij}(T),$$

$$C(T)_{mix} = \sum_{i=1}^{ns} \sum_{j=1}^{ns} \sum_{k=1}^{ns} x_i x_j x_k C_{ijk}(T),$$

where x_i, x_j, and x_k are the mole fractions of species i, j, and k, respectively, and B_{ij} and C_{ijk} are the combined virial coefficients for binary and tertiary interactions, respectively.

The empirical combining laws chosen for relating the binary interaction force constants between unlike molecules are based on the approximate method of Leland and Mueler[21].

Table 6. Force Constants for the Lennard-Jones (6-12) Potential (Reference 8. Reference 9 for N and O.)

Gas	ϵ/K (°K)	σ (Å)	b_0 (CC/mole)
N_2	95.9	3.71	64.4
O_2	118.	3.46	52.2
Ar	122.	3.40	49.6
NO	131.	3.17	40.0
N	91.5	3.10	37.6
O	100.	2.90	30.8

The mixture collision diameter and interaction energy can be obtained from

$$\sigma_m^3 = \sum_{i=1}^{ns} \sum_{i=1}^{ns} x_i x_j \sigma_{ij}^3,$$

and

$$\epsilon_m = \frac{\sum_{i=1}^{ns} \sum_{j=1}^{ns} x_i x_j \sigma_{ij}^3 \epsilon_{ij}}{\sigma_m^3}$$

respectively. The average combined collision diameter, σ_{ij}, is defined for rigid spheres as

$$\sigma_{ij} \equiv 0.5(\sigma_i + \sigma_j)$$

and the combined interaction energy can be obtained from the semi-empirical equation[21]

$$\epsilon_{ij} = \frac{(\sigma_i^3 \epsilon_j \sigma_j^3 \epsilon_j)^{1/2}}{\sigma_{ij}^3}$$

While the above relations are valid for calculating binary interactions between dissimilar molecules, the third virial coefficient requires that tertiary interaction force constants be calculated. Calculations of $C_{ijk}(T)$ are not available for the Lennard-Jones potential function. However, an approximation can be obtained by correcting the square well third virial coefficient which has been calculated analytically for mixtures.[19] Thus,

$$[C_{ijk}(T)]_{L.J.} = [C_{ijk}(T)]_{S.W.} [A(T_i^*)A(T_j^*)A(T_k^*)],$$

where the function A is tabulated in Reference 19. Note that although this relation should provide a reasonably good approximation to the mixture third virial coefficient for spherical molecules, it is unsubstantiated experimentally. Nevertheless, it is deemed adequate for the purposes of this study. The mixture third virial coefficient for the square well potential is a lengthy function and is therefore detailed in the Appendix.

The mixture compressibility factor was calculated for each reservoir condition listed in Tables 3-5. As an approximate check on the calculations, the compressibility factors were compared with those from the air tables of Hilsenrath[14] for the Mach 16 free jet condition for air, and the Mach 20 direct connect condition. Note that the compressibilities were

compared at the temperature and density of the mixing chamber conditions, and that Hilsenrath includes only the second virial coefficient in his calculations. At the Mach 16 free jet condition, the compressibility factor for this calculation is 1.46, and the corresponding value due only to the second virial coefficient is 1.37. The extrapolated value from Hilsenrath is 1.35, and is seen to be within 1.5 percent of the present calculation. However, the contribution due to the third virial coefficient (0.09) is significant, and is in fact comparable with the total number of moles generated at this condition per mole of undissociated air (MW/MW_∞ = 1.10).

At the Mach 20 direct connect condition, the calculated total compressibility factor is 1.23, the second interaction term contribution is 0.204, and so the third term contribution is 0.026. The compressibility factor according to Hilsenrath is 1.20, and hence agrees almost exactly. Moreover, since there is relatively significant ionization at this condition, it seems that the effect of ions on the compressibility of the gas is negligible at these levels of ionization.

Examining the remaining conditions, the compressibility of the test gas at free jet reservoir conditions becomes significant at Mach 12 (Table 3), where the mixing chamber pressure would increase by about 10 percent to 1470 atm (21,600 psia) at the given density and temperature. Naturally, the higher pressure will change the composition of the mixture and hence change the temperature. However, this is probably a second order effect.
The compressibility factor at the stagnated Mach 20 free jet condition in air is seen to be exceedingly high (2.8), but this value is questionable because the gas density (960 kg/m^3) approaches that of liquid air. As was previously mentioned, the series expansion for the compressibility begins to diverge at densities near those of liquids. Nevertheless, it is clear that real gas effects are significant at these conditions and must be accounted for in any detailed analysis of the flow through the EWT.

2.4.a. Impact of Compressibility on Nozzle Chemical Kinetics

The previous discussion indicated that for a given simulated total enthalpy, the total pressure generated is significantly greater (for most of the hypervelocity flight envelope) than the ideal gas assumption would predict. The implications of this effect on facility nozzle performance are, to first order, minimal if the predicted real gas pressure can be contained. In effect, at the real gas pressure, the temperature-density history (and hence the chemistry) through the nozzle would be similar to that for an ideal gas, and the pressure history would vary according to the combined effects of the expansion and the change in the compressibility with density. At the nozzle exit, the density is low enough such that the compressibility factor is unity, resulting in flow conditions that are very near to those of an ideal gas. If, however, the real gas total pressure can not be contained, then the effect would be to reduce the initial density proportionally, resulting in a decrease in the level of recombination. Since most of the recombination occurs early in the nozzle, the net result would be a reduction in recombination which is approximately proportional to the ratio of initial containable pressure to the required real gas pressure. The chemical kinetic nozzle

performance calculations which were made did not incorporate any compressibility effects, so that the results may be assumed similar to those in which compressibility effects were included and the total pressure was increased according to the real gas calculations described above.

2.5. Conclusions Regarding Gas Conditions in the Mixing Chamber

The calculations made in sections 2.2 through 2.4 all indicate that the gas in the mixing chamber must be characterized as a dissociating, calorically and thermally imperfect gas, which has an enormous impact on the simulation capability of the electrothermal wind tunnel, or more correctly, any facility which stagnates the test gas at total enthalpies and pressures typical of the hypervelocity regime. Specifically, the total pressure requirement is the most obvious limitation from the point of view of containing the test gas. On the other hand, the high pressures are favorable from a nozzle chemical kinetics point of view. Since the convective heat transfer near the facility nozzle throat is approximately proportional to the product of the local pressure and velocity, both the high pressures and total enthalpies will make the nozzle wall heat transfer another significant limiting factor. (Calculations were made to assess this latter effect, and are described subsequently.) However, there are other factors which, although more subtle, may be just as limiting. For instance, the extremely high temperatures generated in the mixing chamber may radiate significant amounts of energy to the walls of the chamber. Unknowns which may be of significant consequence are the transport properties of a partially ionized semi-conducting gas at conditions typical at the nozzle throat. Quite obviously, all of the above-mentioned phenomena will require more extensive and rigorous analysis in concert with some experimental verification to properly address and account for these effects.

3.0. Chemical Kinetic Nozzle Performance

One of the major technical issues which must be addressed in the design of this facility is the performance of the facility nozzle. Expansion of the gas through a nozzle to achieve the desired test conditions requires proper consideration of the coupled chemical and gas dynamic processes, the ultimate goal being to assure a test flow which is as consistent as possible with that encountered in flight. The previous section has shown that the stagnation conditions required for Mach 16-20 simulation result in a highly dissociated test gas, even at the total pressures required for free jet simulations. Moreover, relatively significant amounts of NO form for all the conditions examined. As previously mentioned, nitric oxide tends to tie up oxygen atoms and retard the formation of molecular oxygen, making chemical kinetics calculations necessary to predict the state of the gas at the nozzle exit plane.

In flight, very low concentrations of nitric oxide and atomic oxygen are expected in the air stream entering a scramjet combustor even at near-orbital speeds. This is due to the low temperatures prevailing through most of the inlet, and the very short residence time in the last segment of the inlet where the temperatures are high. However, both nitric oxide and atomic oxygen are capable of dramatically altering autoignition characteristics at low temperatures and/or pressures where ignition delay times are significant. It can be argued that practical engine designs should not have ignition delay times so long that facility-induced nitric oxide or atomic oxygen can produce measurable effects. However, the overall heats of combustion of hydrogen, for example, with nitric oxide or with atomic oxygen are considerably higher (36% and 100%, respectively) than with molecular oxygen. Therefore, the presence of nitric oxide and atomic oxygen in the test gas produced by a facility can alter the apparent heat of combustion of the fuel and the inferred combustion efficiency by amounts proportional to the relative concentrations of these dissociation products. Accordingly, reduction of these species to tolerable levels in the test section of the EWT is considered essential.

The focus of the one-dimensional inviscid calculations made here was to maximize the recombination of nitric oxide and atomic oxygen to molecular oxygen in the facility nozzle by various means. In section 3.3, within the framework of the one-dimensional flow restriction, an optimum nozzle area distribution was determined based on oxygen recombination. The effect of ionization reactions on the expansion process is then described. A detailed analysis of the chemical kinetic processes through the nozzle follows in which effect of varying the nozzle expansion angle are considered for each flight condition (design point). The entropy production through the nozzle is then examined in section 3.4. Section 3.5 evaluates oxygen replenishment as a method for replacing the oxygen lost to nitric oxide and to monatomic oxygen. Finally, section 3.6 describes calculations which determine the three body efficiencies necessary to significantly improve the test gas composition. Based on these results, small amounts of water (whose third body efficiency is 16.25 according to the NASP mechanism[22]) were introduced into the flow to enhance

three body recombination. The results of these calculations are also described in section 3.6.

Note that all of the calculations in this section assume that the vibrational mode of the particles is in equilibrium with the translational mode. Although no calculations were made to verify this assumption, it was felt that the high pressures which prevail through the nozzles for these conditions, combined with the relatively low expansion angles examined here will almost certainly produce a flow which is vibrationally equilibrated.

These calculations were intended to provide insight into the chemical kinetics issues relevant to nozzle performance and indicate potential solutions to improve the performance. However, a significant amount of additional work needs to be done to better define the performance of the real (i.e., two or three dimensional, real gas, viscous flow) nozzle under the conditions unique to this facility.

3.1. Description of the Computer Code and Chemical Kinetic Mechanism

The one-dimensional finite rate calculations were made with the NASA-Lewis "LSENS" general chemical kinetics code, which is a revision of the GCKP84 code written by D. Bittker and N. Scullin[23]. The code was modified by the authors to accept high temperature (>5000 K) polynomial curve fits for the thermodynamic properties of the constituents of air, including ionized species. Both the low and high temperature curve fits are identical to those used in the EqState code (see Table 2), except for the addition of the low temperature (<5000 K) properties of NO_2, which was needed for several of the reactions. The high temperature properties of NO_2 were not available at the time the calculations were made, nor were the high temperature properties available of any hydrogen-based compounds. Hence, the only neutral reactions used above 5000 K are those involving atomic and molecular nitrogen and oxygen, and nitric oxide.

The neutral species chemical kinetic mechanism used for the calculations was compiled by the NASP High Speed Propulsion Technology Team[22], while the reactions and rate constants involving ions were obtained from Bortner[24]. The complete set of reactions used is shown in Table 7. Note that although both the reservoir and sonic gas compositions included ionized argon (Ar^+), reactions involving this element could not be found in the literature search. Hence, both the neutral and charged forms of argon were assumed inert in the mechanism.

The assumption implicit in using this mechanism is that all the reactions obey the Arrhenius rate law throughout the range of conditions encountered, which in many cases falls outside the range of temperatures and pressures for which the rate constants were determined. The reaction rate constants for the ion reactions are the average values listed in Reference 24, and in some cases there is a fairly large uncertainty in these constants. The largest uncertainty is for the three body ion recombination reactions, which is two orders of magnitude in all the pre-exponential factors. However, these reactions are sufficiently fast that this uncertainty will probably not affect the results of the calculations to any great extent.

The LSENS code can also accept radiative reactions, which may be important in this facility at the typical operating temperatures of the mixing chamber and facility nozzle throat. Future calculations should assess the significance of these reactions.

Table 7. Reaction Mechanism Used in Chemical Kinetic Nozzle Calculations

NEUTRAL TWO BODY REACTIONS	A* [CGS]	N	E [cal/mole]	Ref.
$O_2 + H \rightarrow O + OH$	1.91^{14}	0.0	16430.2	12
$H_2 + O \rightarrow H + OH$	5.06^{04}	2.67	6287.7	12
$H_2 + OH \rightarrow H_2O + H$	2.16^{08}	1.51	3427.8	12
$OH + OH \rightarrow H_2O + O$	1.50^{09}	1.14	0.0	12
$H + HO_2 \rightarrow OH + OH$	1.50^{14}	0.0	1002.9	12
$H + HO_2 \rightarrow H_2 + O_2$	2.50^{13}	0.0	693.1	12
$O + HO_2 \rightarrow OH + O_2$	2.00^{13}	0.0	0.0	12
$OH + HO_2 \rightarrow H_2O + O_2$	2.00^{13}	0.0	0.0	12
$O + NO \rightarrow N + O_2$	3.80^{09}	1.0	41348.5	12
$O + N_2 \rightarrow NO + N$	1.82^{14}	0.0	76202.8	12
$H + NO \rightarrow N + OH$	1.70^{14}	0.0	48776.2	12
$NO_2 + H \rightarrow NO + OH$	3.50^{14}	0.0	1469.6	12
$NO_2 + O \rightarrow NO + O_2$	1.00^{13}	0.0	595.8	12
$HO_2 + NO \rightarrow NO_2 + OH$	2.09^{12}	0.0	-476.6	12
NEUTRAL THREE BODY RECOMBINATION REACTIONS				
$H + H + M \rightarrow H_2 + M$	7.30^{17}	-1.0	0.0	12
$H + OH + M \rightarrow H_2O + M$	8.62^{21}	-2.0	0.0	12
$O + O + M \rightarrow O_2 + M$	1.14^{17}	-1.0	0.0	12
$O + H + M \rightarrow OH + M$	2.60^{16}	-0.6	0.0	12
$H + O_2 + M \rightarrow HO_2 + M$	8.00^{17}	-0.8	0.0	12
$O + NO + M \rightarrow NO_2 + M$	3.31^{10}	1.0	-8980.7	12
THIRD BODY EFFICIENCIES: H_2 = 2.5, H_2O = 16.25				12
TWO BODY ION REACTIONS				
$N_2^+ + e^- \rightarrow N + N$	5.28^{17}	-0.2	0.0	13
$O_2^+ + e^- \rightarrow O + O$	7.18^{18}	-0.7	0.0	13
$NO^+ + e^- \rightarrow N + O$	2.83^{20}	-1.2	0.0	13
$O^+ + O_2 \rightarrow O + O_2^+$	1.20^{13}	0.0	0.0	13
$N_2^+ + N \rightarrow N_2 + N^+$	6.02^{11}	0.0	0.0	13
$O^+ + O^- \rightarrow O + O$	3.61^{19}	-1.0	0.0	13
$O_2^+ + O^- \rightarrow O_2 + O$	3.61^{19}	-1.0	0.0	13
$NO^+ + O^- \rightarrow NO + O$	3.61^{19}	-1.0	0.0	13
THREE BODY ION RECOMBINATION REACTIONS**				
$O^+ + e^- + M \rightarrow O + M$	5.65^{27}	-2.5	0.0	13
$O_2^+ + e^- + M \rightarrow O_2 + M$	5.65^{27}	-2.5	0.0	13
$N^+ + e^- + M \rightarrow N + M$	5.65^{27}	-2.5	0.0	13
$N_2^+ + e^- + M \rightarrow N_2 + M$	5.65^{27}	-2.5	0.0	13
$NO^+ + e^- + M \rightarrow NO + M$	5.65^{27}	-2.5	0.0	13
$O^+ + O^- + M \rightarrow O_2 + M$	1.13^{29}	-2.5	0.0	13
THIRD BODY EFFICIENCIES: N_2 = 35.9, O_2 = 141., NO = 2120.				13

Table 7. (Continued)

								A* [CGS]	N	E [cal/mole]	Ref.
Collisional Detachment											
O	+	O_2	→	O + e^-	+	O_2		1.39^{15}	0	26,000	13
O	+	N_2	→	O + e^-	+	N_2		1.39^{15}	0	26,000	13
Associative Detachment											
O	+	O	→	O_2 + e^-				8.43^{13}	0	0	13
O	+	N	→	NO + e^-				9.64^{13}	0	0	13

NOTES: * $a^b = a \times 10^b$, $k = AT^n e^{-E/RT}$, ** Exponent of "A" has an uncertainty of ± 1

3.2. Initial Conditions and Nozzle Geometry

The one-dimensional LSENS calculations require that the initial conditions for the facility nozzle correspond to a supersonic state ($M_i > 1.0$). To obtain the initial conditions, the EqState code was modified to calculate the sonic state of the gas for an equilibrium chemistry, adiabatic expansion from the stagnation state. The sonic velocity was then increased slightly to obtain an initial Mach number of about 1.01.

It is recognized that the actual nozzle may be cooled and significant wall heat transfer will occur in this region. We felt that at this stage, however, that without knowledge of the cooling mechanism and the resulting heat transfer rate, and given the other assumptions implicit in this type of calculation, that assuming an adiabatic flow was sufficient. On the other hand, finite rate chemistry calculations were made to see if the equilibrium flow assumption through the subsonic portion of the nozzle was acceptable. Several conditions were examined (Mach 10 and 20 total enthalpies, free jet and direct connect total pressures), and in all cases the residence time of the gas was such that the flow was close to or in equilibrium.

The sonic conditions calculated for the ten design points examined (see Tables 2 to 5) are shown in Tables 8 and 9. The tables list the sonic flow conditions and gas composition, as well as the mass flows and throat areas for the full scale facility. The free jet simulation conditions are shown in Table 8, and the direct connect conditions are in Table 9. The mass flows were assumed to be constant for corresponding free jet and direct connect conditions, and hence the nozzle exit area varies for each direct connect condition. These areas are listed in Table 9. The free jet nozzle exit area is 2 ft^2 (0.1858 m^2).

The nozzle geometry (area distribution) for the calculations was determined by comparing the level of recombination for linear (2-D equivalent) and parabolic (conical) area profiles for the Mach 16 free jet and direct connect conditions. Several calculations were made for nozzle half-angles ranging from two to ten degrees. It was found that for equal half-angles, more recombination took place for the parabolic area distribution than for the linear distribution. The smaller initial expansion rate of the parabolic area profile produces a flow which is initially closer to equilibrium. Hence, that area distribution was chosen for the calculations. Figure 16 shows the geometric relationship of the expansion half-angle to nozzle length for the free jet and direct connect simulated conditions. Since the product of the mass flow and the total enthalpy (power requirement) for a given flight condition is assumed constant, the nozzle area ratio and hence the length will be different between the free jet and direct connect modes.

Table 8. Initial (Sonic) Conditions for Facility Nozzle Chemical Kinetic Calculations - Free-Jet Design Points

	Mach 10 (air)	Mach 12 (air)	Mach 16 (air)	Mach 20 (air)	Mach 16 (17.5% Ar by mass)	Mach 20 (64% Ar by mass)
Pressure, psia (atm)	3530 (240)	10,700 (728)	69,000 (4690)	305,000 (20700)	46,900 (3190)	43,000 (2930)
Temperature (K)	3370	4520	7400	10,700	7510	11,500
Velocity (m/s)	1120	1310	1730	2140	1740	2260
$\dot{m}$ (kg/s), full scale	16.6	15.3	13.5	11.6	13.5	11.6
A* (in^2)	0.917	0.326	0.0589	0.0144	0.0849	0.0931
Species mass fractions						
N_2	0.72396	0.69646	0.66481	0.61388	0.52651	0.075737
O_2	0.19011	0.13752	0.047573	0.023405	0.038886	0.51409^{-2}
Ar	0.01290	0.01290	0.01290	0.012898	0.175	0.63913
NO	0.06729	0.12565	0.17382	0.17201	0.14278	0.029812
NO_2	0.57584^{-3}	0.93671^{-3}	-	-	-	-
N	0.31382^{-5}	0.14653^{-3}	0.95051^{-2}	0.060552	0.011486	0.08156
O	0.51573^{-2}	0.026381	0.091104	0.11497	0.10501	0.16577
e^-	0.0	0.0	0.67360^{-4}*	0.46528^{-3}*	0.93781^{-4}*	0.17428^{-2}*
N_2^+	0.0	0.0	0.0	0.11448^{-3}	0.0	0.10818^{-3}
O_2^+	0.0	0.0	0.32119^{-5}	0.38791^{-4}	0.3848^{-5}	0.47097^{-4}
NO^+	0.0	0.0	0.21508^{-3}	0.14875^{-2}	0.24278^{-3}	0.11773^{-2}
N^+	0.0	0.0	0.0	0.14325^{-4}	0.0	0.12895^{-3}
O^+	0.0	0.0	0.0	0.17000^{-4}	0.0	0.15771^{-3}
Ar^+	0.0	0.0	0.0	0.23270^{-5}	0.0	0.86722^{-3}
O^-	0.0	0.0	0.76382^{-4}	0.61217^{-3}	0.77432^{-4}	0.35582^{-3}

* Mole fraction

Table 9. Initial (Sonic) Conditions for Facility Nozzle Chemical Kinetic Calculations - Direct Connect Design Points

	Mach 10	Mach 12	Mach 16	Mach 20
Pressure, psia (atm)	983 (66.9)	2970 (202)	17,100 (1160)	49,300 (3350)
Temperature (K)	3350	4420	7080	9,780
Velocity (m/s)	1120	1300	1730	2130
$\dot{m}$ (kg/s), full scale	16.6	15.3	13.5	11.6
A* (in^2)	3.30	1.17	0.214	0.0862
Ae (in^2)	0.0369	0.0324	0.0303	0.0290
Species mass fractions				
N_2	0.72497	0.70136	0.67832	0.61448
O_2	0.18744	0.12811	0.032115	0.011798
Ar	0.01290	0.01290	0.01290	0.012899
NO	0.065304	0.11535	0.13602	0.11319
NO_2	0.29667^{-3}	0.44928^{-3}	-	-
N	0.52496^{-5}	0.20894^{-3}	0.013634	0.08756
O	0.90863^{-2}	0.041625	0.12674	0.15841
e^-	0.0	0.0	0.10340^{-3}*	0.68489^{-3}*
N_2^+	0.0	0.0	0.0	0.71190^{-4}
O_2^+	0.0	0.0	0.18168^{-5}	0.19151^{-4}
NO^+	0.0	0.0	0.18038^{-3}	0.12520^{-2}
N^+	0.0	0.0	0.0	0.15437^{-4}
O^+	0.0	0.0	0.0	0.18608^{-4}
Ar^+	0.0	0.0	0.0	0.14821^{-5}
O^-	0.0	0.0	0.79896^{-4}	0.28732^{-3}

* Mole fraction

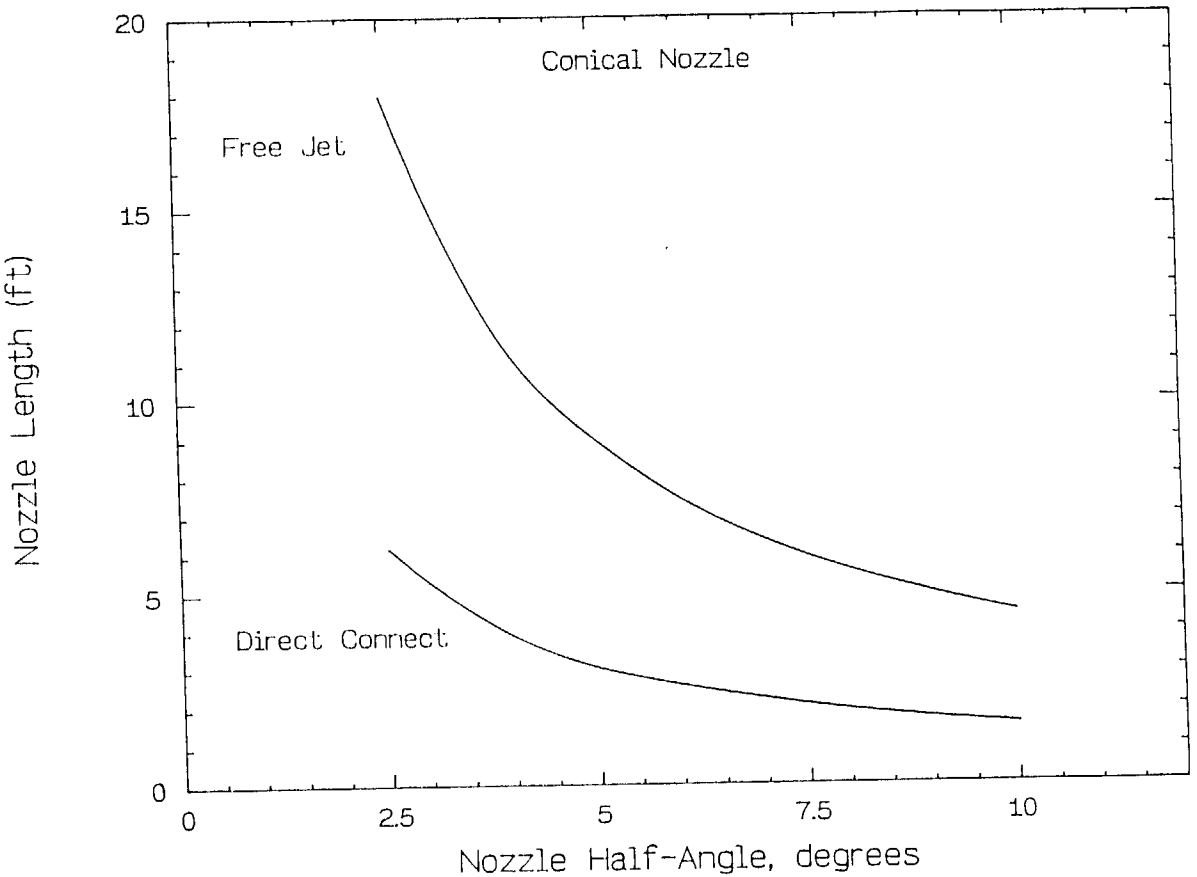

FIGURE 16. FACILITY NOZZLE LENGTHS FOR FREE-JET AND DIRECT-CONNECT SIMULATION VERSUS THE NOZZLE HALF-ANGLE

3.3. Nozzle Performance at the Design Points

The matrix of facility nozzle calculations initially made were for the ten design points listed in Tables 8 and 9, that is: the simulated Mach 10, 12, 16, and 20 free jet and direct connect conditions for air, and the Mach 16 and 20 free jet conditions for the surrogate gas mixtures. The results are shown in terms of the profiles and exit molar concentrations of O_2, O, and NO, the exit flow conditions normalized by the equilibrium, or desired conditions at the test section, and finally the entropy production in the nozzle.

3.3.a. Effect of Ionization

In making the initial set of calculations, it was found that the ionization reactions included in the chemical kinetic mechanism (for the Mach 16 and 20 conditions) increased the computational time significantly over the Mach 10 and 12 cases for which only the NASP neutral mechanism was used. In addition, the accuracy of the solution was compromised somewhat because the relative error tolerance had to be reduced to obtain reasonable run times. The reduced accuracy generally affects the species concentrations more than the fluid dynamic variables, and particularly the trace concentrations. Since all of the ionic species formed under the conditions examined are considered trace species, and in light of the fact that the ionic reaction rate coefficients have large uncertainties associated with them, an assessment of the effect of ion reactions on the flow was deemed necessary.

Several calculations were made to determine if the ion reactions had any effect on the nozzle chemistry. The most significant ionization occurs at reservoir and throat conditions corresponding to Mach 20 simulation. Hence, calculations were made with and without the ion reactions at this condition. In addition, nozzle expansion angles of two and ten degrees were investigated to determine if the rate of chemical freezing affected the final concentration of ions.

There was no noticeable difference in any of the calculations between the results with the full mechanism with ion reactions and those with the NASP neutral species mechanism alone. A negligible percentage of the total enthalpy (about 0.5%) was consumed by ionized species. In addition, their rates of depletion through the nozzles were extremely fast and were independent of expansion angle such that they seemed to be in equilibrium with the flow conditions. Given this result and the uncertainties and errors mentioned above, it was decided to perform the remainder of the calculations without the ion reactions.

3.3.b. Expansion Angle Variation

Calculations were made to determine the extent of oxygen recombination for a range of conical nozzle half-angles from two to ten degrees. All ten design points were examined in

this manner. The results of the calculations are shown in the following set of figures, and illustrate the effect of varying the expansion angle on the exit flow conditions, the exit mole fractions of O_2, O, and NO and their profiles through the nozzle. Note that the very low nozzle half-angles investigated here are not representative of realistic or typical values, but were used to study finite rate chemistry nozzle performance over a relatively wide range of expansion rates. Expansion rates as low as two degrees would most likely introduce excess boundary layer growth and would exacerbate the heat transfer problem near the throat. On the other hand, at flight conditions above about Mach 15, the degree of recombination chemistry is more heavily dependent on the expansion angle, so that consideration must be given to lower initial angles than are typically used for current facility nozzles.

Mach 10 and 12 Solutions:

The solutions for the Mach 10 and 12 conditions indicate that although no atomic oxygen remains after the expansion, nitric oxide freezes at relatively high levels (about 5% by volume), and that the solutions are about the same for free jet and direct connect total pressures. Exit mole fractions of oxygen and nitric oxide are plotted in Figure 17 as a function of expansion angle for the Mach 10 and 12 conditions. The extent of recombination is seen to be fairly independent of expansion angle at these conditions. The mole fraction of oxygen reaching the test section is seen to be between 0.18 and 0.19, which is 85 to 90 percent of the nominal mole fraction in air. The remainder of the oxygen arrives in the form of nitric oxide.

It is instructive to look at the molar concentration profiles through the nozzle for the Mach 12 condition, shown in Figure 18. All of the recombination occurs very early in the expansion. This is typical of most of the nozzle expansions examined in this study (and facility nozzles in general), and indicates that a "horn" geometry may be the optimum. That is, a slow expansion to the freezing point followed by a much more rapid expansion to the required area ratio. (Of course a contoured section will be necessary to cancel the two-dimensional expansion waves so that a uniform, parallel flow exists at the exit. However, the resulting nozzle will still be significantly shorter than a conical nozzle followed by a contoured section.) In addition, the freezing zones are seen to occur at nearly the same area ratio. This implies that due to the high local densities the chemistry is initially in equilibrium with the local thermodynamic conditions and is independent of the expansion rate within the given range of nozzle half-angles. At sufficiently low densities, however, chemical equilibrium cannot be maintained, and the freezing rate then becomes a function of the rate of change of the local conditions. Hence, chemical freezing occurs more quickly in larger expansion rate nozzles.

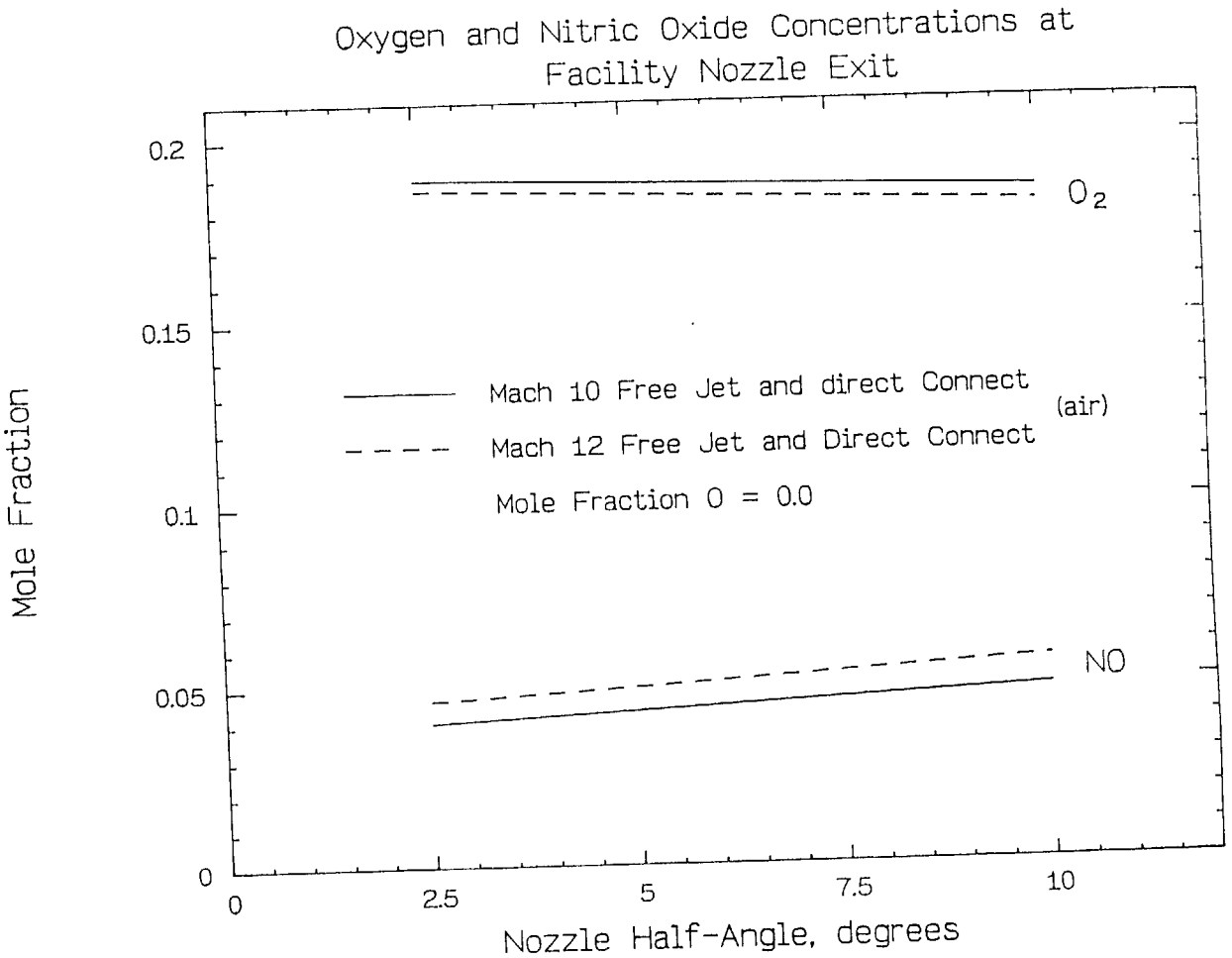

FIGURE 17. CALCULATED OXYGEN AND NITRIC OXIDE CONCENTRATIONS AT FACILITY NOZZLE EXIT VERSUS EXPANSION ANGLE, MACH 10 AND 12 CONDITIONS

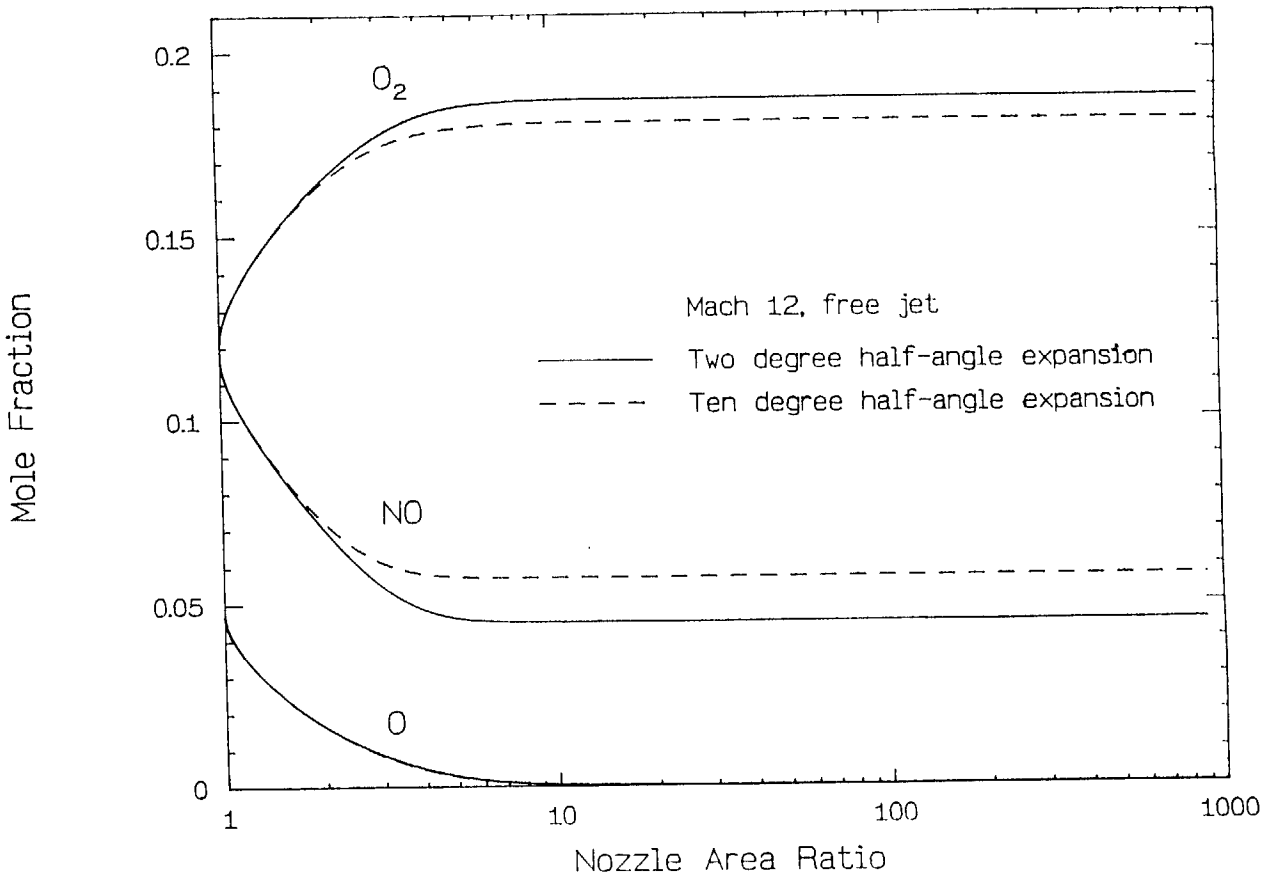

FIGURE 18. FACILITY NOZZLE CONCENTRATION PROFILES FOR MACH 12 FREE-JET SOLUTION

The calculated exit flow conditions for the Mach 10 and 12 conditions are shown in Figure 19, and are seen to be within five to ten percent of their equilibrium values. The temperature is most sensitive to the chemistry and hence is the least well simulated. The velocity ratio will not be very different from one (and hence will appear to be the best simulated) in all of the conditions examined, especially at the higher Mach numbers, because most of the energy is in the form of kinetic energy and is therefore dependent mostly on the nozzle pressure and area ratios. However, as the Mach number increases, small changes in velocity produce progressively larger changes in pressure and temperature and vice-versa.

Mach 16 Solutions (air):

The results for the Mach 16 condition for air are shown in Figures 20 to 23. The dependence of the exit composition on the expansion angle in Figure 20 increases from the Mach 10 and 12 conditions while the difference in composition between free jet and direct connect conditions becomes substantial. The exit mole fraction of oxygen varies from 0.18 to 0.17 (86% to 81% of the undissociated fraction in air, 0.21) for the free jet condition, and from about 0.17 to slightly under 0.15 (81% to about 70% of 0.21) for the direct connect mode. Atomic oxygen freezes out at higher levels (1% to 3% mole percent at free jet conditions and 4% to 7% for the direct connect mode). Interestingly however, the concentration of nitric oxide freezes at about the same level (4% to 5% by volume) as for the Mach 10 and 12 conditions, although the initial concentration is much higher. This is in fact seen to be the case at all the conditions examined here. Admittedly, the influence of the NO_2 reactions on the composition at these conditions is not known, and should be investigated in a future study.

The molar concentration profiles of O_2, O, and NO for the free jet condition (Figure 21) indicates that the flow is in chemical equilibrium up to the freezing zone here as well. On the other hand, the profiles in Figure 22 for the two direct connect nozzles show that the gas is driven out of chemical equilibrium earlier in the expansion.

The flow conditions at the nozzle exit reflect the composition at the exit and in Figure 23 are seen to be more heavily dependent on the expansion angle. Relatively large differences are observed between the free jet and direct connect cases, except for the velocity ratio, which is again constant at a value of unity.

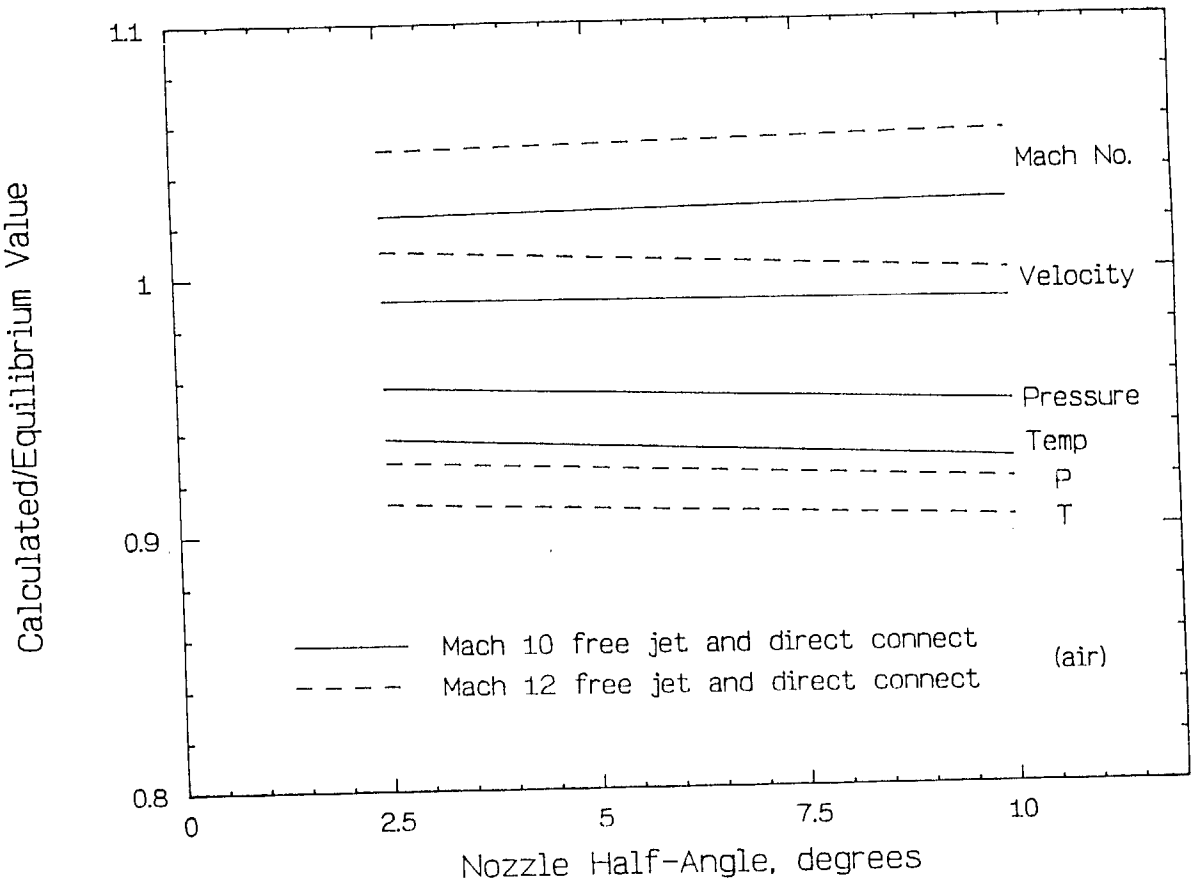

FIGURE 19. CALCULATED FACILITY NOZZLE EXIT FLOW CONDITIONS, MACH 10 AND 12 CONDITIONS

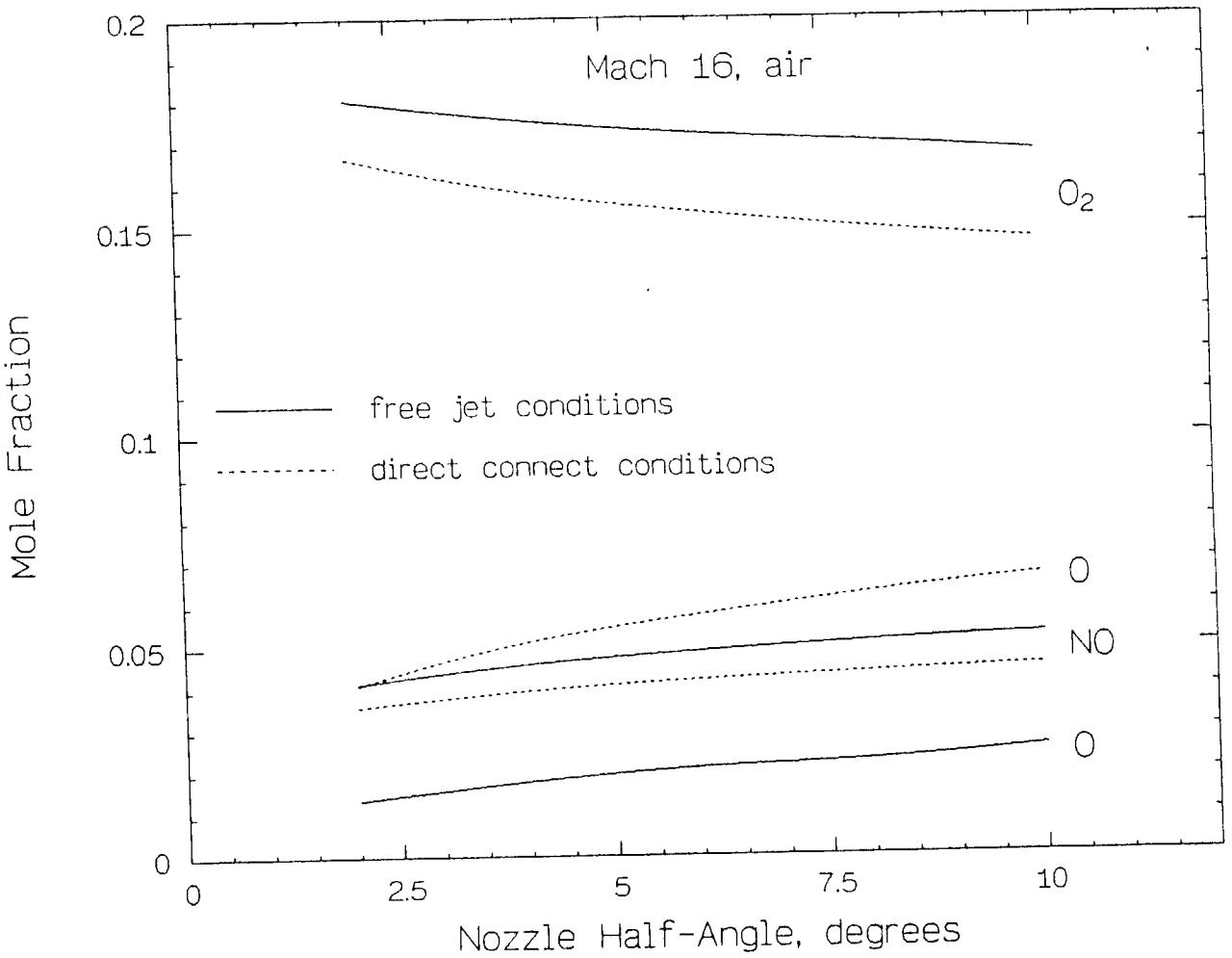

FIGURE 20. CALCULATED ATOMIC AND MOLECULAR OXYGEN AND NITRIC OXIDE CONCENTRATIONS AT FACILITY NOZZLE EXIT VERSUS EXPANSION ANGLE, MACH 16 CONDITIONS

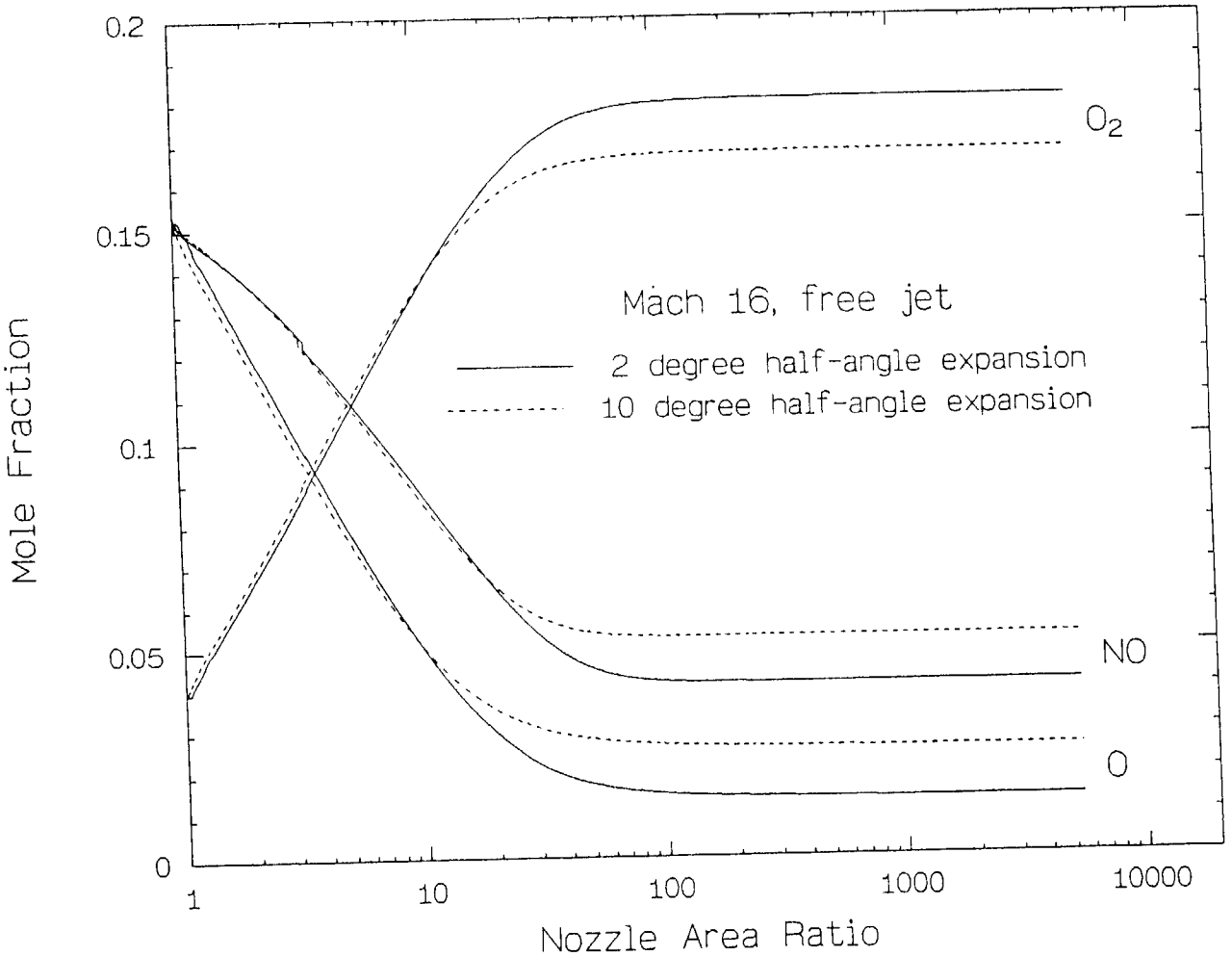

FIGURE 21. FACILITY NOZZLE CONCENTRATION PROFILES, MACH 16 FREE-JET CONDITION

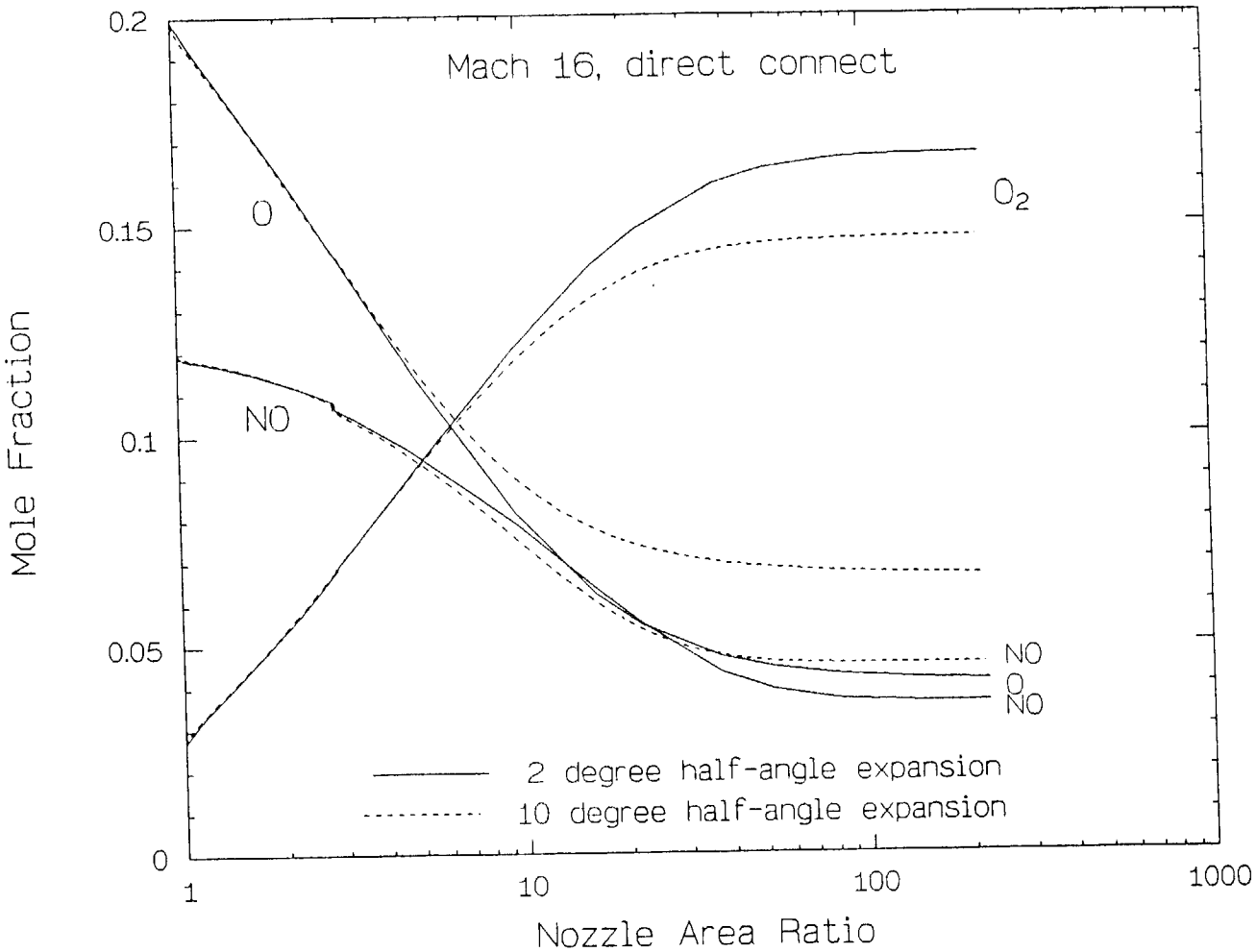

FIGURE 22. FACILITY NOZZLE CONCENTRATION PROFILES, MACH 16 DIRECT-CONNECT CONDITION

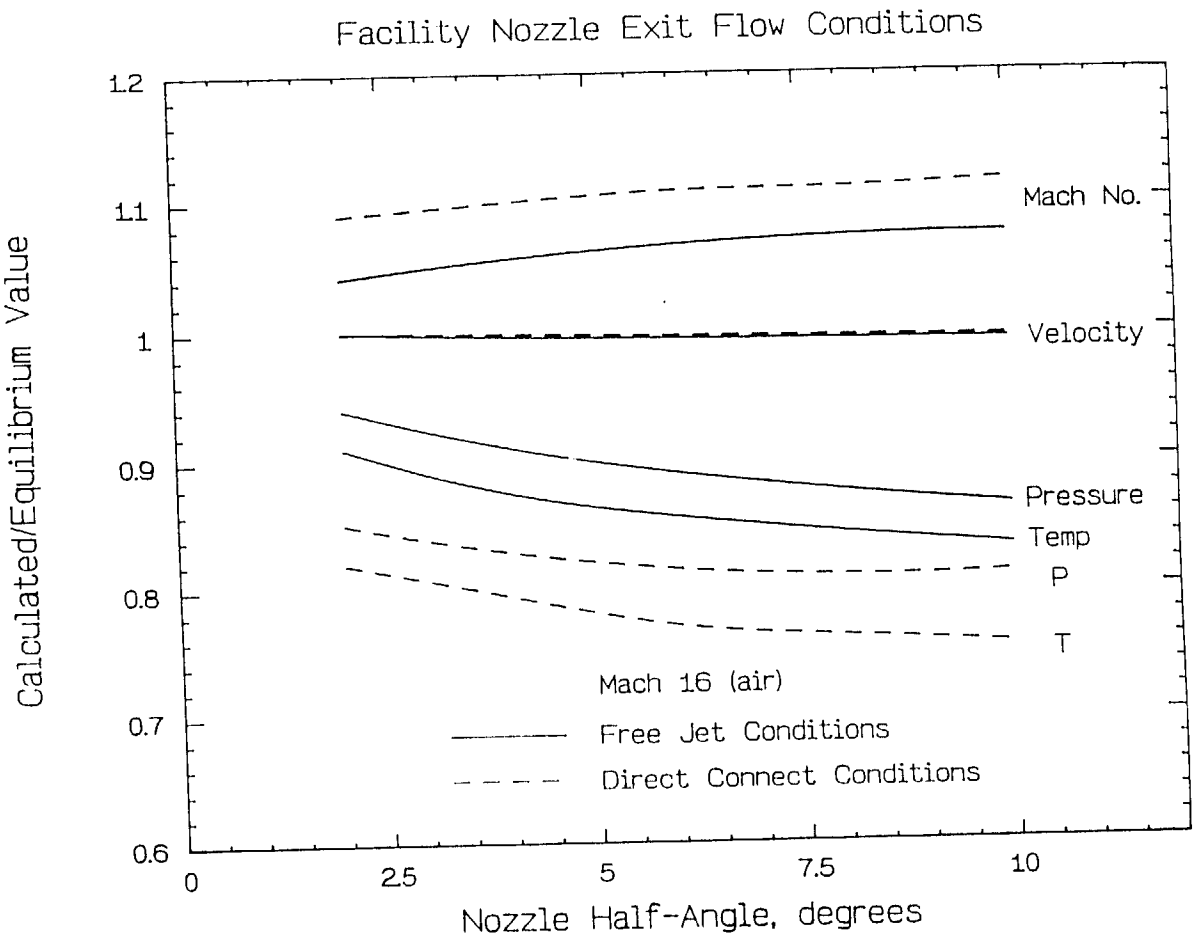

FIGURE 23. CALCULATED FACILITY NOZZLE EXIT FLOW CONDITIONS, MACH 16 CONDITIONS

The deviations from the desired or equilibrium flow conditions do not impact the simulation capability of the facility nearly as much as the gas composition does, as the flight conditions can be varied to closely match the nozzle exit flow conditions. For example, the nozzle exit pressure calculated for the free jet mode is about 90 percent of the equilibrium value, and simulates a 900 psf flight trajectory rather than 1000 psf. The calculated temperature ratio is approximately 85 percent, and simulates the flow underneath a forebody at 6.5 degrees to the flight direction rather than eight degrees. Furthermore, both the conditions and the composition are acceptable for aerodynamic simulation so long as the specific heat ratio and molecular weight are close to those of air. At the calculated Mach 16 free jet exit condition, the specific heat ratio is 1.38, and the molecular weight is 28.6 (for direct connect, $\gamma = 1.32$ at a temperature of 1600 K, and MW=28.0). These properties are in fact close to those for air at the same flow conditions. However, some characteristics of hydrogen-air chemistry cannot be easily simulated with a gas which contains significant amounts of monatomic oxygen and nitric oxide (e.g., ignition delay and reaction times), such as that at the direct connect conditions at this flight Mach number.

Mach 20 Solutions (air):

Considering Mach 20 simulation with air, the nozzle exit compositions shown in Figure 24 are seen to consist mostly of atomic oxygen, and vary substantially with the expansion angle. This is expected since the high total enthalpy reduces the rate at which reactions occur, particularly for the oxygen three body recombination reaction, in which the reaction rate is inversely proportional to the local temperature ($k = AT^{-1}$).

Mach 16 and 20 Free Jet Solutions (surrogate gas):

Finite rate chemistry solutions were generated for the surrogate gas mixtures described in section 2.2 at Mach 16 and 20 equivalent free jet simulation conditions. Initially, it was thought that increasing the amount of argon in the mixture would result in significant amounts of additional oxygen formation. However, only a very modest increase is observed because for a given total pressure and enthalpy, the argon-dominated mixture generates a higher total temperature. Furthermore, the calculations in section 2.2 indicated that the total pressure required to simulate a particular test condition diminishes with increasing amounts of argon in the test gas. Thus, the net effect is to reduce the rate of recombination of oxygen and promote early freezing of the composition.

The nozzle exit molar concentrations for these solutions are shown in Figure 25. The Mach 16 gas composition is almost identical to that of air at the equivalent flight condition (Figure 20). Replacement of some of the nitrogen with argon seems to have no net effect on the chemistry at this condition because of the competing effects mentioned previously, i.e., reduced dissociation products versus higher temperature and lower pressure histories. However, the Mach 20 solution does differ from its "air" counterpart and is observed to produce substantially more atomic oxygen throughout the range of expansion angles considered.

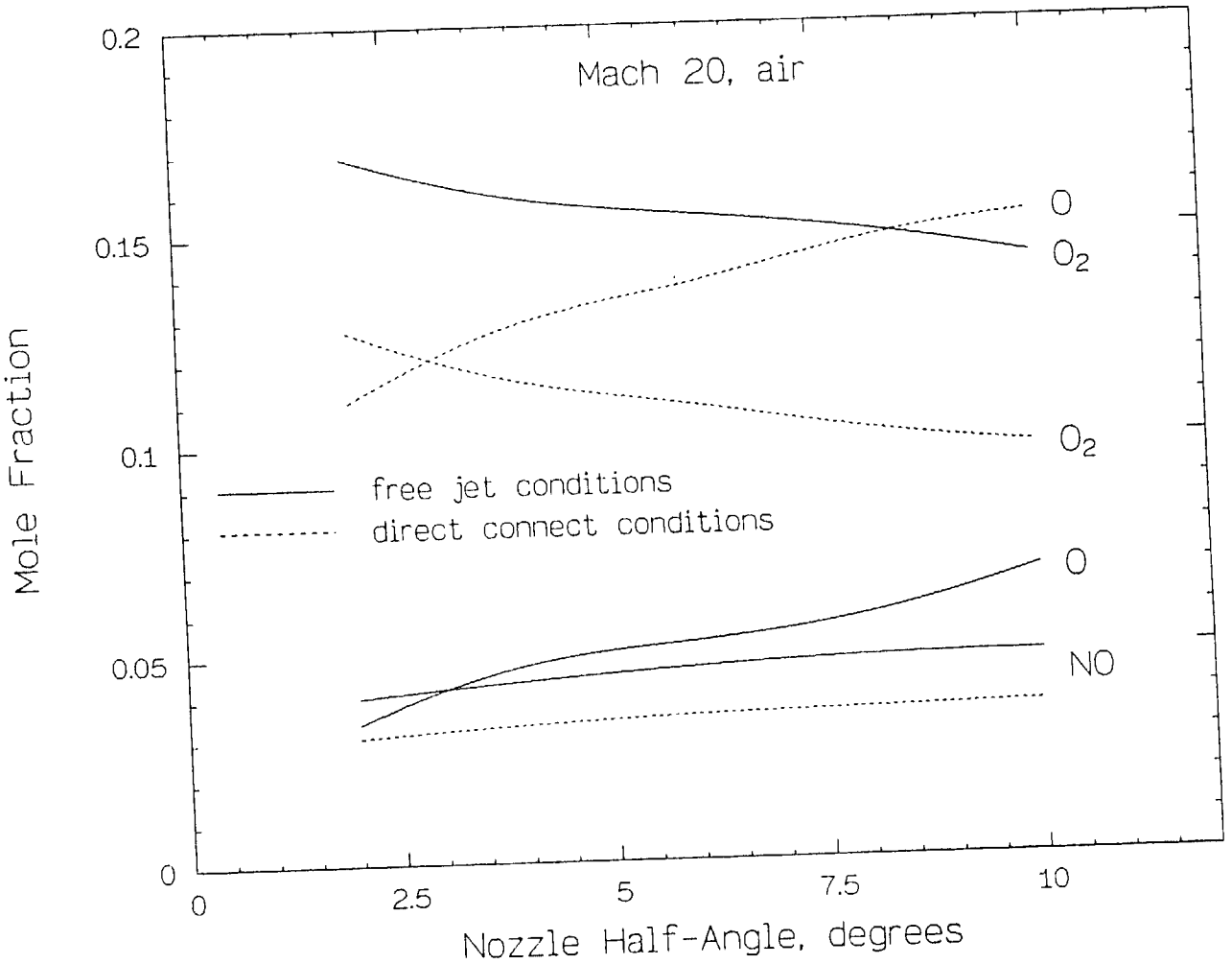

FIGURE 24. CALCULATED ATOMIC AND MOLECULAR OXYGEN AND NITRIC OXIDE CONCENTRATIONS AT FACILITY NOZZLE EXIT VERSUS EXPANSION ANGLE, MACH 20 CONDITIONS

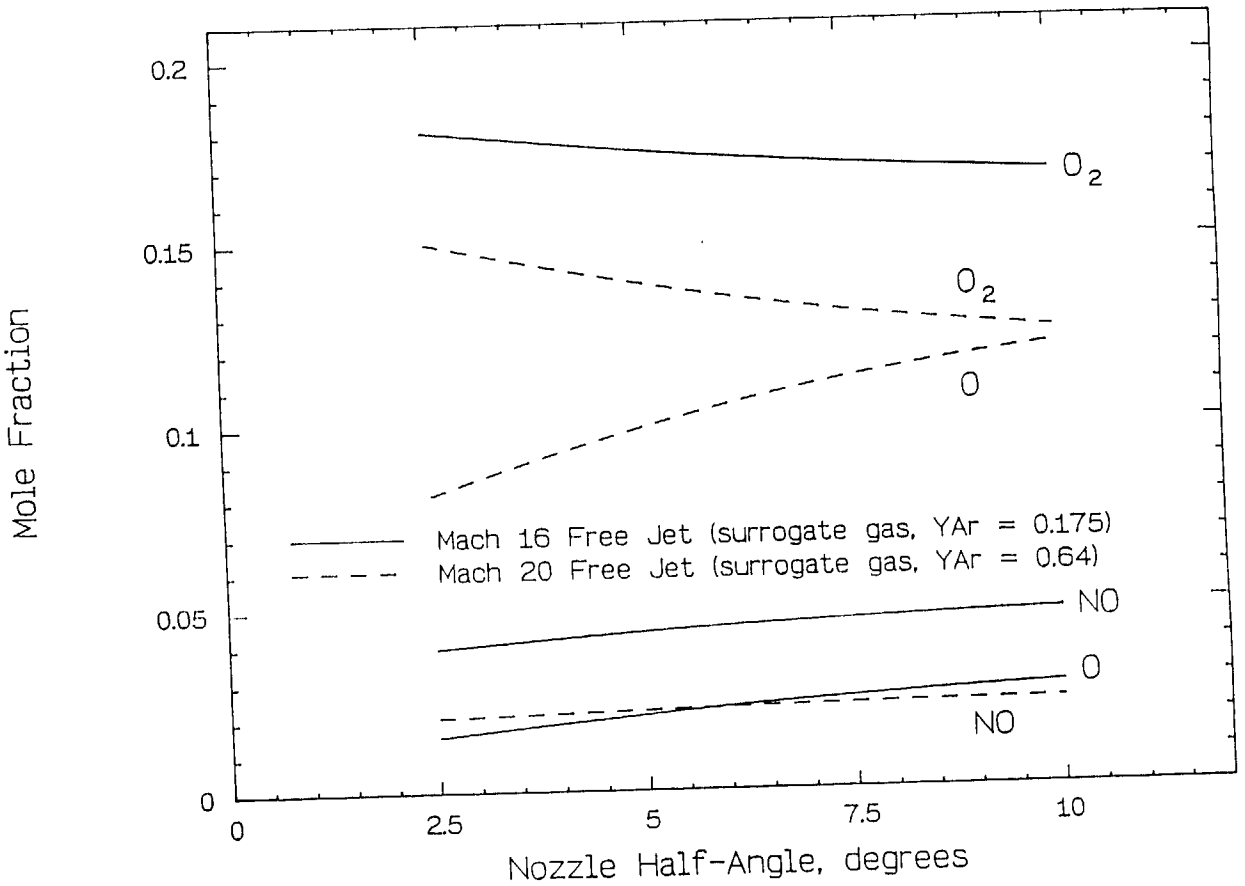

FIGURE 25. CALCULATED ATOMIC AND MOLECULAR OXYGEN AND NITRIC OXIDE CONCENTRATIONS AT FACILITY NOZZLE EXIT VERSUS EXPANSION ANGLE, MACH 16 AND 20 SURROGATE GAS CONDITIONS

Observations:

It is clear from these calculations that neither air nor this surrogate mixture will be suitable for Mach 20 simulation, nor will the generated real gas total pressure be containable. In addition, surrogate gas mixtures are undesirable for combustion simulation regardless of the flight condition simulated. At Mach 16, however, the real gas total pressures for air are within the projected limits of material containment technology, while the predicted gas composition after expansion seems marginally acceptable for free jet simulation (at 1%-3% atomic oxygen) and may be "workable" for direct connect. Hence, this flight condition will be the focus of subsequent calculations. The gas composition at Mach 10 and 12 simulated conditions is acceptable if the predicted amount of nitric oxide can be tolerated or accounted for. Calculations (with EqState), although not described here, show that the oxygen which the nitric oxide consumes can be replaced without additional NO formation in the mixing chamber.

It is clear that the total pressure and the expansion rate are the driving factors in determining the extent of recombination chemistry that occurs in the nozzle for these conditions. If the pressure is great enough and the expansion rate is such that the initial expansion is in equilibrium, then the maximum amount of recombination will occur before "freeze out". Although this seems self-evident, it has a direct bearing on the simulation envelope of the EWT since higher simulated flight dynamic pressures will improve nozzle performance, albeit at the expense of increased throat heat transfer and power requirements (or a smaller test section). The total enthalpy also controls the rate of reaction through the nozzle. Hence, it seems logical that the entropy of the gas both at the reservoir condition and during the expansion should correlate with the level of recombination and chemical freezing in the nozzle for a given geometry.

3.4. Entropy Production

It has been suggested[25,26] that the chemical state of the gas for which freezing occurs after a nonequilibrium expansion correlates with the reservoir entropy. The oxygen concentration at the nozzle exit was therefore examined with respect to the reservoir entropy to determine if this correlation holds for the conditions of interest here.

The calculated nozzle exit mole fraction of oxygen (normalized with respect to the oxygen mole fraction in standard air) was plotted in Figure 26 as a function of the reservoir entropy for the range of reservoir conditions considered and nozzle expansion rates of two and ten degrees (hence, encompassing the range in this parameter as well). Also shown are curve fits of the calculated points for the two expansion angles. The difference in the oxygen fraction between the two expansion angles increases with increasing entropy. In addition, the variation of oxygen fraction with entropy for a given expansion angle is not monotonic.

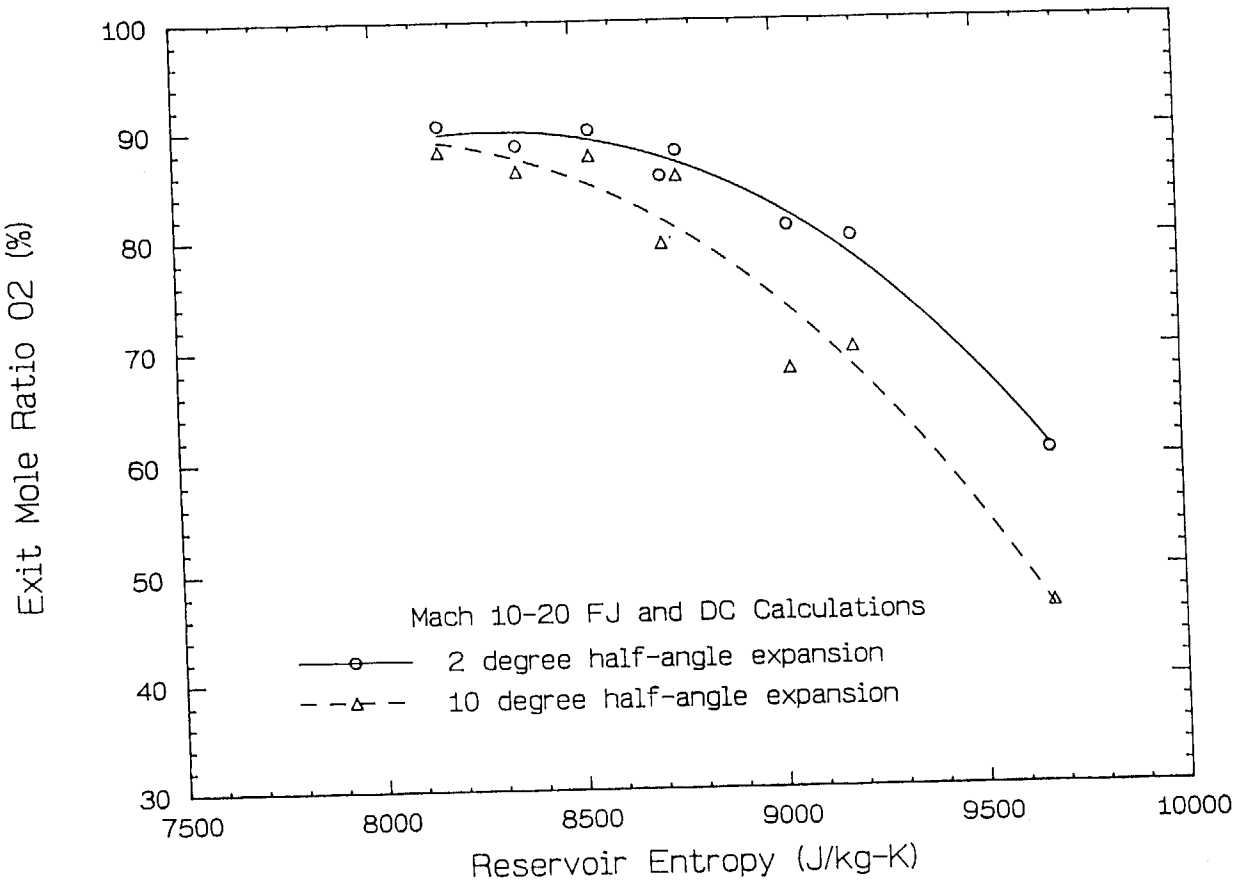

FIGURE 26. CALCULATED FACILITY NOZZLE EXIT MOLE RATIO OF OXYGEN VERSUS RESERVOIR ENTROPY

When the entropy is normalized with respect to the gas constant for standard air as in Reference 25, the abscissa then ranges from 26 to 35, and is seen to be outside of the entropy range examined in Reference 25. The implication is that at least within this entropy range, the nonequilibrium processes which determine the final mixture composition are sensitive to other characteristics of the expansion than just the reservoir entropy. The entropy generated through the nozzles was examined with the objective being to correlate the extent of recombination for the conditions considered.

It is known from the second law of thermodynamics that the entropy generated by either a shifting equilibrium or frozen adiabatic flow is zero. Therefore, the point at which the flow begins to depart from equilibrium, and the point of chemical freezing can be ascertained by plotting the specific entropy through the nozzle. This is shown in Figure 27 for the Mach 16 direct connect condition for expansion half-angles of two and ten degrees. The entropy initially remains constant and indicates an equilibrium flow process. The rate of increase of entropy drops near the end of the nozzle, and although the slope does not go to zero, the increase becomes diminishingly small, indicating that the chemistry has almost completely frozen at the exit.

In contrast, the molar entropy, shown in Figure 28 normalized by the Universal gas constant, illustrates chemical reaction in a slightly different manner. The initially large slope indicates that there is significant recombination occurring, while the flat profile near the exit shows that the flow is essentially frozen. When the ordinate is normalized with respect to the initial (sonic) molar entropy and all the conditions are plotted as in Figure 29, then it becomes clear that the molar entropy rise due to chemical reaction is a function of the total enthalpy, the total pressure, and the nozzle expansion rate.

The profiles are essentially divided into three groups, first by total enthalpy, second by total pressure, and third by expansion rate. For low total enthalpies, the entropy rise is small and corresponds to relatively little recombination in the nozzle. In addition, the entropy rise is independent of the expansion angle, but the dependence increases with increasing total enthalpy, as was seen in the previous section. As the total enthalpy increases, so does the entropy rise, indicating that overall changes in the mixture composition are greater, even though the final composition bears less resemblance to that of natural air. The second grouping is with respect to total pressure. Lower total pressures for a given total enthalpy result in more entropy rise and an increased sensitivity to expansion angle. The effect of expansion angle is the third group. Given the above qualitative discussion of the effects of pressure, enthalpy, and geometry on entropy rise, the functional relationship between the entropy rise and the extent of recombination in the nozzle can be deduced as follows:

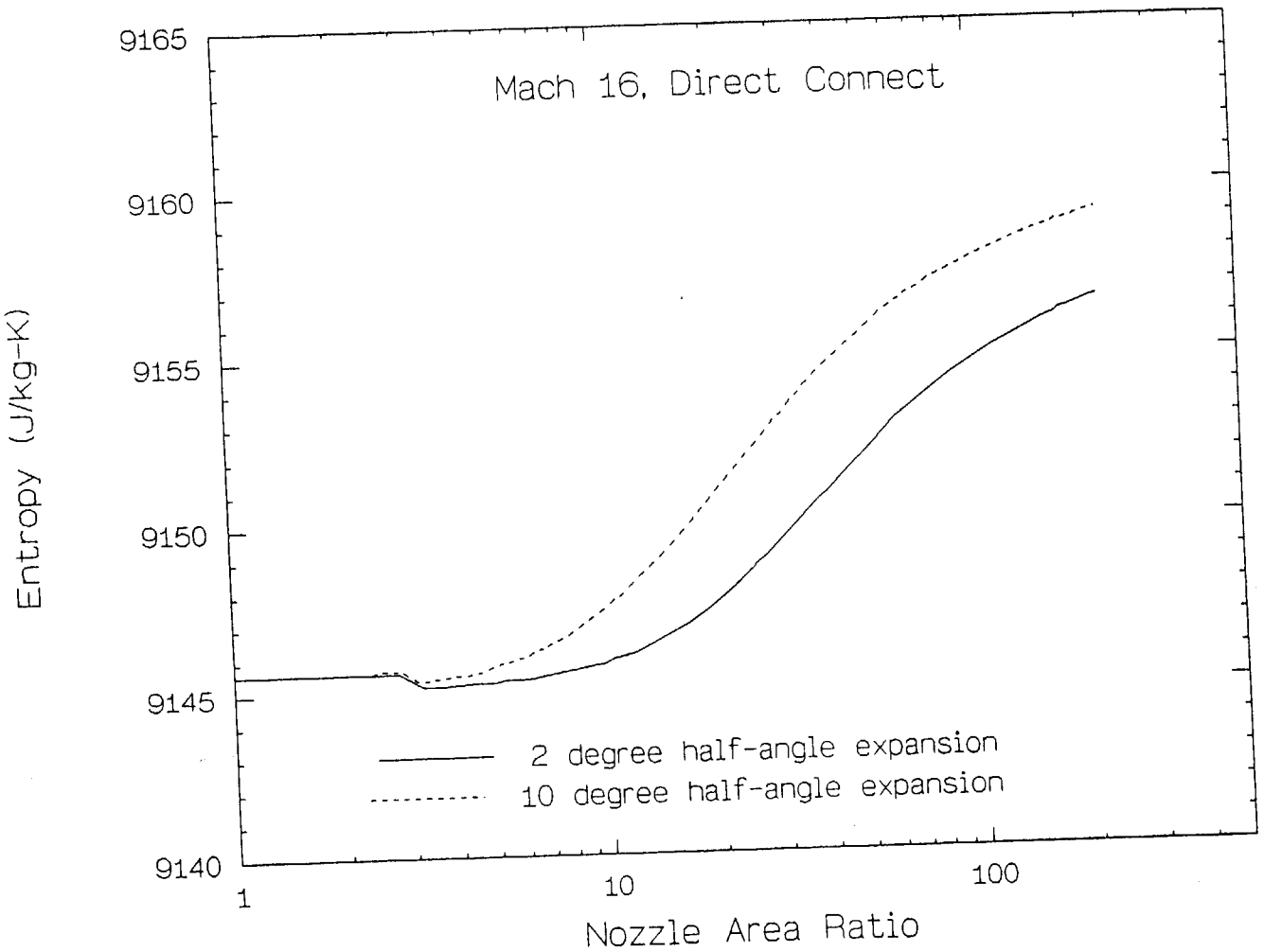

FIGURE 27. FACILITY NOZZLE ENTROPY PROFILES, MACH 16 DIRECT-CONNECT CONDITION

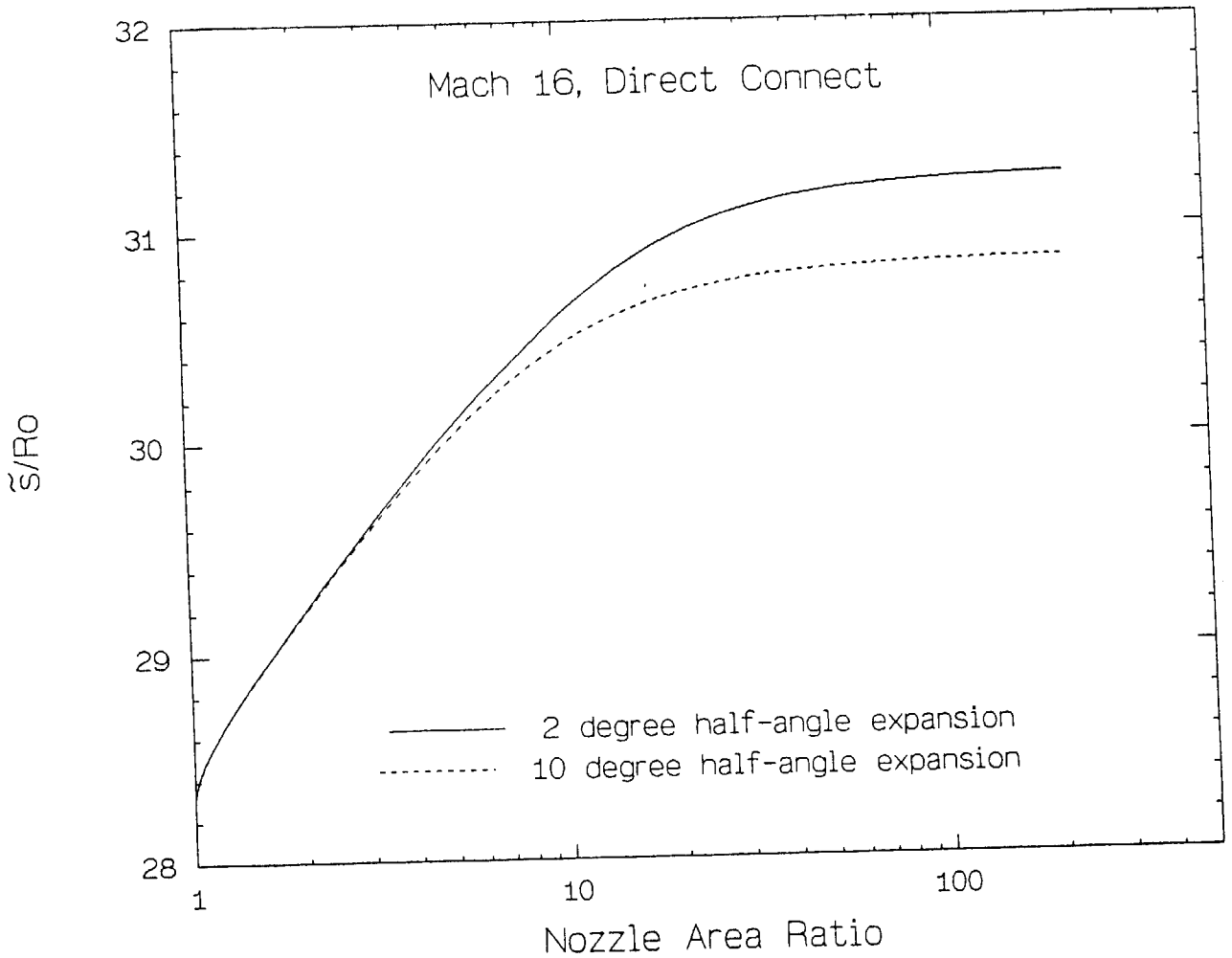

FIGURE 28. FACILITY NOZZLE MOLAR ENTROPY PROFILES, MACH 16 DIRECT-CONNECT CONDITION

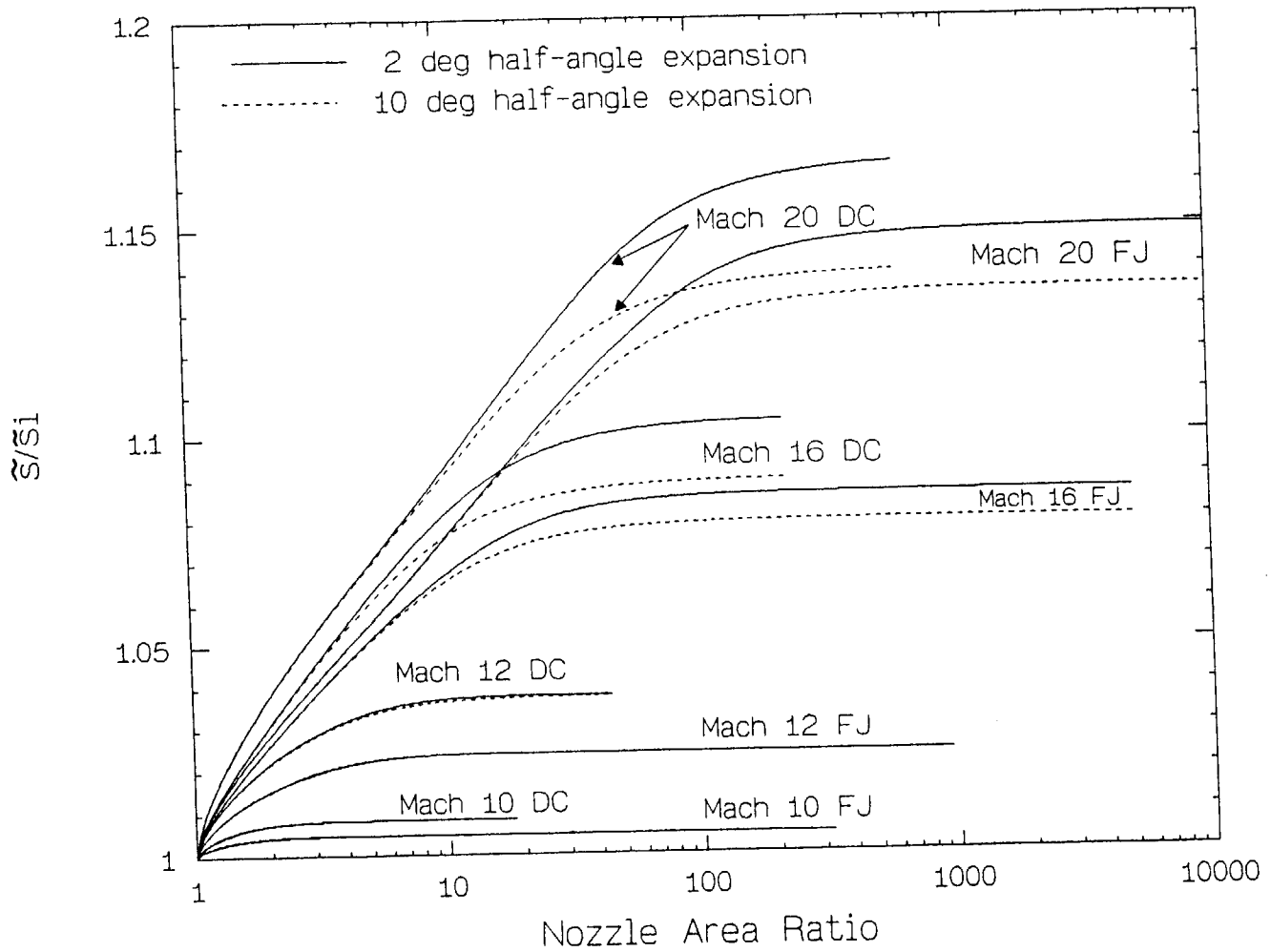

FIGURE 29. MOLAR ENTROPY RISE THROUGH FACILITY NOZZLES, MACH 10 TO 20 CONDITIONS

The irreversibility incurred from reactions which proceed at finite rates can be assessed by calculating the change in the entropy due to changes in the mixture composition. The expression for the molar entropy of an ideal gas mixture can be written as

$$\tilde{s}/R_0 = \sum_{i=1}^{ns} \{\int(\tilde{c}_{p,i}/R_0T)\, dT - \ln(p_i/p_0) + \tilde{s}_{0,i}/R_0\},$$

where $\tilde{c}_{p,i}$ is the constant pressure molar specific heat of mixture component i, R_o is the Universal gas constant, p_i is the partial pressure of component i, and $\tilde{s}_o$ is the entropy at the reference temperature. Taking the derivative implicitly with respect to the mole fractions x_i gives an expression for the entropy change due to a change in mixture composition:

$$d\tilde{s}/R_0 = [(\tilde{c}_p/R_0T)\, dT - dp/p] + \sum_{i=1}^{ns} dx_i \{\int(\tilde{c}_{p,i}/R_0T)\, dT - \ln(p_i/p_0) + \tilde{s}_{0,i}/R_0\}$$

The first term on the right is seen to be the nonreacting contribution to the entropy, while the second term represents the contribution due to chemical reaction. By inspection, the latter is proportional the natural log of the pressure (referenced to atmospheric pressure) and seems to be inversely proportional to the temperature. Since the level of recombination does not correlate directly with the reservoir entropy for these conditions, it is appropriate to correct the entropy in accordance with the functional relationships of the second term in the above equation, i.e., $\ln(p_t)/H_t$. Intuitively this makes sense since higher total temperatures (enthalpies) tend to reduce recombination rates, making chemical performance inversely proportional to the total enthalpy. This is true particularly for air chemistry since the majority of molecular oxygen formation results directly from the three body oxygen reaction, the rate of which is inversely proportional to the local temperature. In contrast, higher total pressures delay chemical freezing and hence will increase nozzle performance. The effect of the expansion angle is essentially to change the effective total pressure, delaying or promoting freezing of the composition. It is therefore reasonable to correct the entropy for pressure by the factor $\ln(p_t/\tan\theta)$, where θ is the conical half-angle. The performance parameter then becomes:

$$\eta_n = \frac{s_t \ln\left(\frac{P_t(atm)}{\tan\theta}\right)}{H_t}, \quad (K^{-1}),$$

where s_t is the reservoir entropy. The nozzle performance parameter η_n is plotted in Figure 30 as a function of the ratio of nozzle exit mole fraction of oxygen to the nominal mole fraction (0.21) in percent, for all the conditions examined (Mach 10 to 20 free jet and direct connect) and for expansion half-angles of two and ten degrees. Almost all the points are seen to lie in a hyperbolic-shaped line which seems to asymptote to slightly above 90 percent recombination of oxygen. The deficit is in the form of nitric oxide. The implication here is that nitric oxide is always formed somewhere in the reservoir or nozzle at the considered conditions and once formed, the oxygen lost to nitric oxide can not be recovered. Values of η_n below about 0.0075 result in a substantial drop in the amount of oxygen recombined. Extrapolating the curve to zero percent oxygen results in a value of η_n of about 0.0025. A reflected shock tunnel operating at Mach 25 flight total enthalpy with about 350 atmospheres of total pressure produces almost 100 percent dissociated oxygen in the test section. The entropy at these conditions is 12,900 J/kg-K. Assuming an effective expansion half-angle of eight degrees, the performance parameter η_n for this simulated condition is 0.0031. The agreement is seen to be good given the slope of the curve at this value of η_n.

Although this nozzle performance parameter seems to predict the nozzle chemical kinetic performance for the given range of conditions, more comparisons with measurements need to be made before it is used with any degree of confidence. This will be done in the future; however, time and funding constraints have precluded further comparisons at this time. Nevertheless, other calculations were made to improve the performance of the facility nozzle, particularly for the Mach 16 conditions. Oxygen replenishment calculations are described next.

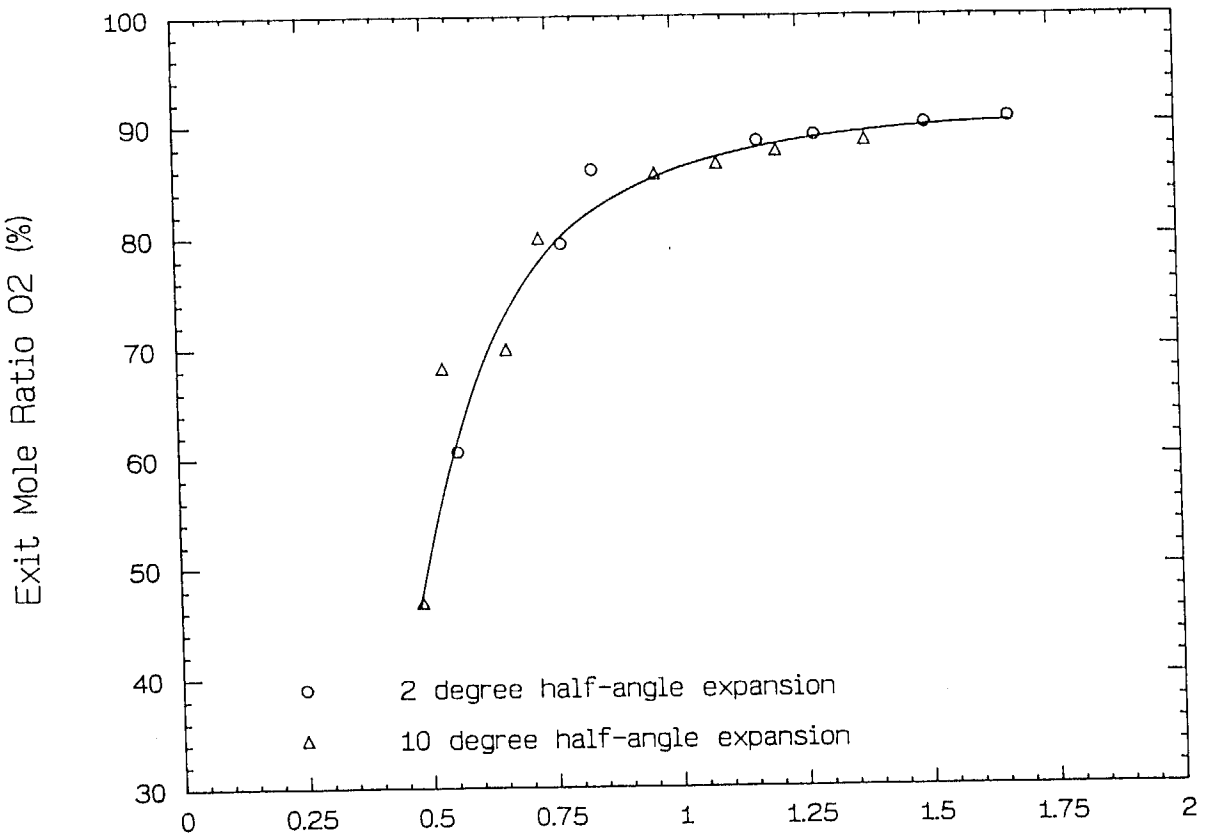

$$\eta_n\ (\text{x } 100) = \frac{s_t \ln\left(\frac{P_t(atm)}{\tan\theta}\right)}{H_t},\ (K^{-1}),$$

FIGURE 30. CORRELATION OF NOZZLE EXIT MOLE RATIOS OF OXYGEN WITH NOZZLE PERFORMANCE PARAMETER, η_n

3.5. Oxygen Replenishment

Calculations were made to evaluate oxygen replenishment as a method for increasing the concentration of oxygen at the facility nozzle exit for the Mach 16 free jet and direct connect conditions. The calculations in section 3.3 indicated that at Mach 10 and 12 simulated conditions, the exit composition contains no atomic oxygen, and about five percent nitric oxide. In addition, the oxygen lost to nitric oxide can be replaced without additional formation of the latter or atomic oxygen. At Mach 16 simulated conditions, however, atomic oxygen concentrations increase to between one and three percent for free jet test conditions and to between four and seven percent for direct connect test conditions, depending on the expansion angle. The objective of the calculations was to determine if the molecular oxygen can be replaced without additional formation of unwanted species.

The methodology was simply to increase the undissociated concentration of oxygen, and observe the exit concentrations calculated by the finite rate solution until a 21 percent mole fraction of oxygen was obtained. The calculations were made for a conical nozzle half-angle of six degrees, and the test conditions were assumed to be identical to those of air.

A summary of the calculations is tabulated below. Shown for each condition is the undissociated mole fraction of oxygen required to obtain 21 percent at the nozzle exit, the exit concentrations of O and NO, and the flow conditions normalized with respect to the nominal (equilibrium) test conditions.

Table 10. Summary of Oxygen Replenishment Calculations

Condition	$XO_{2,\ req'd}$	XO_e	XNO_e	p_e/p_{eq}	T_e/T_{eq}	M_e/M_{eq}
Mach 16, f.j.	0.276	0.0198	0.0552	0.880	0.844	1.07
Mach 16, d.c.	0.292	0.0632	0.0488	0.767	0.772	1.11

The exit to equilibrium molecular weight and gamma ratios are 0.99 and 1.01 for free jet, and 0.975 and 1.01 for direct connect, respectively.

The mole fractions of atomic oxygen and NO for air for a six degree half-angle nozzle are 0.021 and 0.049, respectively. Comparing these values with the oxygen-replenished quantities listed above indicates that for this condition make-up oxygen can be added with no additional penalties to the simulation quality of the gas. The equivalent direct connect quantities for air are 0.0575 mole fraction of O and 0.042 mole fraction of NO. Comparing the present calculation with these values, the differences are seen to be insignificant with respect to the total amount of atomic oxygen and NO formed. Hence, it appears that oxygen replenishment is a reasonable method for obtaining the nominal 21 percent mole fraction of oxygen in the test gas. However, the significant effects of atomic oxygen on the scramjet combustion process require that the concentration of atomic oxygen, particularly for Mach 16 direct connect conditions, be reduced. The next section discusses the

calculations made to enhance the three body recombination of oxygen, the intent being to reduce significantly the amount of atomic oxygen formed and of course increase the molecular oxygen concentration.

3.6. Three Body Recombination Enhancement

It is well known that one way to increase the production rate of oxygen is to introduce efficient third bodies into the flow to catalyze the oxygen three body recombination reaction, this reaction being the principal contributor of oxygen in facility nozzles. Although there are many such catalysts available, their principal disadvantage is that they contaminate the flow with unwanted elements that may have a significant effect on the chemical processes occurring in the combustion zone. For example, metal oxides are known to be among the most efficient third bodies, but their high heats of reaction can affect the combustion process in ways similar to those of atomic oxygen. In addition, condensation near the facility nozzle exit may introduce flow nonuniformity problems and may threaten instrumentation and model survivability despite the fact that only small quantities of these catalysts are typically required to significantly enhance three body recombination.

In contrast, water is an efficient third body that does not have the adverse effects mentioned here for metal oxides. However, introducing water at typical Mach 16 mixing chamber temperatures will surely dissociate it, producing hydroxyl radicals and hydrogen in both atomic and molecular form which may or may not recombine in the nozzle.

Hence, trade-off studies must be performed to compare the adverse effects of the catalyst versus those of atomic oxygen present in the flow. In this section, calculations were made to quantify the degree of third body enhancement (and simultaneously the sensitivity of the chemistry to uncertainties in the reaction rate coefficient) required to recombine most of the atomic oxygen present in the Mach 16 nozzle exit flows. Calculations were then made to assess the effectiveness of water as a three body recombination catalyst.

3.6.a. Artificial Enhancement of the Oxygen Three Body Reaction Rate Coefficient

The sensitivity to the three body reaction rate coefficient was determined by increasing the pre-exponential factor in the oxygen three body reaction rate equation, and observing the species profiles and the concentration of atomic oxygen which remained at the nozzle exit. A six degree half-angle expansion used was for these calculations. Yet it seems that the net effect of increasing the reaction rate would be equivalent to increasing the total pressure of the flow. In essence, the chemistry would remain in equilibrium longer. Since the freezing zone would begin at a larger area ratio, both the density and the concentration of atomic oxygen will probably be lower and would induce faster freezing.

The calculations were made for the Mach 16 free jet and direct connect conditions, and the results are presented in the form of molar profiles in Figures 31 and 32. The solutions for the nominal rate coefficient was plotted with those for which the pre-exponential factor was increased by one and two orders of magnitude. The predicted effects of the increase in rate coefficient on the chemistry do in fact occur, as the flow is seen to remain in equilibrium longer and then freezes more rapidly. In both the free jet and direct connect solutions there is a significant reduction in the amount of atomic oxygen which freezes for a ten-fold increase in the rate coefficient. The reduction is significant for the free-jet case (from 0.021 to 0.0067) but less for the direct connect case (from 0.0575 to 0.0257). Interestingly, however, the nitric oxide freezes at slightly higher levels, 12 and 26 percent (0.055 and 0.0607) for the free jet and direct connect cases, respectively. This may be due to the reduction in atomic oxygen which supplies the rearrangement reaction $O + NO \rightarrow N + O_2$. The net result is that the level of molecular oxygen does not increase to any significant extent.

The solutions for a 100-fold increase in the rate coefficient indicate reductions of atomic oxygen of similar magnitudes beyond the previous calculation. The molar concentrations drop to 0.00166 and 0.009 for the free jet and direct connect nozzles, respectively. The increases in molecular oxygen are also comparable with those of the previous calculation.

The implication of these results is significant since three body efficiencies of 10 or more are not at all unrealistic, and the reduction in atomic oxygen is substantial. Of course the level of atomic oxygen for the direct connect calculation is still considerably higher than that which would exist at the combustor entrance for this flight condition. The results also imply that rate coefficients which differ from the assumed values may potentially have a significant impact on the chemical kinetic performance of the nozzle. Nevertheless, the results are encouraging and warrant additional calculations and investigation into candidate third bodies whose efficiencies are of order ten or higher. As mentioned above, such a calculation was made here with water as the third body.

3.6.b. Oxygen Three Body Recombination Enhancement With Water

The effectiveness of water as a catalyst for the oxygen three body recombination reaction was assessed. A small amount of water (5% by volume) was added to the test gas to determine its effect on the production rate of oxygen and the gas composition at the nozzle exit. Since high temperature curvefits were not available for hydrogen-based compounds, the initial conditions for the finite rate calculation were taken to be those after an equilibrium expansion to an area ratio at which the temperature fell slightly below 5000 K. The remainder of the expansion occurred at a six degree half-angle. The equilibrium chemistry assumption made here was deemed reasonable since the natural air expansions for this flight condition are in equilibrium to larger area ratios than those at the initial conditions in this calculation. The undissociated mole fraction of oxygen (excluding the oxygen in the water) was kept constant at 0.21.

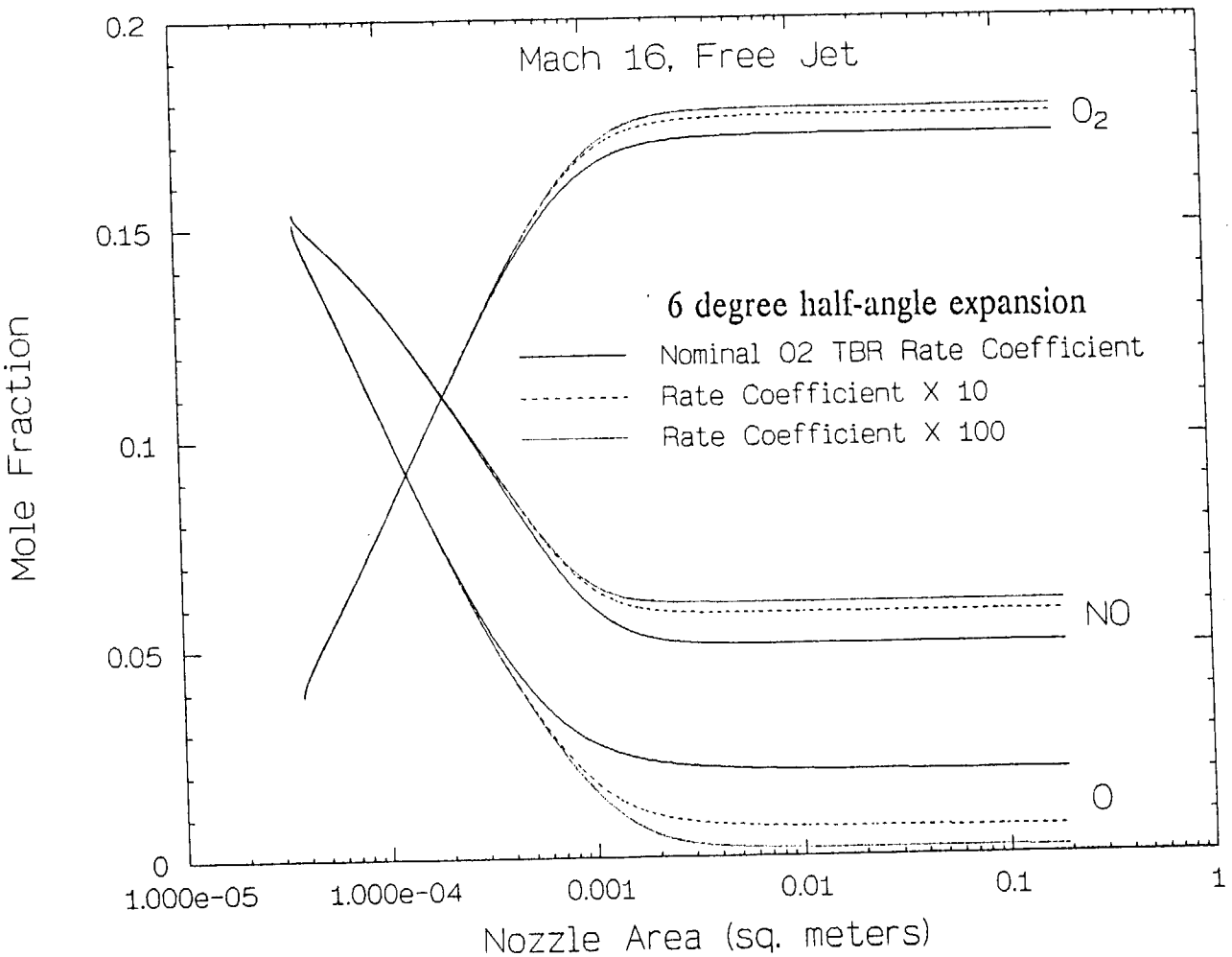

FIGURE 31. RESULTS OF OXYGEN THREE BODY RECOMBINATION ENHANCEMENT CALCULATIONS, MACH 16 FREE-JET CONDITION

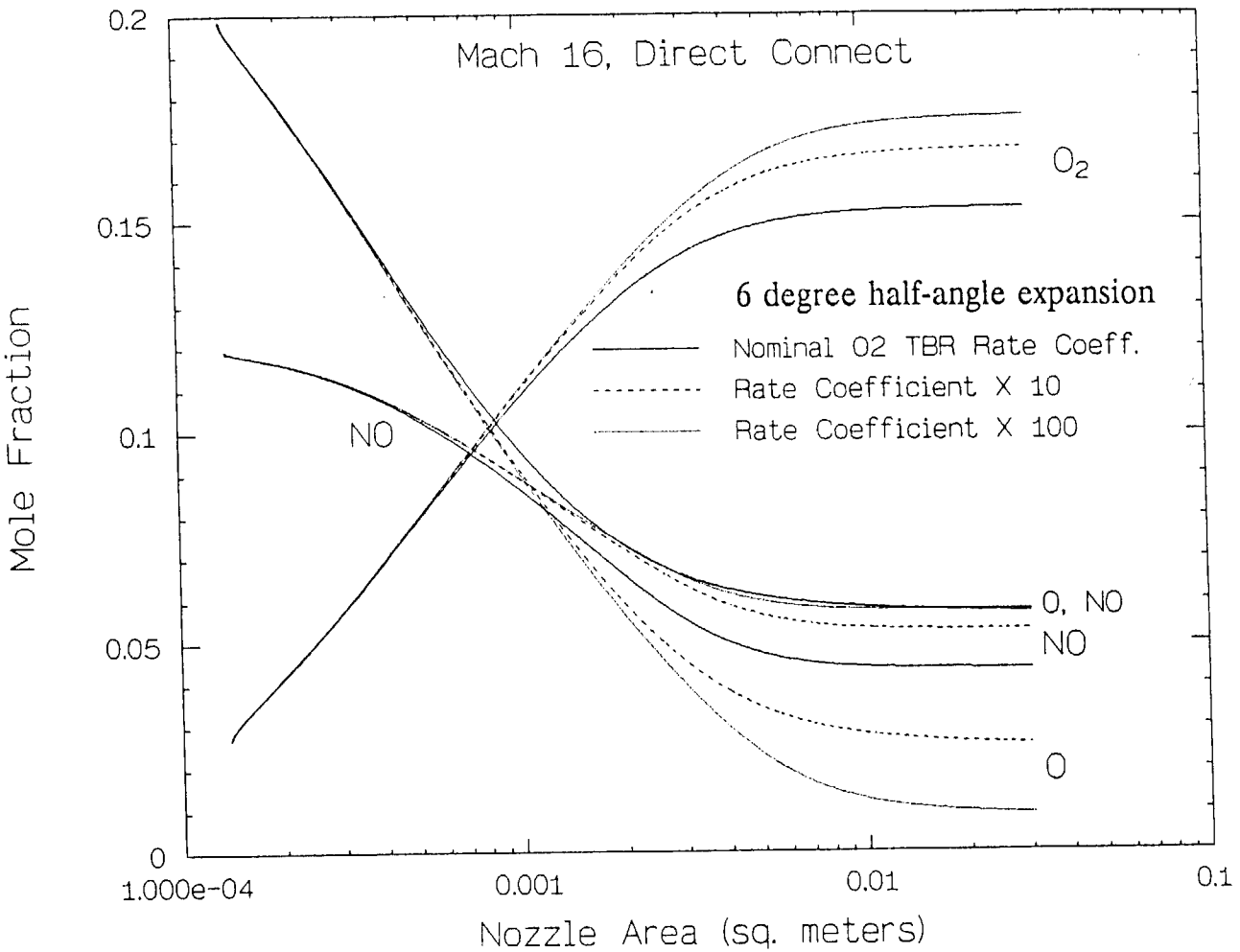

FIGURE 32 RESULTS OF OXYGEN THREE BODY RECOMBINATION ENHANCEMENT CALCULATIONS, MACH 16 DIRECT-CONNECT CONDITION

The results of the calculations are presented in Figures 33 and 34 for the Mach 16 free jet and direct connect conditions. Inspecting first the free jet molar profiles in Figure 33 and comparing them to the six degree expansion rate solution for pure air (Figure 31), the water concentration recombines to the undissociated amount. The molecular oxygen level is slightly greater than for the pure air case (0.813 versus 0.172). More importantly, the atomic oxygen concentration is reduced to trace amounts (1.7×10^{-4}), while the nitric oxide remains approximately constant. The reduction in atomic oxygen is an order of magnitude greater than the calculation in section 3.5.a. where the rate coefficient was increased by a factor of 100. The reactions in the hydrogen-air mechanism seem to further enhance oxygen recombination beyond that due to the third body efficiency of water.

Trace concentrations of hydroxyl radicals and atomic and molecular hydrogen also remain at the exit which, although small, may potentially have a significant impact on ignition delay times. However, the molar profiles indicate that these species (including atomic oxygen) have not frozen at their nozzle exit values so that given some additional reaction time, their concentrations might be further reduced. Nonetheless, the results are encouraging in that there is a significant reduction in the concentration of atomic oxygen over that of natural air due to the inclusion of water in the mixture. The free radical population can probably be reduced by optimizing the amount of water in the mixture.

The direct connect calculations shown in Figure 34 are slightly less encouraging. The atomic oxygen concentration is reduced to less than one percent from almost six percent for natural air, and the amount of molecular oxygen increases by 16 percent from 0.154 to 0.178. However, the hydroxyl concentration is relatively high at 0.64 mole percent. The same is true for atomic and molecular hydrogen. Optimizing the water concentration can probably reduce the concentrations here as well. Other methods include increasing the flight dynamic pressure or adding an isolator to continue the reactions.

To summarize, the calculations presented in this section have demonstrated considerable potential for improving the composition of the test gas for up to and including Mach 16 simulation. It is reasonable to assume that the various methods discussed can be "mixed and matched" to optimize the gas composition for a particular condition or test objective. However, test gas optimization must be preceded by, or conducted simultaneously with, a study to determine the extent to which hydrogen-air combustion intermediates such as O, OH, H must be reduced to obtain acceptable simulation of the combustion chemical kinetics.

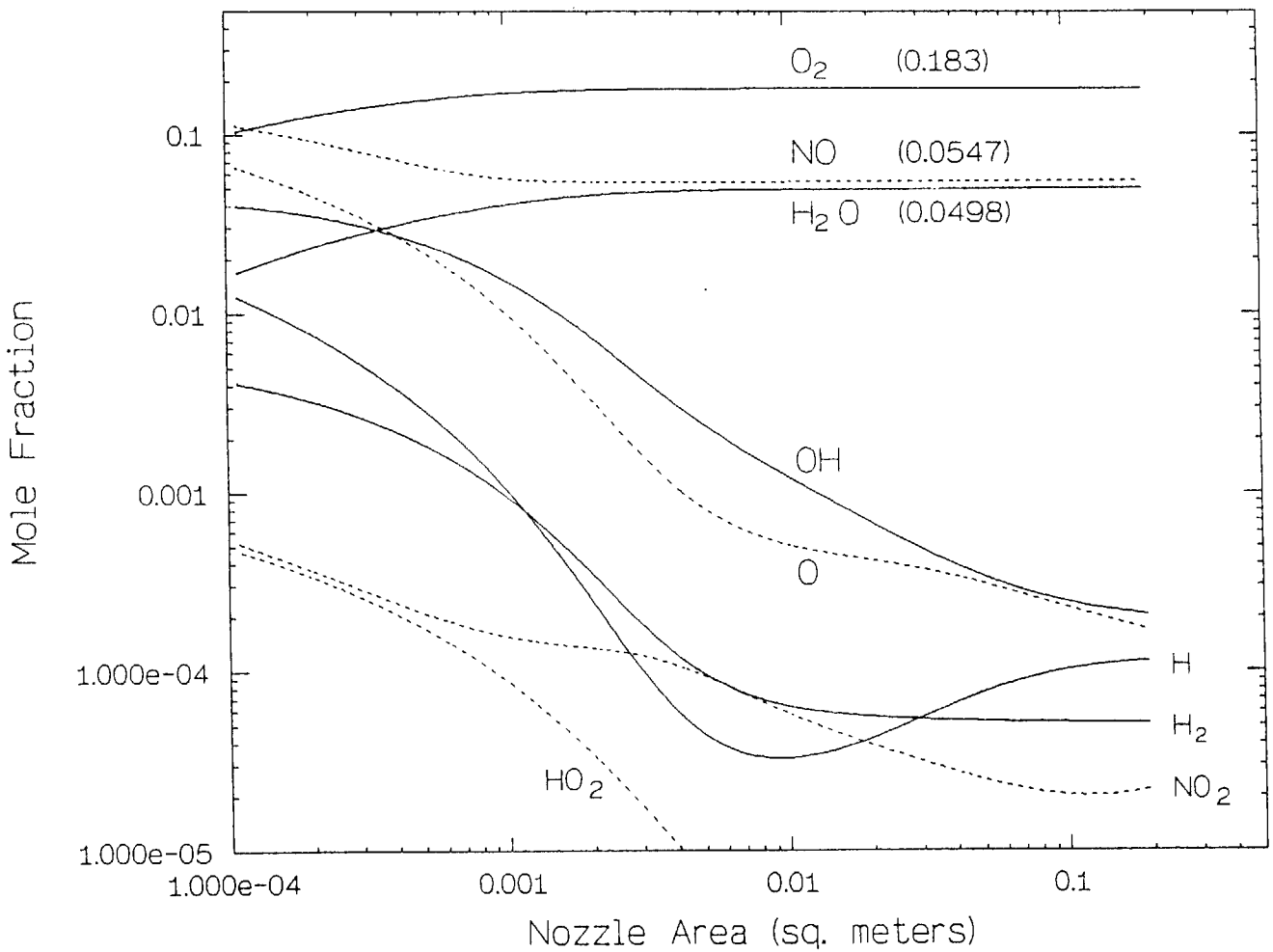

FIGURE 33. RESULTS OF WATER THREE BODY RECOMBINATION ENHANCEMENT CALCULATIONS, MACH 16 FREE-JET CONDITION

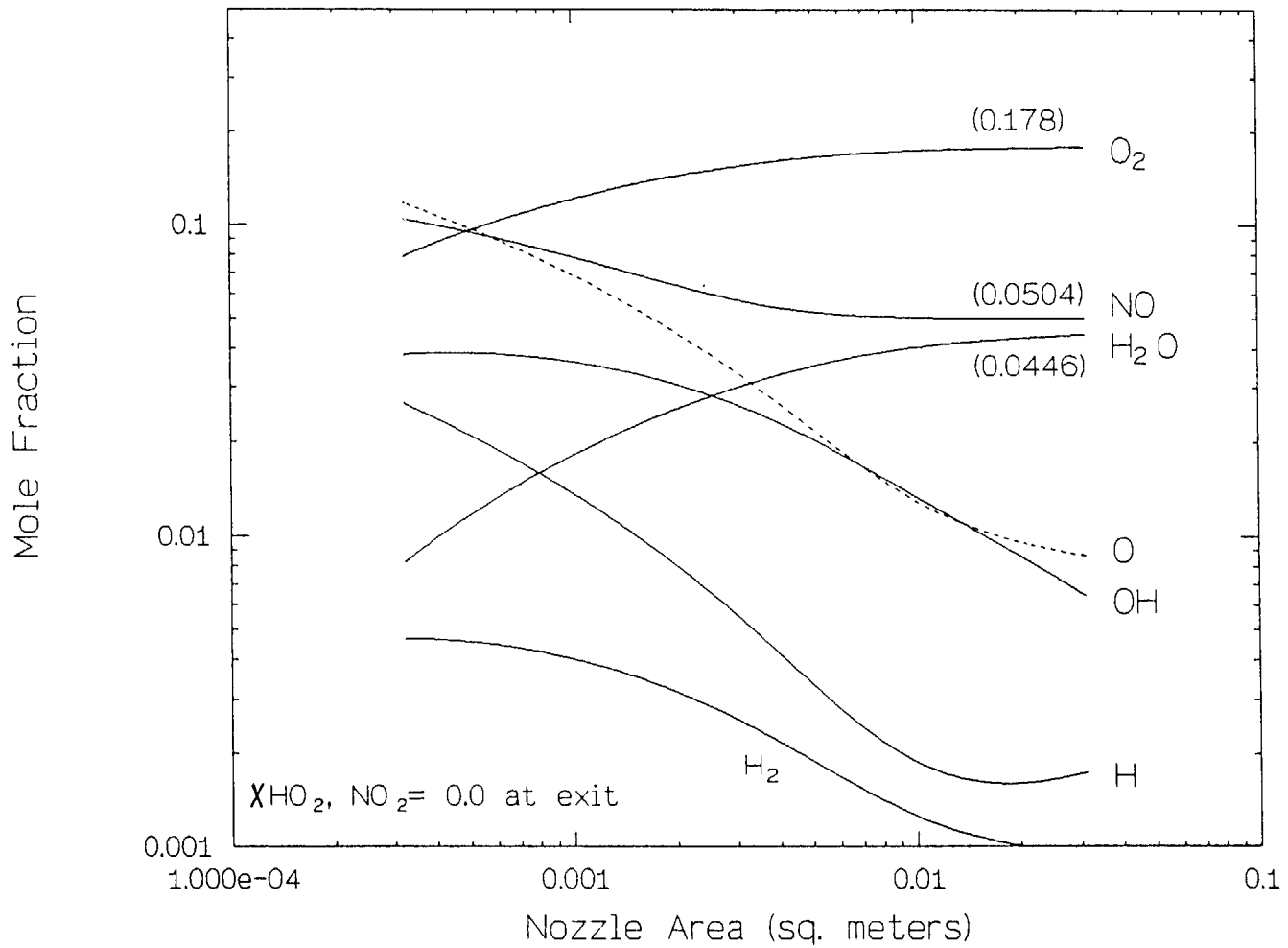

FIGURE 34. RESULTS OF WATER THREE BODY RECOMBINATION ENHANCEMENT CALCULATIONS, MACH 16 DIRECT-CONNECT CONDITION

3.7 Conclusions Regarding Nozzle Chemical Kinetic Performance and Recommended Future Calculations

The conclusions reached in the chemical kinetic facility nozzle performance study can be summarized as follows:

1) At the conditions examined here, the effect of ionization reactions on the chemistry is negligible.

2) The level of nitric oxide which freezes in the nozzle is always between four and six percent at reservoir conditions examined here, and is practically independent of both the conditions simulated and the nozzle geometry. The nozzle performance parameter η_n indicates that the oxygen lost to nitric oxide cannot be recovered once NO is formed.

3) The effect of varying the expansion angle between two and ten degrees on the chemistry is small for Mach 10 to 12 simulation, but becomes significant at about Mach 16. Larger expansion angles result in faster chemical freezing and hence reduce the amount of molecular oxygen reaching the test section, while increasing the level of atomic oxygen.

5) The methods discussed for improving the simulation quality of the test gas, i.e., oxygen replenishment, and three body recombination enhancement (e.g., by water) demonstrate significant potential for all the conditions up to and including Mach 16 simulation. Specifically, the oxygen lost to NO can be replaced with almost no additional formation of dissociation products. At Mach 16 conditions, the atomic oxygen that remains in the test gas can be reduced to trace amounts by adding efficient third bodies into the flow to catalyze the oxygen three body recombination reaction. Water is an extremely efficient catalyst, but leaves behind small amounts of hydroxyl radicals and hydrogen in both atomic and molecular form. This situation is worse for Mach 16 direct connect simulation; however, these latter contaminants can probably also be reduced to trace amounts by optimizing the water concentration and/or increasing the simulated flight dynamic pressure.

6) Mach 20 free jet conditions cannot be simulated with air because the required total pressure is beyond current or projected maximum containment pressures. Simulating Mach 20 direct connect conditions with proper test gas composition does not seem possible from these calculations since the test gas is more than 50 percent dissociated at the nozzle exit.

7) The surrogate gas mixtures discussed here result in at best equal nozzle performance to natural air, and are not acceptable for combustion chemistry simulation.

8) A nozzle chemical kinetic performance parameter was identified which correlates the amount of recombined oxygen in the nozzle to the reservoir entropy, pressure, enthalpy, and the slope of the (conical) nozzle wall for the conditions and geometries examined. This parameter also well predicts the conditions at which a reflected shock tunnel produces a completely dissociated test gas (100% atomic oxygen) after expansion.

Future calculations relating to the facility nozzle chemical kinetic performance should include:

1) Performance optimization of two-dimensional nozzle contours.
2) Investigation of the effects of wall (esp. throat region) heat transfer.
3) Investigation of the influence of active surface cooling on exit flow uniformity.
4) Viscous effects in all of the above.
5) Assessment of coupled real gas effects to all of the above.
6) Assessment of radiative reactions near the nozzle throat.
7) Comprehensive study to determine the most appropriate three body recombination catalyst(s).
8) Influence of NO_2 reactions on the chemistry above Mach 12.

4.0 Facility Nozzle Throat Heat Transfer

The previous sections make clear that for the test conditions considered, the mixing chamber and the facility nozzle throat conditions will be severe due to the high enthalpy and pressure in these regions. In addition, the test times contemplated for this facility are sufficiently long that time-dependent heat conduction will occur through the nozzle walls. Hence, the surface temperature will also vary with time, requiring transient calculations to estimate the magnitude of the temperature rise and to determine the most efficient technique for dissipating heat from the wall.

A preliminary assessment was made of the transient temperature and heat flux distribution to be encountered in the pilot scale facility nozzle throat at Mach 16 direct connect conditions. These calculations were then extended to full-scale dimensions, and from Mach 10 to 20 conditions. Various pure metals and alloys were investigated to estimate typical survival times of the metals, and to indicate if an uncooled throat is feasible. Ablation rates were then estimated to determine if an ablative insert can be used. Finally, transpiration cooling was briefly evaluated as a candidate heat dissipation technique and an estimate was made of the coolant mass flow rate necessary for throat survival. Alternate dissipation techniques are listed and an approach to developing the best solution to this problem is outlined in section 7.

4.1. Temperature Response for a Heat Sink Throat

It was mentioned in the Introduction that the original development program for the EWT called for a pilot facility. An estimate of the transient heat flux and temperature response were therefore required to assess the magnitude of the throat cooling problem at this scale. However, available power supply limitations reduced the dimensions of the facility (from a $1/30^{th}$ scale to $1/50^{th}$), particularly the facility nozzle, to such a small scale as to make the pilot facility concept impractical. In retrospect, even the $1/30^{th}$ scale facility was too small. For instance, the throat radius of the nozzle for a Mach 16 direct connect simulation is one millimeter for a $1/50^{th}$ scale facility and 1.3 mm for the $1/30^{th}$ scale facility. The exit radii are 0.6 inches and 0.75 inches for the two nozzles, respectively. It was subsequently realized, however, upon making similar calculations for the full scale facility, that the transient heat flux per unit surface area was of the same order for both the full scale and pilot scale facilities. The reason for this is described below. Hence, the pilot scale heat flux calculations can be used to approximately represent the heat loads per unit area at the full scale facility nozzle throat.

The transient temperature response of a heat sink throat was modelled by assuming a one-dimensional convection boundary condition for a semi-infinite solid. The solution to this problem is in Reference 27 as a function of the dimensionless variables θ, $h\sqrt{(\alpha t)}/k$ and $x/2\sqrt{(\alpha t)}$. Here, θ is the ratio $(T-T_i)/(T_\infty-T_i)$, where T_i is the initial surface temperature, and T_∞ is the free stream or core flow temperature. Also, h is the convective heat transfer

coefficient of the gas, α is the thermal diffusivity of the solid, t is time, k is the thermal conductivity of the solid, and x is distance into the solid from the surface.

Calculating the convective heat transfer coefficient at the throat requires estimating the transport properties of the gas at the local thermodynamic conditions. This task is not trivial because data is scarce and widely varying at temperatures of about 7000 K. In addition, most of the data collected are at pressures on the order of one atmosphere, and the transport properties of air become fairly strong functions of pressure at high temperatures. The range of calculated viscosity and thermal conductivity coefficients at these conditions is almost an order of magnitude from the references surveyed[15,16,19,28,29,30] because of uncertainties in the collision cross sections and because of increasing levels of atomic and electronic excitation. (Even low levels of ionization greatly influence the thermal conductivity because the electron's high velocity transports a large portion of the kinetic energy.[15]) For this study, the transport properties were obtained by averaging the values predicted from kinetic theory rather than from measured data because of the ability to account for the influence of pressure.

The convective heat transfer coefficient was estimated from an empirical Nusselt number correlation for turbulent, fully developed flow in smooth pipes (entrance effects were found to be small). The estimated transport properties, and the calculated Reynold's number and Nusselt number for a 2 mm diameter throat at Mach 16 direct connect sonic conditions are:

$$k = 0.45 \text{ W/m-K}$$

$$\mu = 2 \times 10^{-4} \text{ kg/m-sec}$$

$$Pr = 0.62$$

$$Re_D = 1.0 \times 10^6$$

$$Nu_D = 1100$$

The resulting heat transfer coefficient is 250 kW/m^2-K or 0.085 Btu/in^2-sec-°F. Note that the Nusselt number is a function of the diameter raised to the 0.8 power. Since the heat transfer coefficient is related to the Nusselt number by the ratio k/D, it is a function of $D^{-0.2}$, or area $A^{-0.1}$. For a 50-fold increase in facility scale, the heat transfer coefficient drops by only 32 percent. In other words, although the actual heat transferred through the full scale facility walls will be much greater, the heat transfer coefficient is only weakly dependent on scale for the assumed flow geometry and boundary layer state. Given the uncertainties associated with the calculation, a 32 percent difference in the heat flux is well within the error bounds of the calculation.

The heat flux was determined using the difference between the adiabatic wall enthalpy and

the enthalpy calculated at the wall temperature assuming equilibrium chemistry. The resulting temporal surface temperature and heat flux distributions are shown in Figures 35 and 36 for an initial surface temperature of 300 K, and for the room temperature material properties of OFHC (Oxygen-Free, High Conductivity) copper. The temperature profile in Figure 35 indicates that in the predicted test time of 0.2 seconds, the surface temperature of the nozzle rises to almost the free stream value. The heat flux profile seen in Figure 36 indicates that the average value over the test time is significantly greater than typical heat fluxes encountered in rocket nozzle throats, which are between 10 to 30 Btu/in^2-sec, and about one order of magnitude greater than the stagnation point heat flux of a ballistic missile during reentry at low altitude.

The heat transfer coefficient, the wall temperature at a test time of 0.2 seconds, and the time-averaged heat flux over a 0.2 sec interval were calculated for Mach 10 through 20 conditions and are shown in the table below. The copper throat was assumed to be initially cryogenically cooled to 70 K.

Table 11. Calculated Average Heat Transfer at the Facility Nozzle Throat Copper Heat Sink; Initially Cooled to 70 K

Flight M	Configuration	h(Btu/in^2-s-° F)	T_w (K) at t=0.2 sec	q(Btu/in^2-s) (average)
10	Direct Connect	0.0061	560.	37.
10	Free Jet	0.017	1380.	98.
12	Direct Connect	0.018	1900.	160.
12	Free Jet	0.051	3450.	415.
16	Direct connect	0.0850	6300.	1030.
16	Free jet	0.260	7100.	3150.
20	Direct connect	0.627	9600.	10,100.
20	Free jet	2.310	10700.	46,500.

The wall temperatures suggest that an uncooled throat will probably suffice for at Mach 10 to 12. However, oxidation will be significant. The heating rates at Mach 20 conditions seem well beyond current technology.

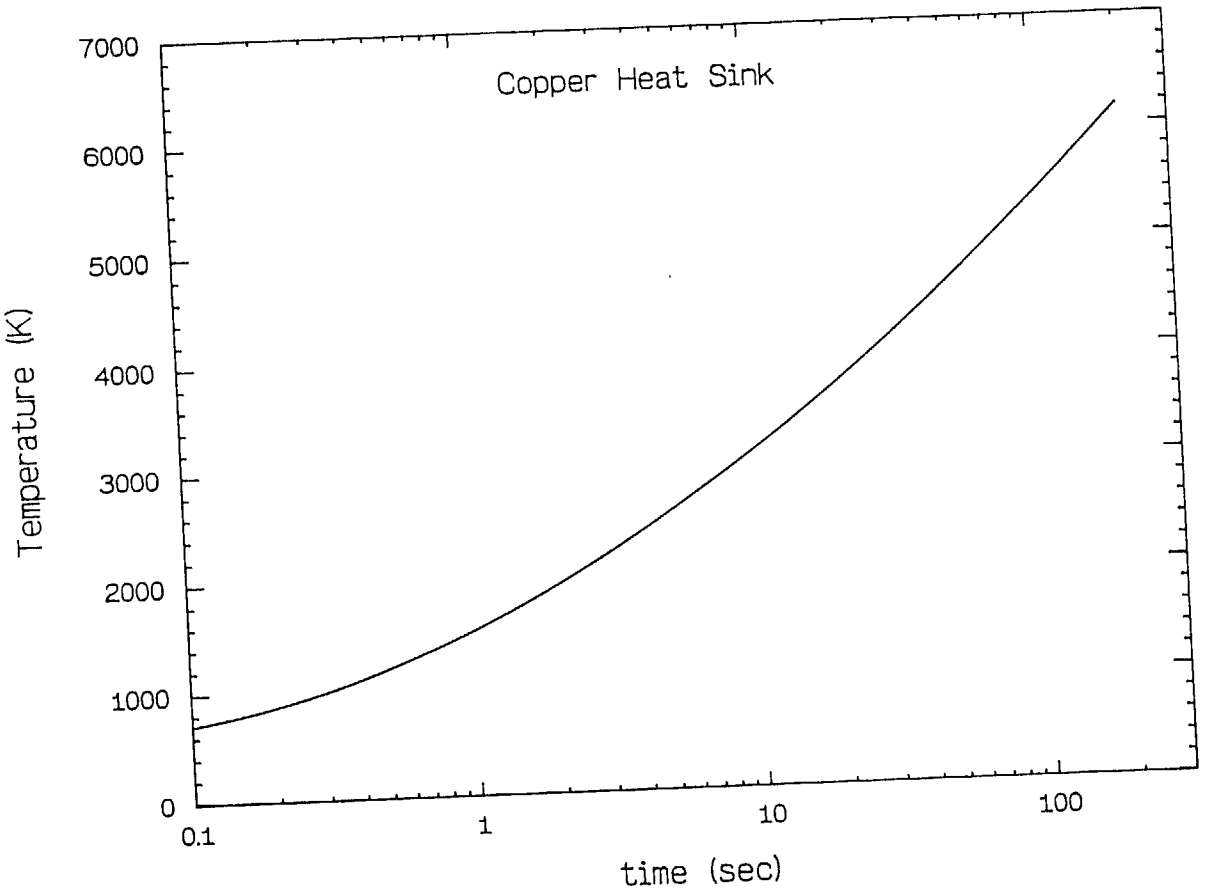

FIGURE 35 CALCULATED WALL TEMPERATURE RESPONSE AT FACILITY NOZZLE THROAT, COPPER HEAT SINK, T_i =300 K

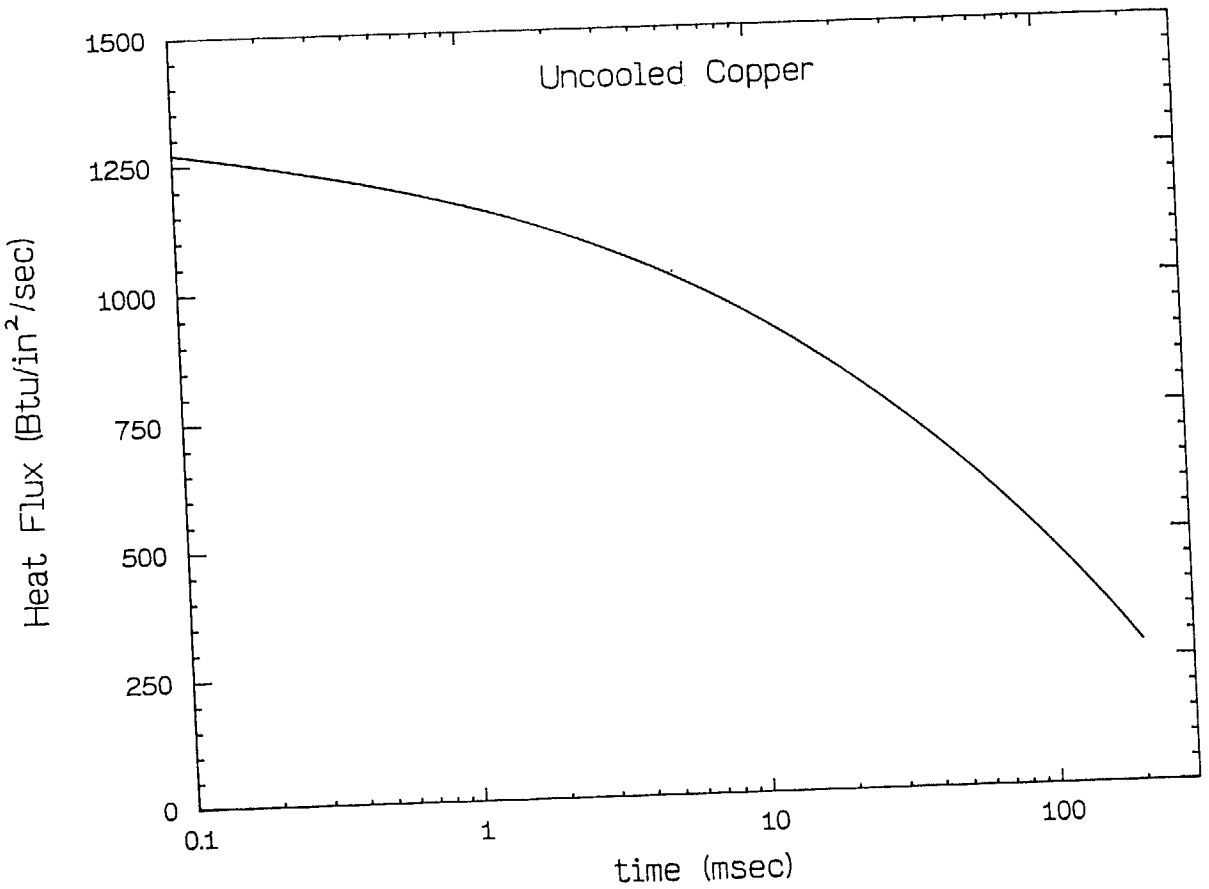

FIGURE 36 CALCULATED WALL HEAT FLUX AT FACILITY NOZZLE THROAT, COPPER HEAT SINK, T_i =300 K

It is immediately apparent that no heat sink material will survive the test duration above about Mach 12 simulation without melting, vaporizing, subliming, and/or ablating to some extent. In spite of this, heat sink calculations of this type are useful for comparing relative survival times and identifying potential materials for use with other cooling methods. Hence, the transient temperature response was determined for several other candidate heat sink materials. The materials investigated were OFHC copper, 1020 carbon steel, pure tungsten, and a 90 percent tantalum - 10 percent tungsten alloy (Ta-10W). Figure 37 shows the transient temperature profiles for these materials. It is seen that the refractory metals are not much better than copper in surviving this environment. In fact, copper alloys having higher melting points than pure copper but retain a high thermal conductivity, e.g., "Naralloy Z" (Cu-0.1Z), may outlast the refractory metals. Steel will melt almost immediately due to its relatively low conductivity and density. The variation of material properties with temperature was not accounted for here, but will affect the performance of the material to some extent.

The figure of merit for evaluating the thermal performance of a heat sink material is the quantity $\sqrt{(\rho Ck)}T_m$, where T_m is the melting point of the material, and C is the heat capacity[18]. Values of this parameter at room temperature for the materials discussed are listed below.

Material	$\sqrt{(\rho Ck)}T_m \times 10^{-6}$, $J/m^2\sqrt{s}$
Carbon steel (1020)	33.0
Ta-10W	38.2
OFHC Copper	51.4
Tungsten	76.5

Although copper has a relatively low melting point, its high thermal conductivity and heat capacity make it comparable to the refractory metals, as was seen in the temperature response profiles in Figure 37. Clearly, one desires high values of all the quantities in this parameter to maximize the heat sink characteristics, all other things being equal. However, other qualities are also important, such as a high yield strength, a low coefficient of thermal expansion, and oxidation resistance. Tungsten has a high tensile strength but oxidizes rapidly above 450 K. A replaceable liner might be used to prevent the load carrying structure from coming in contact with the oxygen. Materials which may be appropriate for this application include tungsten, with an oxidation-resistant coating, and cubic boron nitride which has properties very similar to those of diamond.

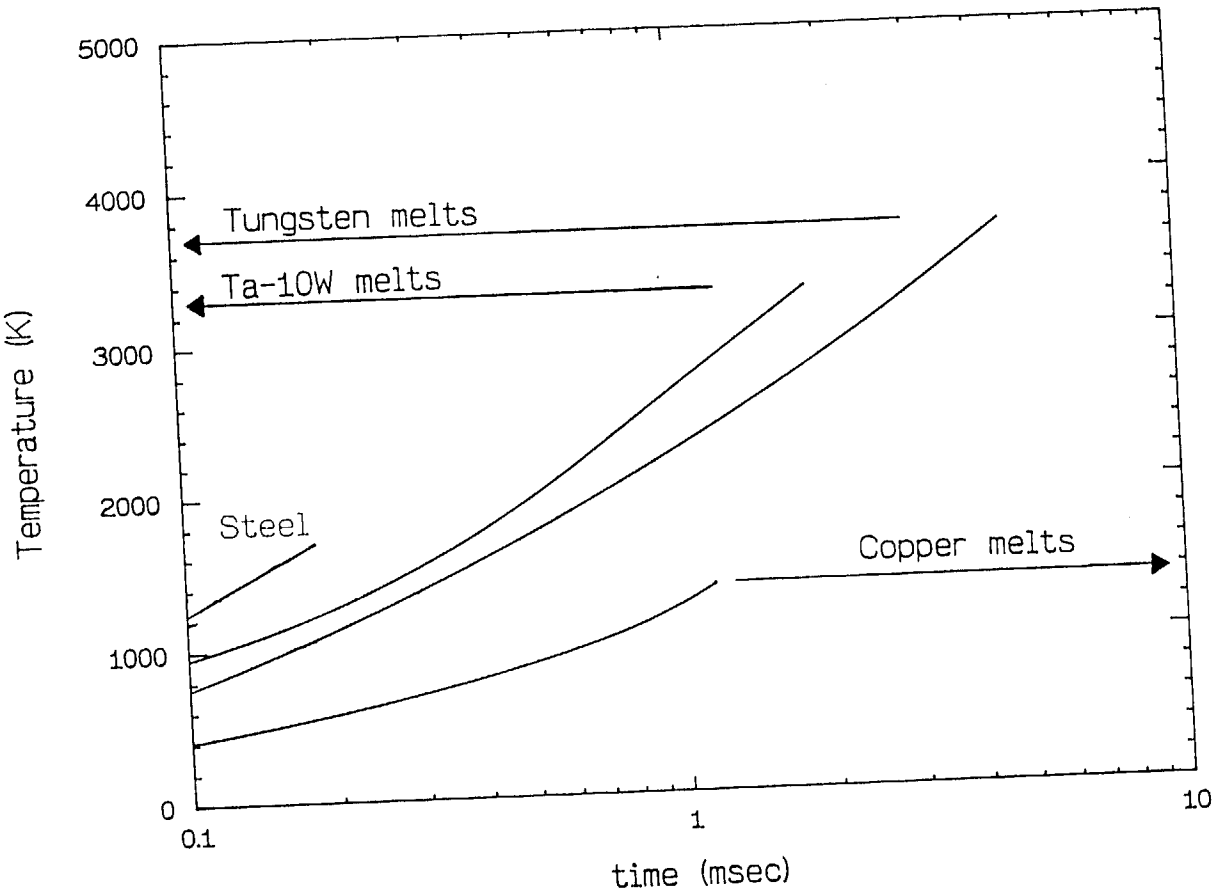

FIGURE 37 WALL TEMPERATURE RESPONSE FOR VARIOUS HEAT SINK MATERIALS, T_i =70 K

4.2 Preliminary Evaluation of an Ablative Throat

Preliminary estimates were made of the possibility of going in the above direction, i.e., designing for an easily-replaceable throat insert (liner) and permitting some minor ablation during each test. The philosophy is: If the throat area increase during the test time is sufficiently small (i.e., so that the facility nozzle exit Mach number change is similar to Mach number changes along a flight path in a similar time frame), then ablation may represent the most cost-effective method of dealing with the high throat heat fluxes.

To this end, the methods developed in Reference 31 were used. The problem treated therein is the reentry stagnation point heat transfer problem, which is clearly a different situation than we face. On the other hand, the lack of data at these extreme conditions ("sublimation" temperatures, latent heats, etc.) required the use of "normal" values for these quantities, driving the results in directions that must be subsequently assessed (see section 6). In any event, assuming tungsten to be the throat insert material, the following area changes were determined for Mach 16 direct connect tests:

Test time, seconds	Percent Area change
0.1	6.7
0.2	13.6

Of consequence here is the fact that the area changes cited above suggest that an ablative wall may be an acceptable approach to dealing with the throat problem. At a minimum, these numbers dictate that further investigations be pursued.

It should be emphasized that pure tungsten may not be the material ultimately selected, but was used here by way of illustration because its properties are well known. Other candidate materials would require evaluation as well (e.g., graphite, phenolic resin with reinforcement, cubic boron nitride, etc.). The idea is to select a material which will not ablate in the usual sense, but will either sublime or "erode" microscopically and be confined to the boundary layer. However, the flow development of a high Mach number nozzle is particularly sensitive to disturbances (mass transfer, oxidation, surface roughness, etc.) in the boundary layer near the sonic region. The effects of these disturbances on the nozzle core flow would of course have to be assessed. In any case, graphite, which sublimes at temperatures as high as 3900 K, dissipates heat through the mechanisms of sensible heat rise, oxidation, latent heat of sublimation and surface radiation. Because of its extremely high ablative efficiency, graphite theoretically offers the minimum amount of ablation and shape change, as well as a high heat capacity. The principal disadvantages of graphite, which are its brittleness and its low resistance to thermal stress, do not detract from its application as a liner since the loads will be carried by the outer containment structure.

Other candidate methods of cooling (besides the heat sink and ablative approaches) must be evaluated carefully. Some of these methods are:

(a) Film cooling
(b) Transpiration cooling
(c) Boundary layer thickening (i.e., by the introduction of material into the boundary layer upstream of the throat)

These alternatives are discussed in the section 7, but transpiration cooling was looked at briefly to indicate whether the required mass flow coolant rates were reasonable compared to the test gas mass flow.

4.3 Preliminary Evaluation of a Transpiration-Cooled Throat

From a thermodynamic point of view, transpiration is the most efficient method for cooling a heated surface[32]. The cooling medium flowing through and out of the porous structure acts to conductively cool the structure and reduce the surface heat transfer rate. The heat transfer is reduced by a thickening and cooling of the boundary layer, in effect reducing the wall temperature and velocity gradients. At sufficiently large coolant flow rates, however, the mass addition, as mentioned above, tends to transition or destabilize the boundary layer or induce separation. Hence, for a given reduction in the heat transfer coefficient ("blocking factor"), the critical parameter for evaluating the feasibility of a transpiration-cooled surface is the required ratio of coolant to boundary layer mass flow rate per unit area, or the "blowing factor".

Estimates of the coolant mass flow required for a given reduction in heat transfer coefficient can be determined from semi-empirical correlations based on a mixing length theory for coolant gases injected into air.[32,33] Figure 38 taken from Reference 20 compares such a correlation with data for several gases injected into a turbulent boundary layer. The ordinate is the blocking factor, and the abscissa is the ratio of coolant mass flow to Nc_o, which is the nominal heat transfer coefficient without cooling.

The blowing factor was calculated from this correlation for the Mach 16 direct connect nozzle throat. The coolant (helium) and porous structure (tungsten) were assumed to be in equilibrium at a surface temperature of 2000 K. The heat transfer coefficient required to maintain this surface temperature is 13.3 kW/m^2-K, and hence the blocking factor is 0.053. The boundary layer mass flow was calculated assuming a linear temperature profile and a 1/n-th-power law velocity profile, with n=8.8 for fully turbulent flow in smooth pipes at the given Reynold's number.[33] The calculated blowing factor of 0.0036 is large compared to typical values of 0.0002.

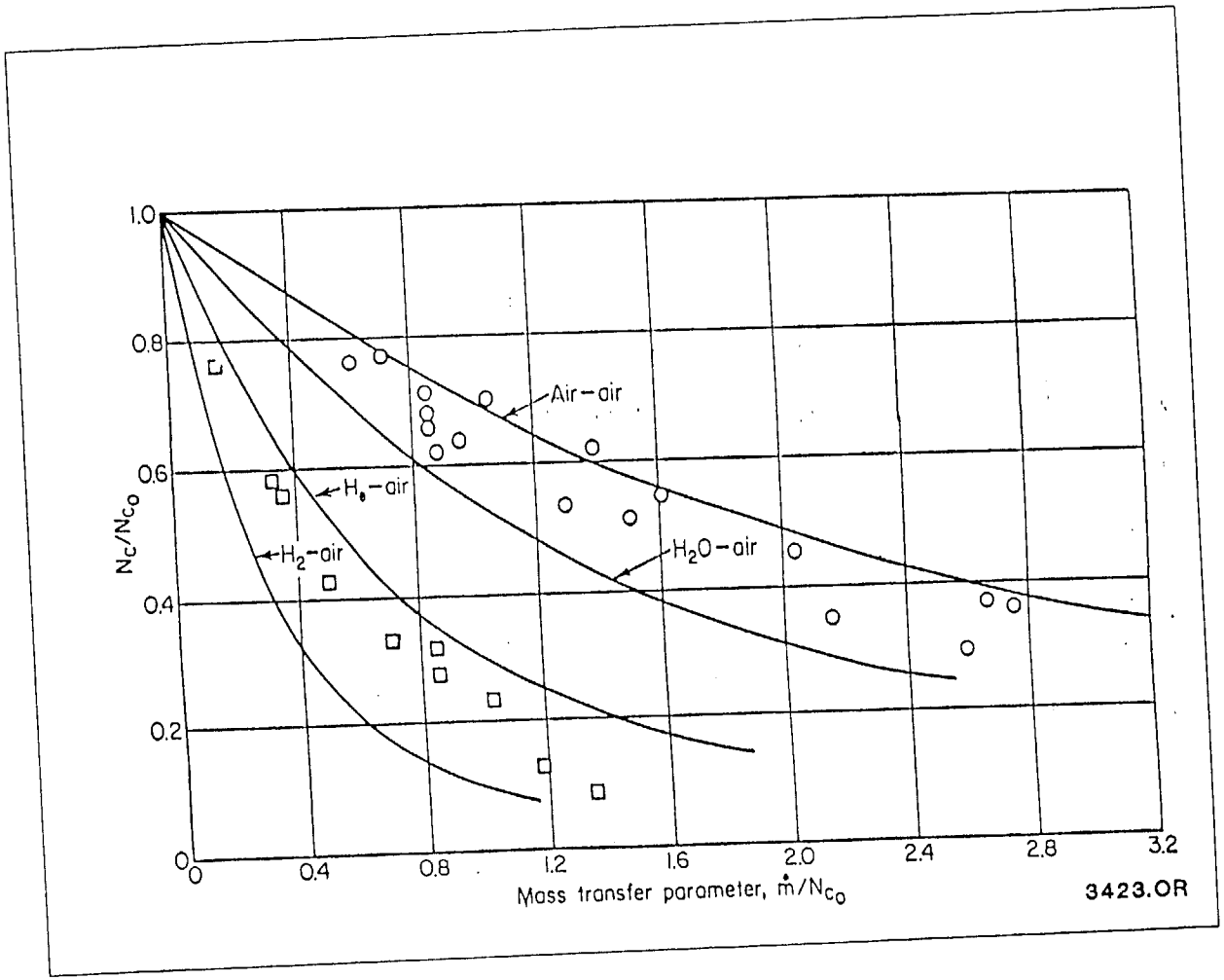

FIGURE 38 THE EFFECT OF MASS TRANSFER ON THE TURBULENT HEAT TRANSFER RATE

There are several other problem areas which must be addressed before transpiration cooling is determined to be a practical solution to the problem at hand. First, the structural material must be formed such that the pores possess small hydraulic diameters on the order less than 0.001 inches. Significantly larger pores result in a decrease in cooling efficiency which approaches that of film cooling. If the porous material has a three dimensional flow characteristic, then the distribution of coolant mass flow will be dependent on the pressure drop through the material, and local hot spots may develop on the surface. Second, the effect of the transpired coolant on the stability and development of the boundary layer and the expanding core flow must be determined, with the obvious objective being to minimize disturbance to the core flow. Resolution of these issues will require sophisticated CFD in concert with experimental verification. Some of the necessary steps are outlined in section 7.

Another concern, and a major cost driver, is the powerplant required for this facility. R. Burton has contributed the next section, which describes the powerplant requirements and evaluates in detail the various types of power supplies suitable for this facility for two test times, 500 milliseconds and 25 milliseconds.

5.0 Powerplant Options for a 500 msec Full Scale Electrothermal Wind Tunnel

General Requirements

The power supply for a full scale electrothermal wind tunnel requires 650 MW at a mass flow of 17 kg/sec (37 lb/sec), when operating at maximum (Mach 20) enthalpy. It is assumed that the electrothermal heater is 50% efficient. The design conditions are summarized below:

Assumed Design Conditions, Full Scale Tunnel

Electric Power	650 MW
Pulse length	0.5 sec
Total electric energy	325 MJ
Heater efficiency	0.50
Stagnation enthalpy (air)	2.3×10^7 J/kg
Nozzle kinetic efficiency	0.80
Exit velocity	6100 m/sec

The power requirements are then:

Power Requirements, Full Scale Tunnel

Electric Power	650 MW
Pulse length	0.5 sec
Electric energy, DC pulse	325 MJ
Total energy, zero-to-zero	500 MJ
Heater resistance	0.5 Ω
Current, DC pulse	36,100 amperes
Voltage, DC pulse	18,000 volts

Operating on a pulsed basis, the flat-top of the pulse is assumed to be 0.5 seconds long. The pulse will consist of a ramp-up of a few tenths of a second, a 0.5 sec flat-top, and a rapid shut-down of a tenth second or less. The start-up and shut-down increase the total energy requirement from current zero to current zero by ~50%, for a total of 500 MW.

Power Transmission

Transmitting the required level of current from the source to the tunnel is not difficult, allowing flexibility in the placement of the power source, which can be some distance away. A 5 cm (2 inch) busbar has an electrical resistance of 10 μΩ/meter, giving only 1 mΩ resistance per 100 m. This is 0.2% of the load resistance, and can be neglected. Even 500 m separation between the source and the tunnel could be tolerated.

Switching

The switching must be considered together with the power source, since requirements vary widely. All sources will require a closing switch to initiate power to the arc heater. Some sources will require an opening switch to disconnect the source from the heater. Other sources will require no closing switch, since the energy store in the source is limited to that required by the pulse.

Switching costs are difficult to estimate and are not included in this discussion. To some extent switching and its costs can be considered as part of the arc heater system, rather than the power source.

Power Supply Options

Four basic power supply options exist: chemical battery, electrical capacitor, mechanical flywheel, and the commercial grid. All of these could do the job, but each has its limitations. The different options are discussed below. The primary factors considered are design, switching, cost, complexity, safety, and maintenance. Costs for all the systems below are sensitive to the assumed pulse length of 0.5 seconds and could be reduced significantly with shorter pulses.

Batteries

Large battery banks, as exist at Eglin AFB, have been constructed. These are lead-acid, 12 volt, and are mounted on racks. A DC charger must be supplied. In order to supply the required voltage, approximately 1000 batteries must be connected in series. The resulting high voltage means that the batteries must be insulated from their racks and undetermined procedures must be evolved to permit maintenance without hazard to the crew. Charging releases hydrogen gas, requiring detectors and fans. A good quality battery can deliver 6500 watts, requiring 100,000 battery units weighing 2500 tons. Maintenance consists of checking electrolyte levels and the tightness of connections, of which there are $2x10^5$. The total energy storage of the system is estimated to be 1 TJ (terajoule=10^6 MJ), or 2,000 times the requirement. [1 TJ is the equivalent of 250 metric tons of He]. This places a stiff requirement on switching, which must be highly reliable to prevent a runaway discharge. At an installed cost including a (40,000 ft^2 building) of $250/battery, the total cost is $25 million, not including switching. Maintenance is roughly estimated as requiring 2-4 full-time workers.

It can be argued that many of the above objections can be overcome by proper design, perhaps packaging the batteries in 1000 volt units for example. The high energy and switching requirements would remain, however.

Capacitors

Electrical storage capacitors are now routinely used up to energy levels of tens of megajoules. Single units storing 0.25 MJ are available, and 1 MJ units are being worked on. The required voltage is not a problem as capacitors are now available from 1 to 100 kV, and current levels of 100's of kiloamperes are not uncommon.

An energy level as large as is required here has never been attempted, but cannot be ruled out. There are other difficulties with capacitors to be addressed, however. The most difficult is the pulse shape. The capacitor is usually connected to inductor coils for pulse shaping, which in effect transfers the capacitor energy to magnetic energy sustained by currents circulating in the inductors. The difficulty is that the inductors, unless made of superconductive material, have an electrical resistance which degrades the pulse. The only remedy is to make the inductors very large (several tons) to reduce their resistance. Even then, inductors can only be discharged for tens of milliseconds, requiring perhaps 10 separate banks to be discharged in sequence, with associated controls, switching and current ripple resulting from the "handoff" from one bank to another.

There is an alternate approach. Assuming that the capacitors stored energy at 30,000 volts, the capacitance for the required storage of 325 MJ would be 0.722 farads. If conductors were not used, the capacitors together with the load resistance would form an RC circuit with a decay time constant of 0.36 seconds, too fast for this application. Assuming a bigger bank so that $RC = 10t_p = 5$ sec, the required capacitance would be 10 farads, 14 times bigger than required. Total bank storage would then be 2 GJ (gigajoules) and the current would slowly decrease during the pulse.

Capacitor units cost 5 cents/joule, and 2-4 times that amount installed. Assuming 10 cents/joule or \$100K/MJ, a 325 MJ bank would cost \$33M and a 4.5 GJ bank would cost \$450M. This implies that the RC approach will not work and that inductors will indeed be required. Since they would have to be quite large to keep their resistance low, it is roughly estimated that they would double the cost of the system. Considering switching and other uncertainties, it is estimated that the total bank would cost ~\$60M.

Motor-Flywheel-Generators

Large currents for the powering of Tokamak magnets, as at the Princeton Plasma Physics Laboratory, are supplied by a mechanical flywheel with generator. This type of equipment is also available at the former Westinghouse pulse power laboratory in Pittsburgh. The current pulse is roughly sinusoidal, requiring that the arc be run only near the top of the pulse. The power output for the Princeton system is roughly 1000 MW for 1 sec, with a total energy storage of 2 GJ. Power for spin-up is supplied by the commercial grid. The 13 MW available at LaRC, assuming that it could be used, would achieve spin-up in 150 seconds for 2 GJ, and less than that for a 325 MJ system. Slower spin-up power levels could also be accommodated.

The cost of the Princeton system was ~$40M when installed about 12 years ago. Since LaRC would require less energy and power, it is suggested that this price could be cut to perhaps $20-$30M. It is possible that a used unit is available somewhere, and could be moved to LaRC for $10M. The building required to house the unit is small, perhaps 4000 ft^2.

Safety and operational aspects of the flywheel approach are favorable. A runaway discharge is not possible, since energy storage is limited. Maintenance requires a half-time technician for the flywheel system. Environmental hazards are small.

It is conceivable that a compatible flywheel unit exists somewhere that could be used for initial testing and component development. This would minimize risk to the program, since all other components could be developed before making a buy decision on a power supply.

Commercial Grid

The commercial grid is an option, and is used at the NASA AMES arc heater facility. Installation cost is probably the lowest, assuming that 650 MW could be tapped off the grid. Drawbacks are obvious in that 650 MW tunnel operations could probably only be performed after midnight. Highly reliable opening switches would be required, as for the battery situation. Re-configuration of power company trip relays and circuit protection devices might be required. Operating costs would be high, since the power companies charge according to peak power drawn, not total energy consumed. Commercial and residential growth in the Hampton, VA area could conceivably force a curtailment or shutdown of activities in the future.

Summary

In our opinion, the possible power supply sources should be ranked as shown below, together with their principal characteristics.

Table 12. Comparison of Power Supplies for a 0.5 Second Full Scale Facility

TYPE	ENERGY	INSTALL COST	OPERATE COST	SAFETY	MAINTENANCE
Flywheel	500 MJ	$10-40M	Low	Good	Low
Comm. Grid	Not Limited	Not Known	High	Good	Low
Capacitors	500 MJ	$60M	Low	Fair	Low
Batteries	10^6MJ	$25M	High	Poor	High

We believe that the flywheel system represents the best overall choice for cost, safety, maintenance, and compatibility with the environment at NASA Langley. We propose that efforts should be concentrated on this approach, particularly with respect to cost, switching and availability of existing facilities.

5.1. Options for a Full Scale, 25 msec Electrothermal Wind Tunnel

General Requirements

If it is assumed that the desired pulse length is 25 msec, producing approximately 30 slug lengths on a 15 foot model, the power requirements are then:

Power Requirements for a 25 MSEC Full Scale Tunnel

Electric Power	650 MW
Pulse Length	25 msec
Electric Energy, DC Pulse	16 MJ
Total Energy, Zero-to-Zero	25 MJ
Heater Resistance	0.5Ω
Current, DC Pulse	36,000 amperes
Voltage, DC Pulse	18,000 volts

Operating on a pulsed basis, the flat-top of the pulse is assumed to be 25 msec long. The pulse will consist of a ramp-up of a few msecs, a 25 msec flat-top, and a rapid shut-down of 5 msecs or less. The start-up and shut-down increase the total energy requirement from current zero to current zero by ~50%, for a total of 25 MW.

Power Supply Options

As in the previous section, four basic power supply options exist, listed in order of preference for the 25 msec application: electrical capacitor, commercial grid, mechanical flywheel, and chemical battery. The primary factors considered are the same as for a 500 msec power supply.

Capacitors

An energy level of 25 MJ as is required here is large for a capacitor system, but is straight forward. The capacitor would be connected to inductor coils for pulse shaping, which in effect transfers the capacitor energy to magnetic energy, sustained by currents circulating in the inductors. The inductors, unless made of superconductive material, have an electrical resistance which degrades the pulse. The inductors must therefore be made large (hundreds of kilograms of copper or aluminum) to reduce their resistance.

Capacitor units cost 5 cents/joule, and 10-20 cents/joule installed. Assuming 10 cents/joule or $100K/MJ, a 25 MJ bank would cost $2.5M. It is roughly estimated that the inductors would double the cost of the system. Considering switching and other costs, it is estimated that the total bank would cost ~$7M. It is estimated that it would take 18 months to design, fabricate, install and checkout a 25 MJ bank.

Power Transmission

Transmitting the required level of current from the source to the tunnel is not difficult, allowing flexibility in the placement of the power source, which can be some distance away. A 5-cm (2-inch) busbar has an electrical resistance of 10 $\mu\Omega$/meter, giving only 1 mΩ resistance per 100 m. This is 0.2% of the load resistance and can be neglected. Even 500 m separation between the source and the tunnel could be tolerated.

Switching

One difficulty for a short pulse is that the switches must operate on a ~5 msec time scale, possibly ruling out electromechanical devices.

Summary

In our opinion, the possible power supply sources should be ranked as shown below, together with their principal characteristics.

Table 13. Comparison of Power Supplies for a 25 msec Full Scale Facility

TYPE	ENERGY	INSTALL COST	OPERATE COST	SAFETY
Capacitors	25 MJ	$7M	Low	Fair
Comm. Grid	High	Not Known	Medium	Good
Flywheel	>25 MJ	$10-40M	Low	Good
Batteries	10^5 MJ	$25M	High	Poor

We believe that for the 25 msec application the capacitor system represents the best overall choice for cost, safety, maintenance, and compatibility with the environment.

6.0 Preliminary Simulation Envelope of the EWT

The simulation envelope of the EWT was estimated based on the calculations in sections 2 through 5. That is, the range of flight conditions which would result in acceptable nozzle performance, containable total pressures, throat heat flux considerations, and power supply limits. The results of these calculations are shown in Figure 39, which maps the portions of the flight envelope where these conditions are met. The solid lines represent flight paths for flight dynamic pressures of 500 to 2000 psf. The dashed and dotted lines bound the simulation regime for the direct connect and free-jet conditions, respectively. Simulation of free-jet conditions is seen to be limited by the total pressure and throat heat flux generated. The test gas composition at the facility nozzle exit for these conditions is comparable with that for the Mach 16 free jet condition. Direct connect simulation is limited by nozzle kinetic performance to Mach 16 at q=1000 psf and to about Mach 13 at q=2000 psf. The remainder of the upper flight envelope is bounded by power limitations.

Note that the simulation envelope does not take into account off-design performance of the cryogenic arc or cryogenic pump and capillary mass flow limitations. A preliminary design of the full scale facility is necessary before such factors can be properly incorporated.

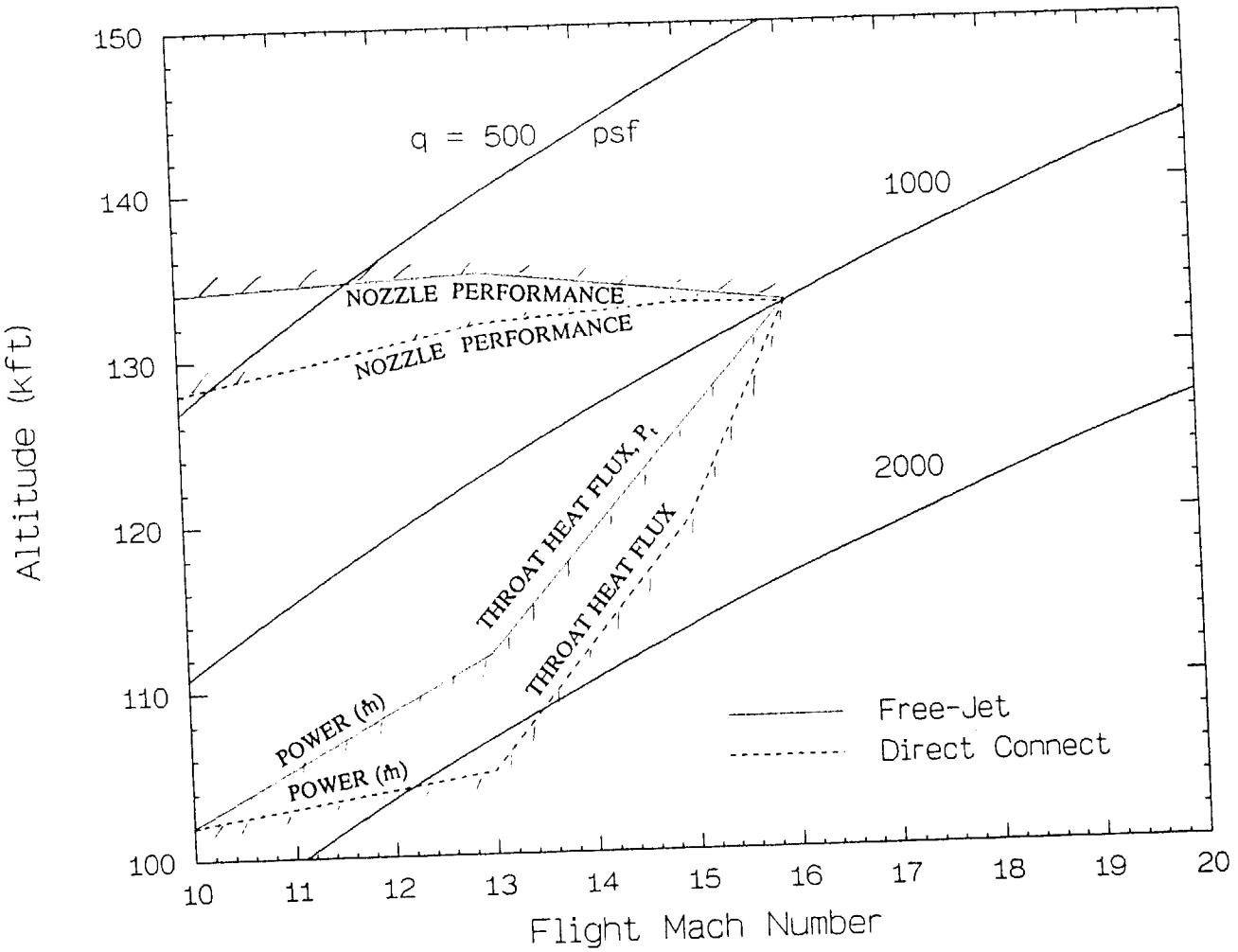

FIGURE 39 PRELIMINARY EWT SIMULATION ENVELOPE

7.0 Recommendations for Phase II Studies

The previous sections enumerated the various technical problems to be encountered in the development of a full scale electrothermal wind tunnel, and discussed feasible solutions to those problems. Before recommending a plan for performing the work required, we felt it appropriate at this point to consider once again some of the other facility concepts capable of providing similar simulation capabilities. Consideration will then be given to addressing the unique problems which will be encountered in the design of this facility.

7.1 Alternate Facilities Comparison

The alternative facilities investigated were:

1. a. Free piston-driven reflected shock tunnel
   b. Free piston-driven expansion tube/tunnel
   c. Free-flight facilities, e.g. Aeroballistic range, Aerophysics facility, ram/scram accelerators, etc.
   d. MHD accelerator

The criteria considered were:

2. a. Total cost (for a facility having one second test duration)
   b. Test flow quality
   c. Cost per test
   d. Model constraints

This list does not attempt to encompass all the necessary criteria nor does it attempt to prioritize them in an absolute sense. Certainly, other criteria could be added and more detailed studies made. However, we felt that within the scope of this report, the following study was sufficient to reassure ourselves that the EWT concept still holds the promise of fulfilling the "near term" (i.e., the next decade) needs of the hypervelocity airbreathing propulsion community.

All of the facilities mentioned here including the EWT are (more or less) capable of simulating the conditions required for hypervelocity propulsion testing, albeit via fundamentally different concepts. However, their practicality is limited by the length of time that they can sustain these conditions if the test time of the EWT ($\sim$ 1 sec) is considered the reference value and the minimum required for testing many aspects of a propulsion system. Therein lies the major drawback to both the free piston-driven reflected shock tunnel and expansion tube, and all of the free flight facilities mentioned in 1. c. In the case of the reflected shock tunnel and the expansion tube/tunnel, the test duration scales, to first order, with facility length. However, the tube diameters must be scaled up linearly (at least) with tube lengths to keep boundary layer effects from dominating the test time, i.e., shock

attenuation effects in the expansion tube and driver gas contamination in the reflected shock tunnel. The cost of a 1 msec reflected shock tunnel (e.g., T5 at Cal Tech) is (roughly) on the order of $3 million, of which about one-half is in hardware. The hardware replacement cost of the HYPULSE 6" expansion tube is of the order of $4 million. If the hardware costs scale with weight only, then a 10^3-fold increase in test duration implies a 10^6-fold increase in cost, assuming that the length to diameter ratio is maintained. Obviously, pulse facilities are viable candidates for no more than a 10-fold increase in test time, unless alternate, low cost manufacturing techniques for large, high pressure containment structures can be devised.

The reflected shock tunnel inherits an additional disadvantage in its limited total pressure simulation capability. The relatively low total pressure causes substantial dissociation of the test gas behind the reflected shock and results in extremely poor nozzle recombination kinetics. Consequently, the oxygen is almost completely dissociated in the test section at the higher flight conditions ($\geq$ Mach 15). The expansion tube, on the other hand, adds kinetic energy rather than thermal energy to the gas. This produces a very clean test gas with minimal contaminants and dissociation. The cost per test for both the shock tunnel and the expansion tube are comparable and lower than for the EWT, the primary difference being the maintenance and operational costs of the power supply, and the number and cost of expendable items per shot (e.g., capillary linings, liquid air, possible throat inserts, etc.). Model constraints are for the most part similar among all three facilities since each must expand the flow through a facility nozzle to obtain reasonable test section dimensions.

The free-flight facilities possess some unique features, but the drawbacks appear to be overwhelming at this time. It is the only type of facility, for instance, that truly duplicates hypervelocity test conditions, including ambient turbulence levels. But the cost per test can approach that of actual flight tests, with similar remote instrumentation, telemetry, and survivability costs. Additionally, the model and its instrumentation must withstand tremendous acceleration loads on the order of 20,000 g's. The constraints placed on the types of models tested in the free flight facilities are perhaps the most restricting of any facility. Besides the limitation that the mass of the model must decrease rapidly with test velocity, the model shape must permit flight stability, yet produce zero net lift. However, knowing precisely the aerodynamic forces on the model implies the ability to predict the results of the experiment a priori. Model survivability rates must therefore be assumed low, increasing further the cost per test which has been estimated at between $100,000 and $1M.

The last type of facility considered, the MHD accelerator, may perhaps hold the most promise in the long run for simulating hypervelocity combustion test conditions for significant test times. Like the expansion tube, the MHD concept allows energy to be added to the test flow kinetically rather than thermally. Test gas dissociation is therefore minimized. However, contaminants are present in the form of the alkali metal seed material used to enhance the ionization, which can compromise the simulation of chemical kinetics. Unseeded MHD accelerator concepts have been proposed where, for instance, microwave radiation increases ionization in the test gas by raising the electronic temperature

independently[34]. However, these concepts are largely untested and probably will require significant development efforts and funding to prove the technology. The EWT is estimated to require 2500 MW/m^2 based on demonstrated ET gun technology. The power required for an MHD facility producing static pressures suitable for combustion testing at Mach 20 is of the order of 4,000 MW/m^2 for an assumed energy conversion efficiency of 50%. Assuming similar model constraints, the EWT is then the most cost effective facility at this time for hypervelocity propulsion development.

7.2 Critical Issues Development Tasks and Schedules

The original concept called for building and testing a one-fiftieth-scale pilot facility at NASA LaRC prior to proceeding to a full-scale facility. These initial studies have made clear, however, that a number of unique problems must be addressed prior to the design of any facility; viz.,

1. Appropriate design and operation of intensifier pumps at cryogenic conditions;

2. Investigation of optimum techniques for dealing with the extreme conditions at the facility nozzle throat (i.e., throat "cooling");

3. Acquisition or development of an appropriate electrical power supply;

4. Proper design of high-pressure-holding vessels (mixing chamber, facility nozzle, etc.);

5. Proper aerodynamic design of the facility nozzle;

6. Proper test chamber and exhaust system design.

Most of the above are facility-dependent; i.e., effectively, design concepts must be re-developed for each new facility and cannot be carried over from a sub-scale facility (e.g., items 2, 3, 4 and 6 above). As a result, it is recommended that Phase II be scaled back from the building of, and testing in, a pilot facility to experimental and analytical studies oriented toward dealing with the problems enumerated above, as well as those discussed below, as applied to a full-scale facility. A subsequent Phase would then proceed directly to the full-scale facility.

Table 14 clarifies the various tasks required to arrive at a successful full-scale design, indicates the lead and supporting organizations for each task, and sets forth a schedule to accomplish these tasks over an 18-month period. Table 15 focusses upon Task 2, the facility nozzle throat heat flux problem, and indicates the alternatives and approaches as we see them at this time.

Table 14. Phase II Tasks and Schedule

TASK	LEAD/SUPPORT	Months from Contract Start: 0 1 2 3 4 5 6 7 8 9 10 11 12 13 14 15 16 17 18
1. Continued development of intensifier pump	GASL/GT-D	
2. Intensifier pump manifolding	GASL/GT-D	
3. Facility nozzle throat heat flux investigation	GASL	
4. Facility nozzle design	GASL	
5. Pressure vessel design	GASL	
6. Test chamber design, instrumentation	GASL	
7. Exhaust system design	GASL	
8. Electrical power source	GT-D/GASL	
9. Scaling up of the capillary	GT-D	
10. Full-scale facility A. Preliminary design B. Final design	GASL/GT-D	
11. Quarterly reports	GASL/GT-D	
12. Final report	GASL/GT-D	

Table 15

Task 3. Facility Nozzle Throat Heat Flux Investigation

Subtask	Description
3.1	Survey available approaches and materials: • Film cooling (slot, platelets); coolants • Transpiration cooling (holes, sintered materials); coolants • Ablation (materials) • Boundary layer thickening (materials, introduction configuration).
3.2	Develop a quasi-one-dimensional analysis to predict required coolant rates (film and transpiration cooling) and required ablation rates.
3.3	Use GASL Shape Change code to assess interaction of coolant/ablation materials on the facility nozzle exit flow quality.
3.4	Validate and "tune" analyses of 3.2 and 3.3 by conducting relatively simple experiments: • HYPULSE • Blow-down wind tunnels • Sub-scale EWT tunnel at GT-Devices
3.5	Use validated analyses to arrive at final configurations, materials selections, flow rates.

References

1. Roffe, G., "Hypersonic Scramjet Test Facility Concept Study", GASL TR 295, June, 1988.

2. Thomas, Scott R., and Guy, Wayne, "Scramjet Testing from Mach 4 to 20, Present Capabilities and Needs for the Nineties", AIAA paper 90-1388, June, 1990.

3. Wagner, D.A., et. al, "Hypersonic Facility Requirements and Design Considerations", AIAA paper 88-1991, May, 1988.

4. Wagner, D.A., et. al, "Hypersonic Test Facility Requirements for the 1990's", AIAA paper 90-1389, June, 1990.

5. Anderson, Griffin Y., "An outlook on Hypersonic Flight", AIAA paper 87-2074, June-July, 1987.

6. Anderson, G., Kumar, A., and Erdos, J., "Progress in Hypersonic Combustion Technology with Computation and Experiment", AIAA paper 90-5254, October, 1990.

7. Rizkalla, Oussama, Bakos, Robert J., Chinitz, Wallace, Pulsonetti, Maria V., and Erdos, John I., "Use of an Expansion Tube to Examine Scramjet Combustion at Hypersonic Velocities", AIAA paper 89-2536, July, 1989.

8. Bakos, R.J., Tamagno, J., Rizkalla, O., Pulsonetti, M.V., Chinitz, W., and Erdos, J.I., "Mixing and Combustion Studies in the GASL HYPULSE Facility", AIAA paper 90-2095, July, 1990.

9. Bakos, R.J., Tamagno, J., Trucco, R., Rizkalla, O., Chinitz, W., and Erdos, J.I., "Mixing, Ignition, and Combustion Studies Using Discrete Orifice Injection at Hypervelocity Flight Conditions", AIAA paper 91-2396, June, 1991.

10. Winsor, N.K., et al., "Facility Description: A 20 mm Electrothermal Gun," GT-Devices, Inc., 38th Meeting, Aeroballistic Range Association, Tokyo, Oct. 1987.

11. Burton, R.L. et al., "Experiments on a Repetitively Pulsed Electrothermal Thruster," J. of Propulsion and Power, 6:2, March-April 1990. pp. 139-144.

12. Pratt, D.T., "Calculation of Chemically Reacting Flows with Complex Chemistry," in *Studies in Convection*, Lauder, B.E., Vol. 2, Academic Press, 1977.

References (continued)

13. McBride, B.J., Heimel, S., Ehlers, J.G. and Gordon, S., "Thermodynamic Properties to 6000 K for 210 Substances involving the First 18 Elements", NASA SP-3001, Lewis Research Center, Cleveland, Ohio, 1963.

14. Hilsenrath, J. and Klein, M., "Tables of Thermodynamic Properties of Air in Chemical Equilibrium Including Second Virial Corrections from 1500 K to 15,000 K", AEDC-TR-65-58, National Bureau of Standards, Washington, DC, 1965.

15. Hansen, C.F., "Approximations for the Thermodynamic and Transport Properties of High-Temperature Air", NACA TN 4150, 1958.

16. Hansen, C.F., "A Review of the Thermodynamic, Transport, and Chemical Reaction Rate Properties of High-Temperature Air", NACA TN 4359, 1958.

17. Moeckel, W.E. and Weston, K.C., "Composition and Thermodynamic Properties of Air in Chemical Equilibrium", NACA TN 4265, 1958.

18. Billig, F.S., et. al, "Proposed Supplement to Propulsion System Management Support Plan", JHU/APL-NASP-88-1, The Johns Hopkins University Applied Physics Laboratory, Laurel, Maryland, July, 1986. Unclassified, Controlled Need to Know.

19. Hirschfelder, J.O., Curtiss, C.F. and Bird, R.B., *Molecular Theory of Gases and Liquids*, John Wiley and Sons, New York, 1954.

20. Glasstone, Samuel, *Textbook of Physical Chemistry*, Second Edition, D. Van Nostrand Company, Inc., Princeton, NJ, 1946.

21. Reid, R.C., and Leland, T.W., Jr., "Pseudocritical Constants", *A.I.Ch.E. Journal*, March 1965, pp. 228-237.

22. Oldenborg, R., et. al., "Status Report of the Rate Constant Committee, NASP High Speed Propulsion Technology Team", December, 1989.

23. Bittker, D.A., Scullin, V.J., "GGKP84 - General Chemical Kinetics code for Gas-Phase Flow and Batch Processes Including Heat Transfer Effects", NASA TP 2320, 1984.

24. Bortner, M.H., "Reaction Rate Handbook", DASA 1948, General Electric Company, Chapter 19, October, 1967.

25. Harris, Clarence J., "Comment on 'Nonequilibrium Effects on High-Enthalpy Expansion of Air'", AIAA Journal, Vol. 4, No. 6, June, 1966.

References (continued)

26. Lordi, J.A., and Mates, R.E., "Nonequilibrium Effects on High-Enthalpy Expansions of Air", AIAA Journal, Vol. 3, No. 10, October, 1965.

27. Holman, J.P., *Heat transfer*, 6th ed., McGraw-Hill, New York, 1986.

28. Lee, R.E., "Additional Comparisons of Approximations of the Thermodynamic and Transport Properties of Equilibrium Air," NASP Contractor Rept. 1010, Jan. 1988.

29. Cooper, D.M., et. al., "Real Gas Properties of Air and Air Plus Hydrogen Mixtures," NASP Tech. Memo. 1031, Oct. 1988.

30. Yos, J.M., "Transport Properties of Nitrogen, Hydrogen, Oxygen, and Air to 30,000°K," AVCO Rsch. & Dev. Div. Rept. TM RAD-TM-63-7, March 1963.

31. Truitt, R.W., *Fundamentals of Aerodynamic Heating,* Ronald Press, New York, 1960; Chap. 11.

32. Rohsenhow, Warren M., and Hartnett, James P., *Handbook of Heat Transfer*, McGraw-Hill, New York, 1973, p. 19-32.

33. Schlichting, H., *Boundary Layer Theory*, McGraw-Hill, New York, 1979.

34. Simmons, G., Nelson, G., Heirs, R. and Western, A., "An Unseeded Air MHD Accelerator Concept for High Mach Number Hypersonic Propulsion," Paper No. 89-2535 presented at the 25th Joint Propulsion Conference, Monterey, CA, July 10-12, 1989.

APPENDIX

Square Well Third Mixture Coefficient*

$$3C_{ijk}(T) = I(0) - [I(1,1)\Delta_{ij} + I(1,2)\Delta_{ik} + I(1,3)\Delta_{jk}] + [I(2,1)\Delta_{ij}\Delta_{ik} + I(2,2)\Delta_{ij}\Delta_{jk} + I(2,3)\Delta_{ik}\Delta_{jk}] - [I(3)\Delta_{ij}\Delta_{ik}\Delta_{jk}],$$

where,

$$(b_0)_{ij} = \tfrac{2}{3}\pi N\sigma_{ij}^3, \qquad \Delta_{ij} = [\exp(\epsilon_{ij}/kT) - 1],$$

$$I(0) = J(\sigma_{ij}, \sigma_{ik}, \sigma_{jk})$$

$$I(1,1) = J(R_{ij}\sigma_{ij}, \sigma_{ik}, \sigma_{jk}) - I(0)$$

$$I(1,2) = J(\sigma_{ij}, R_{ik}\sigma_{ik}, \sigma_{jk}) - I(0)$$

$$I(1,3) = J(\sigma_{ij}, \sigma_{ik}, R_{jk}\sigma_{jk}) - I(0)$$

$$I(2,1) = J(R_{ij}\sigma_{ij}, R_{ik}\sigma_{ik}, \sigma_{jk}) - [I(0) + I(1,1) + I(1,2)]$$

$$I(2,2) = J(R_{ij}\sigma_{ij}, \sigma_{ik}, R_{jk}\sigma_{jk}) - [I(0) + I(1,1) + I(1,3)]$$

$$I(2,3) = J(\sigma_{ij}, R_{ik}\sigma_{ik}, R_{jk}\sigma_{jk}) - [I(0) + I(1,2) + I(1,3)]$$

$$I(3) = J(R_{ij}\sigma_{ij}, R_{ik}\sigma_{ik}, R_{jk}\sigma_{jk}) - [I(0) + \sum_{k=1}^{3} I(1,k) + \sum_{k=1}^{3} I(2,k)],$$

$$R_{ij} = R_{ik} = R_{jk} = 1.87$$

The function J(a,b,c), which occurs in the formulae for the I's is

$$J(a,b,c) = \frac{16\pi^2}{9} b^3c^3 \qquad a \geq b+c$$

$$J(a,b,c) = \frac{\pi^2}{18}\left[\begin{array}{l} a^6 + b^6 + c^6 + 18a^2b^2c^2 \\ + 16(b^3c^3 + c^3a^3 + a^3b^3) \\ - 9\{a^4(b^2+c^2) + b^4(c^2+a^2) + c^4(a^2+b^2)\} \end{array}\right] \qquad a \leq b+c$$

---

* Reproduced from Reference 8, p. 161.

Acknowledgements

The authors wish acknowledge Dr. John I. Erdos for his contributions and for the benefit of many useful discussions regarding the work carried out under this contract.

REPORT DOCUMENTATION PAGE

Form Approved
OMB No. 0704-0188

1. AGENCY USE ONLY *(Leave blank)*	2. REPORT DATE	3. REPORT TYPE AND DATES COVERED
	November 1991	Contractor Report

4. TITLE AND SUBTITLE
Mach 10 to 20 Electrothermal Wind Tunnel Feasibility Study and Demonstration
Vol. I, Executive Summary and Analytical Study

5. FUNDING NUMBERS
C NAS1-18450, Task 20
WU 505-62-40-02

6. AUTHOR(S)
O. F. Rizkalla and W. Chinitz, General Applied Science Laboratories, Inc.
R. Burton (University of Illinois)

7. PERFORMING ORGANIZATION NAME(S) AND ADDRESS(ES)
General Applied Science Laboratories, Inc.
77 Raynor Avenue, Ronkonkoma, NY 11779
University of Illinois
Urbanna, IL 61801

8. PERFORMING ORGANIZATION REPORT NUMBER
GASL TR-342

9. SPONSORING / MONITORING AGENCY NAME(S) AND ADDRESS(ES)
NASA Langley Research Center
Hampton, VA 23681-0001

10. SPONSORING / MONITORING AGENCY REPORT NUMBER
NASA CR-191427, Volume I

11. SUPPLEMENTARY NOTES
Langley Technical Monitor: Allen G. McLain

12a. DISTRIBUTION / AVAILABILITY STATEMENT
Unclassified - Unlimited

Subject Category 09

12b. DISTRIBUTION CODE

13. ABSTRACT ***(Maximum 200 words)***

The objective of the electrothermal wind tunnel (EWT) concept study is to demonstrate, both analytically and experimentally, the feasibility of a high total pressure and enthalpy airbreathing propulsion test facility. The key element of this wind tunnel is a high pressure heater developed by GT-Devices which uses a continuous high power (100 to 650 MW) arc discharge to heat cryogenic liquid air (or possibly a surrogate fluid) to high temperature and pressure. The vaporized fluid is mixed with cooler fluid to obtain the desired reservoir conditions, then expanded through a nozzle to produce the test conditions (or expanded directly from the arc). The full-scale facility was initially sized to produce Mach 10 to 20 total enthalpies at mass flows up to 17 kg/sec (35 lbm/sec) for total test times of 0.5 seconds.

14. SUBJECT TERMS
Electrothermal Wind Tunnel
Liquid Arc
Airbreathing Research Facility

15. NUMBER OF PAGES
127

16. PRICE CODE
A07

17. SECURITY CLASSIFICATION OF REPORT	18. SECURITY CLASSIFICATION OF THIS PAGE	19. SECURITY CLASSIFICATION OF ABSTRACT	20. LIMITATION OF ABSTRACT
Unclassified	Unclassified	Unclassified	